ESA STUDY – FINAL REPORT

ESA Contract No:	SUBJECT:	INSTITUTE/COMPANY:
4000133961/21/NL/SC	Application of the data received from Liulin-MO dosimeter aboard ExoMars TGO (TGORad)	Solar-terrestrial physics department Space Research and Technologies Institute Bulgarian Academy of Sciences (STPD SRTI BAS) SUB-CONTRACTORS: NA
ESA Proposal No: 1186/26.11.2019	Revision No.: 0	INSTITUTE'S REFERENCE: 4/18.02.2021

ABSTRACT (Summary of the Project):

The dosimetric telescope Liulin-MO for measuring the radiation environment onboard the ExoMars Trace Gas Orbiter (TGO) is a module of the Fine Resolution Epithermal Neutron Detector (FREND) (**https://doi.org/10.1007/s11214-018-0522-5**). Liulin-MO operated successfully during TGO transit to Mars, on the high elliptic Mars capture orbits and since April 2018 on Mars scientific circular orbit. The activity under the project concerns application of the data received from Liulin-MO dosimeter aboard ExoMars TGO. Data will be used for assessment of the radiation conditions in the interplanetary space and in Mars orbit. The obtained data may also be of interest to ESA for comparison of the measured fluxes by other instrument for radiation measurements in the interplanetary space as e.g. SREM on ESA mission Rosetta.

The outcomes of the activity will have an actual use in ExoMars 2016 mission. These results will be very important regarding planning and radiation risks to future manned flights to Mars. The developed products have the potential for further use or development in Human Space flight and Exploration ESA Programmes, Robotic Exploration, Space Science

The work described in this report was done under ESA PECS Contract. Responsibility for the contents resides in the author or organisation that prepared it.

Names of authors: Rositza Koleva, Jordanka Semkova

Name of ESA Technical Officer: Mr Stephane Combes

ESA PECS PROGRAMME (IPL-IPS)

	Doc. No. 4000133961-003- FR Issue: I Revision: 1 Date: 12.07.2023

Application of the data received from Liulin-MO dosimeter aboard ExoMars TGO

(TGORad)

Final Report

Change Log

Issue/ Revision	Date	Modified paragraphs
4000133961-003-FR	10.07.2023	First Issue
4000133961-003-FR, revision 1	12.07.2023	Corrections made and some text added in sections “Introduction”, “Highlight Summary”, “Action Items”, Conclusions and Recommendations”. Section "Acknowledgements" is added

Table of Contents

Applicable Documents

1. ESA Contract No. 4000133961-003/20/NL/Nde with Solar Terrestrial Physics Department, Space Research & Technologies Institute, Bulgarian Academy of Sciences (STPD SRTI BAS): Application of the data received from Liulin-MO dosimeter aboard ExoMars TGO (TGORad);
2. The signed Minutes of the Negotiation Meeting held on 05 January 2021, reference "BG5_13_MoM_V2;
3. Appendix 1 to the above contract: Requirements for Management, Reporting, Meetings and Deliverables;
4. The Contractor's Proposal, reference "Proposal No. 1186/26.11.2019" dated of 30 November 2019.

List of Acronyms

AtRIS	Atmospheric Radiation Interaction Simulator
BAS	Bulgarian Academy of Sciences
CSV	Comma Separated Values
EAICD	Experiment Archive Interface Control Document
ESAC	ESA European Space Astronomy Centre
ESOC	European Space Operations Centre, ESA mission control
FREND	Fine Resolution Epithermal Neutron Detector for the TGO
FOV	Field of view
GEANT	A Monte Carlo GEometry ANd Tracking code
IKI, IKI-RAS	Space Research Institute at the Russian Academy of Sciences
IMBP	Institute for Medico-Biological Problems at the Russian Academy of Sciences
HEND	High Energy Neutron Detector
LASCO	Large Angle and Spectrometric Coronagraph
LET	Linear Energy Transfer
Liulin-MO	A particle telescope for measurement the radiation environment, a module of the Fine Resolution Epithermal Neutron Detector (FREND) onboard the ExoMars 2016 TGO
MGNS	Mercury Gamma-ray and Neutron Spectrometer
PDS	Planetary Data System
PhF-SU	The Physical Faculty of Sofia University
PI	Principal Investigator
PM	Project manager
PPP	Partially processed (data) products in PSA
PSA	ESA Planetary Space Archive
SOC	ESA Science Operations Centre
SDO	Solar Dynamics Observatory
SOHO	Solar and Heliospheric Observatory
SPICE	Observation geometry information system developed by NASA
SREM	ESA Standard Radiation Environment Monitor
SRTI	Space Research and Technologies Institute
STPD	Solar-terrestrial physics department
S/W	SoftWare
SWT	ExoMars Science Working Group

SWOG	ExoMars Science Operations Working Group
TEC-EPS	ESA Space Environments and Effects Section
TGO	Trace Gas Orbiter of ExoMars 2016 mission
UTC	Coordinated Universal Time
WP	Work Package

1. Introduction

The final report pulls together the technical information that exhibits the work completed of the project "Application of the data received from Liulin-MO dosimeter aboard ExoMars TGO (TGORad)" from 01/02/2021 to 01/06/2023.

The aim of this project according the contract was to: Provide to ESA, Roscosmos and the international science community experimental data and results for the radiation environment conditions in Mars' orbit and in the interplanetary space, necessary for planning the future manned missions to Mars.

The experimental data for the radiation conditions in the interplanetary space and Mars orbit obtained during the contract has been reported to ESA in the technical notes, provided to ESA PSA and uploaded at the Liulin experiments database created during a previous contarct with ESA, reported at the regular SWT&SOWG ExoMars meetings and published in number of science publications and conference presentations.

The main technical objective is to assess the radiation conditions in Mars orbit and in the interplanetary space from Liulin-MO data

1.1 To obtain values for the radiation doses and particle fluxes necessary for the actualisation of the existing models of cosmic ray fluxes and the evaluation of the radiation hazard to the space vehicles and the crew of future interplanetary missions;

1.2 To improve the level of calibrated data and prepare the derived data intended for ESA PSA;

1.3 To cooperate with TEC-EPS for comparison of the measured fluxes by Liulin-MO to SREM flux data on ESA Rosetta mission;

1.4 To bring Liulin-MO data to the state of the art level, accounting for adverse effects to the measured data

2. Highlight Summary

The technical objectives and tasks of the contract are completed successfully. The main science and technical results are:

- Investigation of the radiation conditions in Mars orbit and in the interplanetary space based on Liulin-MO data were conducted. The dependence of the particle fluxes and dose rates on the solar cycle development are investigated. Shown is that f**rom** March to August 2020 the measured radiation values are maximal, corresponding to the minimum of 24th cycle and transition to 25th cycle. The highest values of the dose rate (15.5/16.2 µGy h^{-1} at two perpendicular directions) and particle flux (3.24/3.33 cm^{-2} s^{-1} at two perpendicular directions) are registered in this period. Since September 2020 a decrease of the dose rates and fluxes is observed, corresponding to the decrease of GCR intensity during the inclination phase of the 25th cycle. Analysed are the radiation characteristics of the solar energetic particle (SEP) events, registered since July 2021 in Mars orbit. Compared are measurements of GCR time profiles and SEP events by different radiation detectors, including Liulin-MO, located on different satellites in the heliosphere and a good agreement is observed.
- The values for the radiation doses and particle fluxes necessary for the actualisation of the existing models of cosmic ray fluxes and the evaluation of the radiation hazard to the space vehicles and the crew of future interplanetary missions were obtained. We have compared with model results Liulin-MO measurements during the transit to Mars, on the high elliptic orbit and in Mars science orbit. The obtained results show that in all cases the measured dose rate and flux behind the shielding of the detectors of Liulin-MO are higher than the simulated values. The reasons for that are the secondary particles in the surrounding materials of the detectors, anomalous cosmic rays and the gradient of GCR spectrum from 1 AU to 1.5 AU which are not included in the models. Accounting for these differences, the calculated flux and dose rate may increase to match the measurement results. The results can serve for the benchmarking of GCRs models**.**
- A method and a S/W for extrapolating Liulin-MO data in Mars orbit to values in deep space at 1.5 a.u. were developed**.** The method and the S/W account for the contribution of GCR and albedo radiation from Mars surface and atmosphere as well as for the shading effect of Mars on the measured fluxes and dose rates in Mars orbit. The recalculated values represent the derived Liulin-MO data.
- Liulin-MO particle flux and dose rates data from TGO science phase were processed to calibrated and derived levels and in formats agreed with PSA developers as described in FREND Experiment Archiving Interface Control Document (EAICD, EXM-FR-ICD-IKI-0086). The obtained accuracy is within: ± 10% for the calibrated dose rates; ± 5% for the calibrated particle flux; ± 15% for the derived dose rate; ± 10% for the derived particle flux. Mutual work of Liulin-MO team and PSA collaborators led to a more readable structure of the raw data products, removing raw files with wrong data, appropriate structure of partially processed data products and a lot of improvements in the EAICD. Currently all calibrated data for the period 2016 - 2022 are provided to PSA in ESAC, stored and approved. (contact point: Daniela Coia, **Daniela.Coia@ext.esa.int**)

- A comparison of the measured by Liulin-MO fluxes to SREM flux data on Rosetta mission and their dependence on the solar activity were performed. Reviewed are the results from the comparison of Liulin-MO fluxes on ExoMars TGO mission with SREM TC1, S32 and S14 count rates on Rosetta mission obtained in the period April - September 2016 at different heliocentric distances in the interplanetary space. A long-term enhancement of all parameters is observed. This is in response of the falling trend of the solar activity in 2016 toward the solar cycle 24 minimum. All measured parameters from SREM and Liulin-MO instruments follow relatively well the shorter-term variations of the GCR flux, monitored by Oulu Neutron Monitor on Earth.
- A numerical model of Liulin-MO was created to investigate and account for the effect of the materials surrounding the instrument on the measured LET spectra. For that purpose a specialized application G4AAP was built, working in GEANT4 environment. The application allows for simulating the processes of Liulin-MO measurements. The results show that the behaviour of the simulated spectra of deposited energy very well follows the course of the measured spectra and provides the possibility to clean the measured LET spectra from false coincidence signals due to secondaries produced in the surrounding matter.
- A method, algorithm and S/W have been developed for subtracting the secondary effects on LET spectra measured by Liulin-MO dosimeter onboard ExoMars TGO during the transit to Mars in May-September 2016. They are based on the developed numerical model of Liulin-MO and the processes in the surrounding materials. The S/W also allows calculation of $\langle Q \rangle$ from the measured spectra with subtracted secondary effects.
- Liulin-MO data were processed to the state of the art level, accounting for adverse effects to the measured data. The data for the LET spectra, radiation quality factor $\langle Q \rangle$ and dose equivalent rates H from the beginning of Liulin –MO operations were reprocessed and analysed by the above method and S/W. The results from the reprocessing the data show that during the TGO transit to Mars in May-September 2016: $\langle Q \rangle$=3.9±0.29 for AB telescope and $\langle Q \rangle$=3.7±0.27 for CD telescope; H = 1.89±0.29 mSv day^{-1} in detectors B(A) and 1.79±0.28 mSv day^{-1} in detectors D(C). These are the data for GCRs. The above results are in good agreement with previous estimations of the corresponding values, based on measurements in single detectors of Liulin-MO and with the values of $\langle Q \rangle$ and dose equivalent rates obtained by RAD instrument aboard of NASA MSL during its cruise to Mars. All above mentioned results prove the reliability of the simulations of Liulin-MO instrument and processes in it and the reliability of the newly developed method of calculating the LET.
- The scope and schedule of the activity were reviewed and the status of Liulin-MO data and science results have been reported in regular participation in totally 7 SWT&SOWG ExoMars meetings held during the reporting period.
- Totally 9 publications in science journals and 14 conference presentations relevant to the objectives of the contract were published.

3. Management Overview

Management summary

After the kick off of the project the management activities of the contract have started. The management activities are described in WP3

Project management and reporting

Planning meetings. At a meeting of the team held immediately after the kick-off meeting the tasks and labour cost of every team member for the whole period of the project were planned. Periodically planning meetings of the team as well as meetings with the international partners were conducted.

The Director of SRTI-BAS issued an order assigning the team working under the contract.

The Project Website was created and installed online at the following URL: **http://esa-pro.space.bas.bg/ExoMars//**. In contains the following main menus: Home, ExoMarsNews, Project team. The site was linked with SRTI-BAS web. A full description of the website was presented in TN03.01.

Every 3 months a project Progress report was submitted and approved by ESA. Totally 7 Progress reports were submitted.

A Table of the meetings of the team and meetings with the ExoMars partners is given below.

Contractual management

Advanced payment request and Milestone 1 confirmation and invoice for milestone payment were submitted via esa-p system on achievement of a milestone and preliminary approval by ESA.

A Document list and an Action list have been created and maintained during the contract (see below the Action list).

Resources management

The distribution of the resources is monitored by PM in compliance with PSS forms.

The expenditures are recorded and compliance of the expenditures with PSS forms is monitored by PM permanently.

Risk management

A “Risk register” has been created at the beginning of the contract and updated regularly during the contract. The register was delivered to ESA together with each progress report every 3 months. Totally 7 Risk registers were submitted. The Risk register helps to maintain the risks connected with the technical and schedule domains.

Problems, Issues and Risk Areas were reported in Progress reports to ESA and thus maintained. The main problems and risks of the contract was connected with the restrictions imposed in Bulgaria because the COVID 19 pandemic. They provoked no access to the computer of the Faculty of Physics at Sofia University as planned and prevented the assistance of specialists from the university necessary for the numerical simulation. This led to a delay in starting the work of WP2. They were resolved in communications with ESA.

Schedule updates

Originally the duration of the contract was scheduled from 1 February 2021 to 1 March 2023. Because of the delay in work of WP2 we requested extension of the contract. On 31 January 2023 we received a notification from ESA that upon our request the delivery date of all deliverables due under the contract 4000133961/21/NL/SC is extended to 1 June 2023.

Planing

Updated Gantt chart

GANTT CHART

	Code	Task Name		Duratio	Start	Finish	Predece
1		Kick-off meeting		0 days	01-02-21	01-02-21	
2	**WP 1**	**Developmental works for the provision/pipeline of Liulin-MO fluxes and dose rates**	**M**	**500 days**	**01-02-21**	**30-12-22**	**1**
3	Task 1.1	Develop a method and a S/W for extrapolating Liulin-MO fluxes and dose rates in Mars orbit to values in deep space		217 days	01-02-21	30-11-21	
4	TN 01.01	Review of method and S/W for extrapolating Liulin-MO fluxes and dose rates to deep space. MS1.	10	0 days	30-11-21	30-11-21	3
5	SW 01.01	S/W for extrapolating Liulin-MO fluxes and dose rates in Mars orbit to values in deep space. MS1.	10	0 days	30-11-21	30-11-21	
6	Task 1.2.	Works for provision/pipeline to ESA PSA of Liulin-MO data		283 days	01-12-21	30-12-22	3
7	TN 01.02	Review of Liulin-MO results during the first year of the contract. MS1.	12	0 days	29-01-22	29-01-22	
8	Review 1 with ESA	Review of MS1	13	0 days	28-02-22	28-02-22	
9	TN 01.04	Liulin-MO data products prepared for delivery to ESA PSA: Review of results. MS2.	23	0 days	30-12-22	30-12-22	6
10	Task 1.3.	Agree with TEC-EPS and compare Liulin-MO and SREM-Rosetta fluxes and solar activity		413 days	03-05-21	30-11-22	
11	TN01.03.	Review of results from comparison Liulin-MO, SREM fluxes and solar activity. MS2.	22	0 days	30-11-22	30-11-22	10
12	Review 3 with ESA	Review of TN01.03, TN01.04	23	0 days	30-12-22	30-12-22	
13	**WP 2**	**Numerical simulations of Liulin-MO**	**De**	**607 days**	**03-02-21**	**01-06-23**	
14	Task 2.1.	Develop a numerical model of Liulin-MO and the processes in the surrounding materials		434 days	04-10-21	01-06-23	
15	TN02.01	Numerical simulations of Liulin-MO: Review. MS2.	20	0 days	01-06-23	01-06-23	14
16	Review 2 with ESA	Review of TN 02.01	21	0 days	01-06-23	01-06-23	
17	Task 2. 2.	Develop an algorithm and S/W for accounting the secondary effects on LET spectra		413 days	02-11-21	01-06-23	
18	TN02.02.	Algorithm and S/W for subtracting the secondary effects on LET spectra. Review. MS2.	22	0 days	01-06-23	01-06-23	17
19	SW02.02	S/W for subtracting the secondary effects on LET spectra. MS2.	22	0 days	01-06-23	01-06-23	
20	Review 4 with ESA	Review of TN 02.02, SW 02.02, TN 02.03	23	0 days	01-06-23	01-06-23	
21	Task 2.3.	Task 2.3. Subtract the contamination effects from measured data		457 days	01-09-21	01-06-23	
22	TN02.03.	Reprocessed data for LET spectra, Q and dose equivalent rates and analysis. Review. MS2.	24	0 days	01-06-23	01-06-23	21
23	**WP 3**	**Management and reporting.**		**609 days**	**01-02-21**	**01-06-23**	
24	**Task 3 .1**	**Project management and reporting. Contractual ma**		**609 days**	**01-02-21**	**01-06-23**	
25	TN 03.01	Project Website updated. MS1.	4	0 days	29-05-21	29-05-21	
26	PR1	I Progress report and Risk register. MS1.	3	0 days	30-04-21	30-04-21	
27	PR2	II Progress report and Risk register. MS1.	6	0 days	30-07-21	30-07-21	
28	PR3	III Progress report and Risk register. MS1.	9	0 days	30-10-21	30-10-21	
29	PR4	IV Progress report and Risk register. MS1.	12	0 days	29-01-22	29-01-22	
30	PR5	V Progress report and Risk register. MS2.	15	0 days	30-04-22	30-04-22	
31	PR6	VI Progress report and Risk register. MS2.	18	0 days	30-07-22	30-07-22	
32	PR7	VII Progress report and Risk register. MS2.	21	0 days	22-10-22	22-10-22	
33	**Task 3.2**	**Task 3.2. Preparation and submission of the Contrac**		**0 days**	**01-06-23**	**01-06-23**	
34	TDP	Technical Data Package. MS2.		0 days	01-06-23	01-06-23	
35	FR	Final Report. MS2.		0 days	01-06-23	01-06-23	
36	ESR	Executive Summary Report . MS2.		0 days	01-06-23	01-06-23	

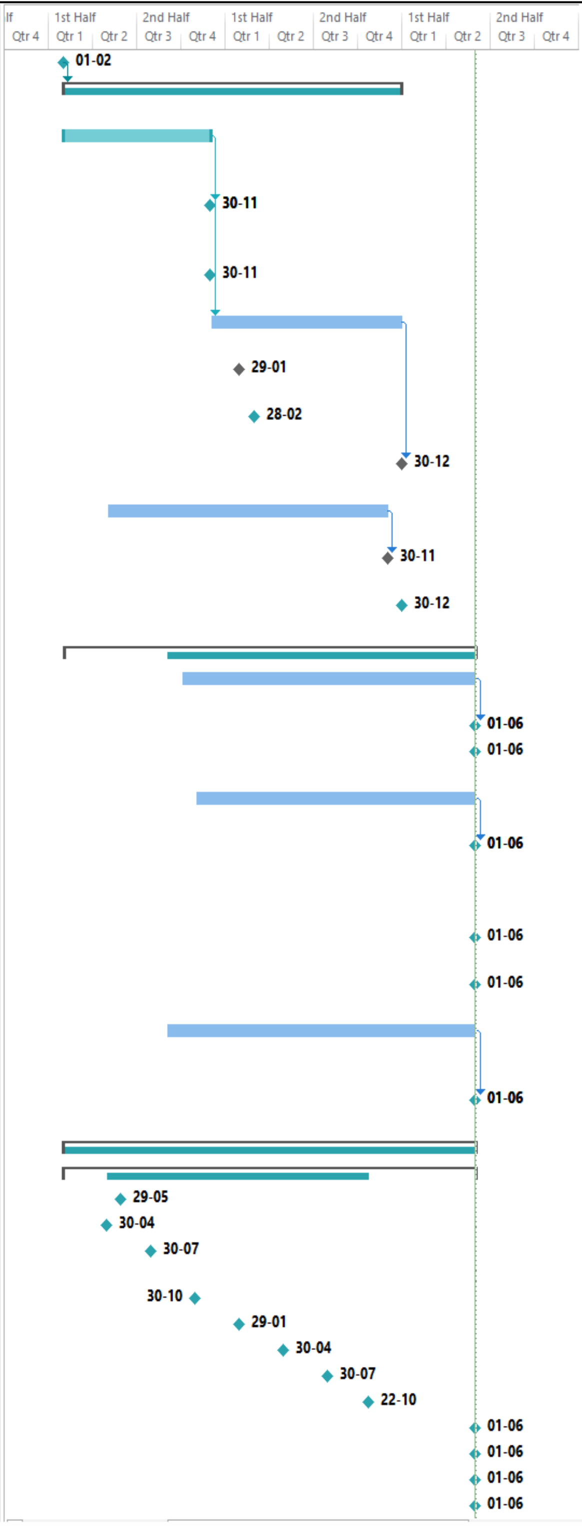

Meetings

Meeting Name	Description/ Purpose	Location	Baseline Delivery Date	Planned or Actual Delivery Date	Attendees
First planning meeting	Presentation of the contract. Planning the tasks and labour cost of every team member for the whole period of the project.	Telecon	10th February 2021	25th February 2021	The key personnel of the contract
Time mismatch	Discussing the difference in times related to measurement data in PSA raw data and Liulin-MO calibrated data	Telecon	April 2021	5th April 2021	WP leaders, FREND manager IKI RAS
What we know about Mars particle albedo	Discussion of albedo evaluations done by Bulgarian and Russian participants in Liulin-MO	Telecon	5th May 2021	5th May 2021	STDP, IMBP Russia
Requirements for albedo modeling	Possibility to model albedo contribution to Liulin-MO data using dMEREM or AtRIS models	Telecon	13th May 2021	13th May 2021	STDP, IMBP, F. Da Pieve J. Guo
Second planning meeting	Planning the tasks of every team member for the next 3 month period of the project. Signing contracts IKIT-BAS and each team member for the whole period of the project	STDP	10th May 2021	10th May 2021	The key personnel of the contract
Contribution of Mars albedo particles to Liulin-MO data	Discussion of a different approach to evaluate albedo contribution	Telecon	19th May 2021	19th May 2021	R.Koleva, J.Semkova, K. Krastev

SWT#23&SWOG#25	Regular meetings of ExoMars Science Working Team and Science Operations Working Group	Telecon	23-25 June 2021	23-25 June 2021	Participants from TGORad team J. Semkova R. Koleva
Third planning meeting	Planning the tasks of every team member for the next 3 month period of the project.	Telecon	10th August 2021	10th August 2021	The key personnel of the contract
Discussion on Liulin-MO numerical modelling	Problems arising from constructing the geometrical-mass model	STDP	12th August 2021	12th August 2021	Members of WP2
'Albedo' discussion	Review on results obtained, planning the next steps	Telecon	September 2021	16th August 2021	WP1 participants, IMBP Russia
Discussion on Liulin-MO numerical modelling -2	Questions connected with geometry and materials of TGO	STDP	14th September 2021	14th September 2021	J. Semkova, K. Krastev, V. Benghin from IMBP
Fourth planning meeting	Planning the tasks of every team member for the next 3 month period of the project.	Telecon	5th November 2021	5th November 2021	The key personnel of the contract
Contribution of Mars albedo particles to Liulin-MO data	Discussion the method to extract the contribution of albedo particles from Liulin-MO measurements	Telecon	8th November 2021	16th November 2021	R. Koleva, J. Semkova, N. Bankov, V. Benghin from IMBP
TGO_SWT#24_MEX_SWT#49_Hybrid	Update of Liulin-MO results	Telecon	16th -18th November 2021	16th -18th November 2021	J .Semkova R. Koleva
Fifth planning meeting	Planning the tasks of the team members for the next period	Telecon	February 2022	8th February 2022	The key personnel of the contract
Discussion on Liulin-MO numerical modelling -3	Discussion on problems with GRAS s/w, consecutive steps of work	STDP	February 2022	10th March 2022	Members of WP2

Provision of Liulin-MO data to PSA	Discussion on the new format of Liulin-MO label files, preparation for submission	STDP	February 2022	10th March 2022	R. Koleva, J. Semkova, N. Bankov
Times and other problems in Liulin-MO data products.	How to overcome the mismatch in Liulin-MO PSA files	Telecon	April 2022	28th March 2022	R.Koleva, A. Villacorta fom PSA
Discussion on Liulin-MO numerical modelling - 4	Discussion on input-output of the model	STDP	March 2022	19th April 2022	Members of WP2
TGO_SWT#25 and SOWG#27 meeting	Update of Liulin-MO results	Telecon	6th -8 th April 2022	6th -8 th April 2022	J.Semkova R. Koleva
Sixth planning meeting	Planning the tasks of the team members for the next period	Telecon	May 2022	12th May	The key personnel of the contract
Discussion on Liulin-MO numerical modelling - 5	Discussion on input-output of the model	STDP	June 2022	26th May	Members of WP2
Numerical model	Installation of the s/w and the model	STDP	June 2022	15 th June	Members of WP2, consultants
Provision of Liulin-MO data to PSA	Discussion on the new format of Liulin-MO label files, preparation for submission	Telecon	June - July 2022	26 th July	R. Koleva, J. Semkova, N. Bankov
Seventh planning meeting	Planning the tasks of the team members for the next period	Telecon	August 2022	16th August	The key personnel of the contract
Discussion on Liulin-MO numerical modelling - 6	Review of the first results	STDP	August-September 2022	13th September	Members of WP2
Discussion on Liulin-MO numerical modelling - 7	Discussion on the new inputs and conditions to the model	STDP	September 2022	20th October	Members of WP2

Provision of Liulin-MO data to PSA	Some problems in data preparation	STDP	October 2022	21st October	R. Koleva, N. Bankov
SWT#26&SWOG#28	Regular meetings of ExoMars Science Working Team and Science Operations Working Group	Telecon	22-24 November 2022	22-24 November 2022	Participants from TGORad team J. Semkova R. Koleva
Discussion on Liulin-MO numerical modelling - 8	Coincidence problems	STDP	November 2022	6th December 2022	K. Krastev, R. Koleva, J. Semkova,
Liulin-MO/SREM comparison	Review of the results from the comparison with SREM fluxes on Rosetta mission	Telecon	November 2022	28th November 2022	Members of WP1
Discussion on Liulin-MO numerical modelling - 9	Problems with the full construction model. How to account for the secondary effects on LET spectra	STDP	December 2022	19th January 2023	Members of WP2
Eight planning meeting	Planning the tasks of the team members till the end of the contract	Telecon	2 February 2023	2 February 2023t	The key personnel of the contract
SWT meeting	Regular meetings of ExoMars Science Working Team	Telecon	15 February 2023	15 February 2023	Participants from TGORad team J. Semkova, R. Koleva
Discussion on Liulin-MO numerical modelling - 10	Results for “cleaned LET spectrum”	STDP	March 2023	15th March 2023	J. Semkova, R. Koleva, K. Krastev
Liulin-MO calibrated data	Problems with the backward time jumps	STDP	March 2023	29th March 2023	J. Semkova, R. Koleva, N. Bankov

Liulin-MO partially processed data	How to resolve the problem of backward time jumps	Telecon	5 April 2023	5 April 2023	R. Koleva, from PSA D. Coia, E. Racero
SWT meeting	Regular meetings of ExoMars Science Working Team	Telecon	20 April 2023	20 April 2023	Participant from TGORad team J. Semkova
Liulin-MO numerical model	How to overcome the problems with the full geometrical model	STDP	21 April 2023	21 April 2023	K. Krastev, consultants
Discussion on Liulin-MO numerical modelling - 11	Problems with LET spectrum and Q Factor	STDP	10 May 2023	10 May 2023	J. Semkova, R. Koleva, K. Krastev
Discussion on Liulin-MO numerical modelling - 12	Results for the obtained Q factor and dose equivalent	STDP	23 May 2023	23 May 2023	J. Semkova, R. Koleva, K. Krastev
SWT meeting	Regular meetings of ExoMars Science Working Team	Telecon	21 June 2023	21 June 2023	Participants from TGORad team J. Semkova, R. Koleva

Action Item – Status List

ID	Description	Actionee	Due Date	Status	Closure Date	Comment/ Closure Reference
KOM 01	Ask permission to use GRAS S/W	STDP, ESA	November 2021	Closed	8th December 2021	
PM 01	Receive an approval of the TNs foreseen for MS1	ESA	March 2022	Closed	26th May 2022	
PM 02	Request for re-scheduling of TN 02.01 and TN 02.02	ESA	August 2022	Closed	23rd August 2022	
PM 03	Request for extension of the contract	ESA	25th January 2023	Closed	31st January 2023	

4. Technical Overview

Requirements targeted

- A method and a S/W for extrapolating Liulin-MO data in Mars orbit to values in deep space at 1.5 a.u. shall be developed**.** These recalculated values represent the derived Liulin-MO data. The result shall be made available to ESA by reports and description of the method.
- Liulin-MO particle flux and dose rates data from TGO science phase shall be processed to calibrated and derived levels and in formats agreed with PSA developers as described in FREND Experiment Archiving Interface Control Document (EAICD, EXM-FR-ICD-IKI-0086). The accuracy should be within: ± 10% for the calibrated dose rates; ± 5% for the calibrated particle flux; ± 20% for the derived dose rate; ± 10% for the derived particle flux. The requirements for the accuracy of the results should be verified through analysis. The results shall be made available to ESA by reports and reviews of data.
- A comparison of the measured by Liulin-MO fluxes to SREM flux data on Rosetta mission and their dependence on the solar activity shall be performed in cooperation with TEC-EPS. The outcome shall be reported to ESA.
- A numerical model of Liulin-MO shall be prepared to investigate and account for the effect of the materials surrounding the instrument on the measured LET spectra. The results shall be made available to ESA by report and description of the method.
- A method and a S/W for subtracting the contamination effects of the surrounding materials from the measured LET spectra shall be developed, based on the results of the numerical simulation. The results shall be made available to ESA by report and description of the method.
- The data for the LET spectra, Q and dose equivalent rates from the beginning of Liulin – MO operations shall be reprocessed and analysed by the above method and S/W. The accuracy should be: ± 10% for Q; ± 20% for the dose equivalent rate. The results shall be made available to ESA by review.
- The scope and schedule of the activity shall be reviewed and the status of Liulin-MO data and science results reported in regular participation in SWT&SOWG ExoMars 2016 meetings. The results shall be made available to ESA by progress reports.
- The science results shall be published in scientific journals and conferences. The results shall be made available to ESA by progress reports.

5. Work Summary

Work package	Activities / Tasks	Responsible Person	Status
WP1: Developmental works for the provision/pipeline of Liulin-MO fluxes and dose rates	1.1. Develop a method and a S/W for extrapolating Liulin-MO fluxes and dose rates in Mars orbit to values in deep space	Jordanka Semkova	Completed
	1.2. Works for provision/pipeline to ESA PSA of Liulin-MO data	Rositza Koleva Nikolay Bankov	Completed
	1.3. Compare Liulin-MO data and SREM fluxes on Rosetta mission	Tsvetan Dachev Jordanka Semkova	Completed
WP2: Numerical simulations of Liulin-MO	2.1. Develop a numerical model of Liulin-MO and the processes in the surrounding materials, using the GEANT4 S/W	Rositza Koleva Krasimir Krastev	Completed
	2.2. Develop an algorithm and S/W for accounting the secondary effects on LET spectra	Jordanka Semkova Krasimir Krastev	Completed
	2.3. Subtract the contamination effects from measured data	Krasimir Krastev Jordanka Semkova	Completed
WP3 Management and reporting	3.1. Project management and reporting. Contractual management. Resources management	Rositza Koleva	Completed
	3.2. Preparation and submission of the Contract Closure Documentation	Rositza Koleva Jordanka Semkova	On-going

Deliverables Status

Deliverable Identifier	Title/ Description	Baseline Delivery Date @ KO	Actual Delivery Date/ Delivery of revised version	Associated Payment Milestone/ Review	Status (Planned / Delivered /Accepted)
Documents					
TN 03.01	Project website created	31.05.2021.	31.05.2021	MS1	Accepted
TN01.01	Description of the method and S/W for extrapolating Liulin-MO data to deep space	30.11.2021	03.12.2021	MS1	Accepted
TN01.02	Review of Liulin-MO results during the first year of the contract	31.01.2022	02.02.2022	MS1	Accepted
TN01.03	Review of the results from the comparison with SREM fluxes on Rosetta mission.	30.11.2022	30.11.2022/ 19.12.2022	MS2	Accepted
TN01.04	Liulin-MO data products prepared for delivery to ESA PSA: Review of results.	31.12.2022	19.04.2023/ 18.05.2023	MS2	Accepted
TN02.01.	Numerical simulations of Liulin-MO; Review of results	31.09.2022 rescheduled 01.06.2023	15.05.2023/ 23.05.2023	MS2	Accepted
TN02.02	Algorithm and S/W for subtracting the secondary effects on LET spectra. Review.	30.11.2022 rescheduled 01.06.2023	25.05.2023	MS2	Accepted
TN02.03.	Reprocessed data for the LET spectra, quality factors and dose equivalent rates and science analysis. Review.	31.01.2023 rescheduled 01.06.2023	30.05.2023	MS2	Accepted
ESR	Executive Summary Report	01.03.2023 rescheduled 01.06.2023	In preparation	MS2	Planned
FR	Final Report	01.03.2023 rescheduled 01.06.2023	This document	MS2	Planned
CCD	Contract Closure Documentation	After acceptance of the final report	After acceptance of the final report	MS2	Planned
TDP	Technical Data Package			MS2	Planned
Software					
SW01.01	S/W for extrapolating Liulin-MO data to deep space.	30.11.2021	03.12.2021	MS1	Accepted
SW02.02	S/W for subtracting the secondary effects on LET spectra.	30.11.2022 rescheduled 01.06.2023	25.05.2023	MS2	Accepted

6. Detailed Review of Work

6.1. Brief description of Liulin-MO instrument

The description of Liulin-MO instrument is necessary to understand the details of all the work done under the current contract and described in technical notes TN 01.01 – TN 02.03.

The Liulin-MO particle telescope contains two dosimetric telescopes – AB and CD arranged at two perpendicular directions (Semkova *et al,* 2018, 2021). Each pair of the dosimetric telescopes consists of two 300 µm thick, 20x10 mm area rectangular Si PIN photodiodes. The distance between the parallel Si PIN photodiodes is 20.8 mm. Fig. 6.1.1 is a sketch of the sensor unit.

The parameters, provided by Liulin-MO simultaneously for two perpendicular directions have the following ranges: absorbed dose rate from 10^{-7} Gy h^{-1} to 0.1 Gy h^{-1}; particle flux in the range 0 - 10^4 cm^{-2} s^{-1}; energy deposition spectrum and coincidence energy deposition spectrum in the range 0.08 - 190 MeV.

To meet the requirement to measure spectra in a wide energy range (and correspondingly linear energy transfer Wide LET range) one of detectors in every telescope measures and provides the energy deposition spectrum in the range 0.08-18 MeV (detectors B and D), and the other in the range 0.32-190 MeV (detectors A and C). The energy deposition spectra of B (D) in the range ~ 0.08-15.9 MeV and of A (C) in the range ~ 16-190 MeV are later summarized and used to obtain the energy deposition spectrum in a single detector in the direction of A-B (C-D). The energy deposition spectra measured in A and B detectors in coincidence mode are recorded separately and used to obtain the LET spectrum in the direction of A-B. This LET spectrum consists of low and high LET parts. The low LET part is obtained from the B coincidence spectrum in the energy deposition range ~ 0.08 - 15.9 MeV and the high LET part is obtained from the A coincidence spectrum in the energy deposition range ~ 16 - 190 MeV. Similarly the energy deposition spectra measured in the C and D detectors in coincidence mode are recorded separately and used to obtain the LET spectrum in the perpendicular C -D direction.

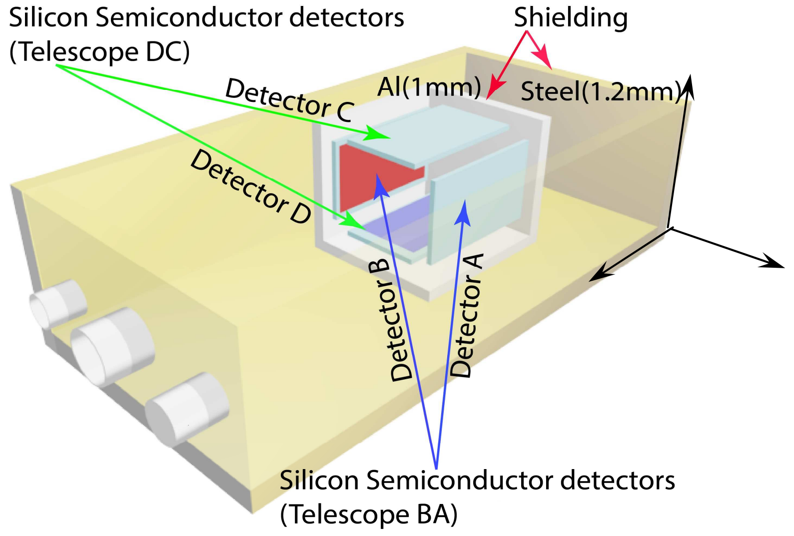

Fig. 6.1.1 A schematic view of Liulin-MO detectors' location in the dosimeter box and TGO axes

Totally 9 energy deposition spectra in anti-coincidence and coincidence modes are measured and provided in Liulin-MO output data:

- B0 and D0 – spectra measured by detectors B and D in anti-coincidence (0 denotes the lower energy part of the full spectrum);
- BA0, BD0, DC0 – spectra measured by B or D in coincidence with detectors A, D or C respectively;
- A1 and C1 - spectra measured by detectors A and C in anti-coincidence (1 denotes the higher energy part of the spectrum);
- AB1 and CD1 – spectra measured by detectors A or C in coincidence with B or D.

Quantities for the particle flux are denoted by F, those for the dose – by D. For example the flux measured by detector B in anti-correlation is FB0, the corresponding dose – DB0. The full quantity of the flux (dose) measured by a single detector is obtained by summarizing the corresponding parts:

FBA=FB0+FBA0+FDB0+FA1+FAB1; DAB= DB0+DBA0+DBD0+DA1+DAB1

FDC=FD0+ FDC0+FDB0+FC1+FCD1; DCD=DD0+ DDC0+DDB0+DC1+DCD1

The dose rates and the fluxes are resolved every minute and recorded in the output data – further called “minute quantities”, while the energy deposition spectra and the LET spectra are resolved every hour.

Liulin-MO data are stored in a specially created database (MSSQL Express 2012) located on a separate host computer. The database was developed under Contract No. 4000117692/16/NL/NDe DOSIMETRY: Dosimetry science payloads for ExoMars TGO & surface platform. Unified web-based database with Liulin type instruments' cosmic radiation data and described in Dosimetry_Deliverable_D04.03-Rev1.pdf. Any registered user can get access to the DB data remotely using the login procedure.

To use Liulin-MO data measured on Mars circular orbit for verification and benchmarking of the radiation environment models, they should be corrected for the shading of GCR by Mars and the contribution of Mars albedo particles.

Reference documents common for all technical notes

1. *Krastev, K., et al,* (2019). The Shading Effect for Doses and Galactic Cosmic Rays Fluxes Measured by Liulin. Eleventh workshop "Solar Influences on the Magnetosphere, Ionosphere and Atmosphere", Book of Proceedings, 2019, ISSN:2367-7570, DOI:10.31401/WS.2019.proc, 31-34
2. *Mitrofanov I., et al,* (2018). Fine Resolution Epithermal Neutron Detector (FREND) onboard the Trace Gas Orbiter, Space Sci Rev, August 2018, 214:86, **https://doi.org/10.1007/s11214-018-0522-5**
3. *Semkova, J., R. Koleva, V. Benghin, et al*, (2018). Charged particles radiation measurements with Liulin-MO dosimeter of FREND instrument aboard ExoMars Trace Gas Orbiter during the transit and in high elliptic Mars orbit, Icarus, 303, (2018) 53–66, **https://doi.org/10.1016/j.icarus.2017.12.034**
4. *Semkova Jordanka, Rositza Koleva, Victor Benghin et al,* (2021). “Results from radiation environment measurements aboard ExoMars Trace Gas Orbiter in Mars science orbit in May 2018 - December 2019”, Icarus, June 2021, 114264, **https://doi.org/10.1016/j.icarus.2020.114264**.
5. *Semkova Jordanka, Rositza Koleva, Victor Benghin et al,* (2023). Observation of the radiation environment and solar energetic particle events in Mars orbit in May 2018- June 2022, Life Sciences in Space Research, 2023, **https://doi.org/10.1016/j.lssr.2023.03.006**

6.2. Activities for WP1

Work Package 1 is aimed at developmental works for the provision/pipeline of Liulin-MO fluxes and dose rates. The work is organized in 3 tasks and is reported in 5 deliverables:

Deliverable number	**Deliverable title**
TN01.01	Description of the method and S/W for extrapolating Liulin-MO data to deep space
SW01.01.	S/W for extrapolating Liulin-MO data to deep space
TN01.02	Review of Liulin-MO results during the first year of the contract
TN01.03	Review of the results from the comparison with SREM fluxes on Rosetta mission.
TN01.04	Liulin-MO data products prepared for delivery to ESA PSA: Review of results.

6.2.1. TN01.01. Description of the method and S/W for extrapolating Liulin-MO data to deep space

The goal of the work described is to develop a method and a S/W for extrapolating Liulin-MO data for the particle fluxes and dose rates measured in Mars orbit to values in deep space at 1.5 a.u. The method shall account for the effect of "shading" the particle flux by Mars, the effect of the detectors' orientation and the albedo particles effect on the measured values

Additional reference documents for TN01.01.

1. *Benghin V., et al, 2019*. Comparison of Liulin-MO Dosimeter Radiation Measurements during ExoMars 2016 TGO Mars Circular Orbit with Dose Estimations Based on Galactic Cosmic Ray Models, paper presented at the 11 th workshop "Solar Influences on the Magnetosphere, Ionosphere and Atmosphere", Primorsko, Bulgaria, June 3-7, 2019, Program & Presentations, **http://ws-sozopol.stil.bas.bg/**
2. *Guo J., S. Banjac, L. Rostel, et al.* (2019). Implementation and validation of the GEANT4/AtRIS code to model the radiation environment at Mars, SWSC, 9, A2
3. *O'Neill, P., Golge, S., & Slaba, T.* (2015). Badhwar–O'Neill 2014 galactic cosmic ray flux model (p. 218569). NASA/TP. **https://ntrs.nasa.gov/archive/nasa/casi.ntrs.nasa.gov/20150003026.pdf**
4. *Semkova, J., Koleva, R., Benghin, V.,* et all, (2020) Radiation environment in the interplanetary space and Mars orbit in 2016-2020 according measurements aboard ExoMars TGO, Proceedings of (SES 2020, http://space.bas.bg/SES/archive.html, e-ISSN 2603 – 3321, pp. 23-34
5. *Jordanka Semkova, Victor Benghin, Jingnan Guo et al* (2022), Comparison of the flux measured by Liulin-MO dosimeter in ExoMars TGO science orbit with the calculations, LSSR, ISSN 2214-5524, **https://doi.org/10.1016/j.lssr.2022.08.007**

Method and S/W for extrapolating Liulin-MO data to deep space

Mars shading effect on GCR flux and dose rate

In Mars circular orbit the planet shades single detectors' field of view (FOV), thus cutting part of GCR flux. The cut part of FOV is an angle dependent on TGO orientation and its altitude. TGO orientation can vary by 180^0 though not often; TGO altitude varies within 50 km in every orbital pass. We investigate the dependence of the flux and dose rate measured by Liulin-MO on the distance of TGO from Mars and the orientation of dosimeter detectors.

When calculating the effect of shading of the flux we neglect the size of the detector and take into account only its orientation and the distance to Mars. The principal configuration is

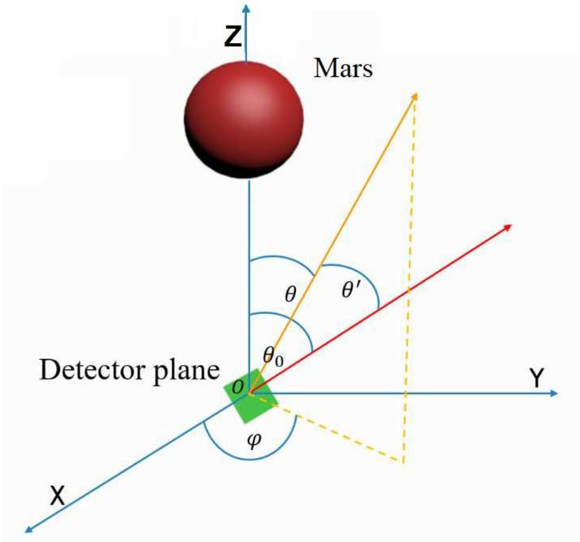

Fig. 6.2.1.1 Scheme for calculation of the shading effect by Mars on GCR flux. The red line marks the normal to the detector plane, θ' is the angle between the normal and the differential flux, θ_0 is the angle between the normal and Mars direction.

shown in Fig. 6.2.1.1. (Krastev *et al*, 2019). Let $j(\theta, \varphi)$ denotes the differential flux and F_{sh} - the part of GCR flux shaded by Mars. Then

(1) $$F_{sh} = \int_0^{2\pi}\int_0^{\theta_1} J(\theta,\varphi)|\cos\theta'|\sin\theta d\theta d\varphi$$

where θ' is the angle between the normal to the plane of the detector and the differential flux, θ_0 is the angle between the normal and the Mars direction, $\theta = \theta_0 - \theta'$,

(2) $$\sin\theta_1 = \frac{\text{Mars radius}}{\text{Distance to Mars}}$$

We define the shading coefficient K_{sh} as

(3) $$K_{sh} - \frac{F_{sh}}{2\pi J(\theta,\varphi)}$$

For the calculation of the shading effect on the dose we use the following:

Let the GCR flux falls on the surface of the detector at an angle θ as shown in Fig. 6.2.1.2. The dose received from this flux is, on one hand, proportional to the flux, on other hand, to the path it travels in the sensitive area of the detector.

(4) $D = kJ.S \quad J = J_0 \cos\theta,$, where D is the dose, S is the path in the detector,

J_0 is the GCR flux (isotropic).

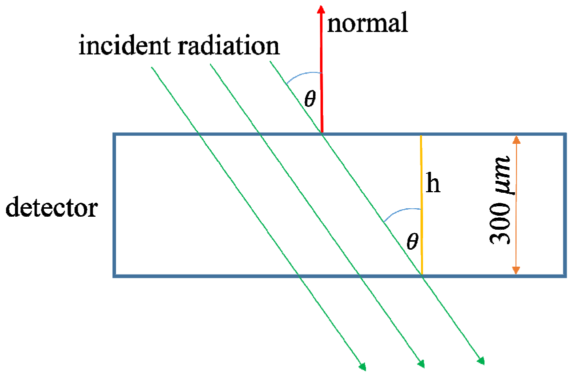

Fig.6.2.1.2. Scheme for calculation of the shading effect by Mars on GCR dose. The red line marks the normal to the detector plane, θ is the angle between the normal and the differential flux, orange line h is the thickness of the detector.

From Fig. 6.2.1.2. it is seen that

(5) $$S = \frac{\boldsymbol{h}}{\cos\theta}$$

(6) $D = kJ_{\mathbf{0}}.\boldsymbol{h}$, *h* is the detector thickness

Integrating for all directions we receive:

(7) $$D_{total} = \int_{\mathbf{0}}^{2\pi}\int_{-\pi}^{\pi} kJ_{\mathbf{0}}.\boldsymbol{h}\ \sin\theta d\theta d\varphi$$

(8) $D_{\ total} = 4\,\pi\, kJ_{\mathbf{0}}.\boldsymbol{h}$

For the shielded dose we receive:

(9) $$D_{shielded} = \int_{\mathbf{0}}^{2\pi}\int_{\mathbf{0}}^{\theta_{\mathbf{1}}} kJ_{\mathbf{0}}.\boldsymbol{h}\sin\theta d\theta d\varphi = kJ_0.\boldsymbol{h}\int_0^{2\pi}\int_0^{\theta_1}\sin\theta d\theta d\varphi$$

where $$\sin\theta_1 = \frac{\text{Mars radius}}{\text{Distance to Mars}}$$

The comparison of the experimental flux and dose rate data with the analytical estimates of the shadow coefficient is shown in Fig 6.2.1.3 (Semkova *et al,* 2020). From top to bottom are plotted: particle dose rate measured by B(A) detectors from 8 July to 9 July 2018; the particle flux measured by the same B(A) detectors; the shading coefficient; the angle between detector's axis and Mars direction; the altitude of TGO. Most of the time the angle between detector's axis and Mars direction is ~ 90^0 and the shading effect is about 0.23, the change in the altitude results small variations in the shading coefficient K_{sh}. The narrow sharp drops of the measured flux coincide with the increases of the shading effect up to about 0.4 due to changing of the angle between detector's axis and Mars direction.

It can be seen that, as a first approximation, the absorbed dose depends insignificantly on the change of the shading coefficient. Two mutually compensating effects can explain the

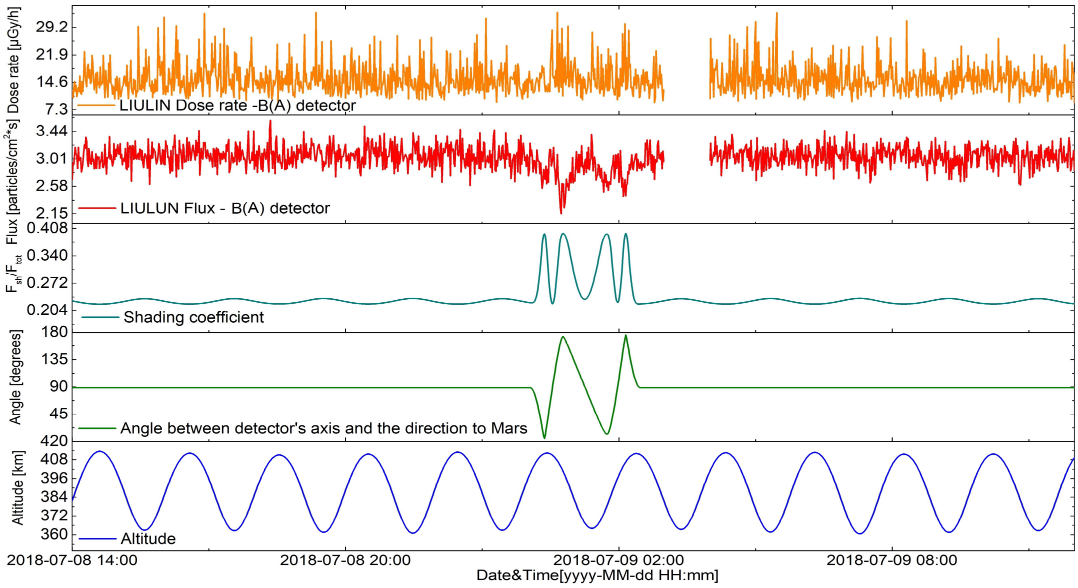

Fig. 6.2.1.3. Comparison of the experimental dose rate and flux data with the analytical estimates of the shadow coefficient. From top to bottom are plotted: minute values of the dose rate measured by B(A) detectors from 8 July to 9 July 2018; minute values of the particle flux measured by the same detector; the shading coefficient; the angle between detector's axis and Mars direction; the altitude of TGO.

above peculiarity. When the detectors normal is perpendicular to the nadir to Mars – we call this 'nominal position' - the planet blocks GCR particles that would hit the detectors at sharp angles. These particles would have a small effective area on the detectors and would contribute less to the registered particle flux but their path in the detector would be long thus contributing more significantly to the absorbed energy. In case when the detector normal is parallel to the nadir, the hampered GCR particles would hit the detectors at small angles with considerable absorbed energy. As a result the decrease in the dose rate is insignificant when compared to the dose rate measured in nominal position.

Evaluation the contribution of Mars albedo particles

First approach: using measurements at high elliptic orbit

To account for the albedo particles contribution we used the measurements conducted near the pericenter in high elliptic TGO orbit (Benghin *et al,* 2019, Semkova *et al,* 2020). At almost all pericenters TGO was oriented nominally, Liulin-MO detectors' axes are at 90^{o} to nadir. In Fig. 6.2.1.4 on the top are plotted the flux (left) and dose rates (right) measured by Liulin-MO on 25 February 2017 near and at the pericenter of TGO. On the middle plots are plotted the same **values corrected by a simple geometrical correction of FOV shading by Mars. The result from this correction systematically overestimates the flux. We interpret this overestimation as a consequence of the presence of albedo radiation in the measured flux.**

In order to estimate the deep space flux from data measured on Mars orbit we replace the altitude by an 'effective altitude' - the real altitude multiplied by an allowance factor. For a circular orbit at an altitude of 380 – 430 km taking into account the selected allowance factor, the effective height is about 1000 km. In Fig.6.2.1.5. is shown the dependence of the non - shaded part of flux on the altitude above Mars for 3 different orientations of Liulin-MO sensors relative to the nadir. The difference in the fraction of unshaded flux for the actual and effective height gives estimates of the albedo radiation.

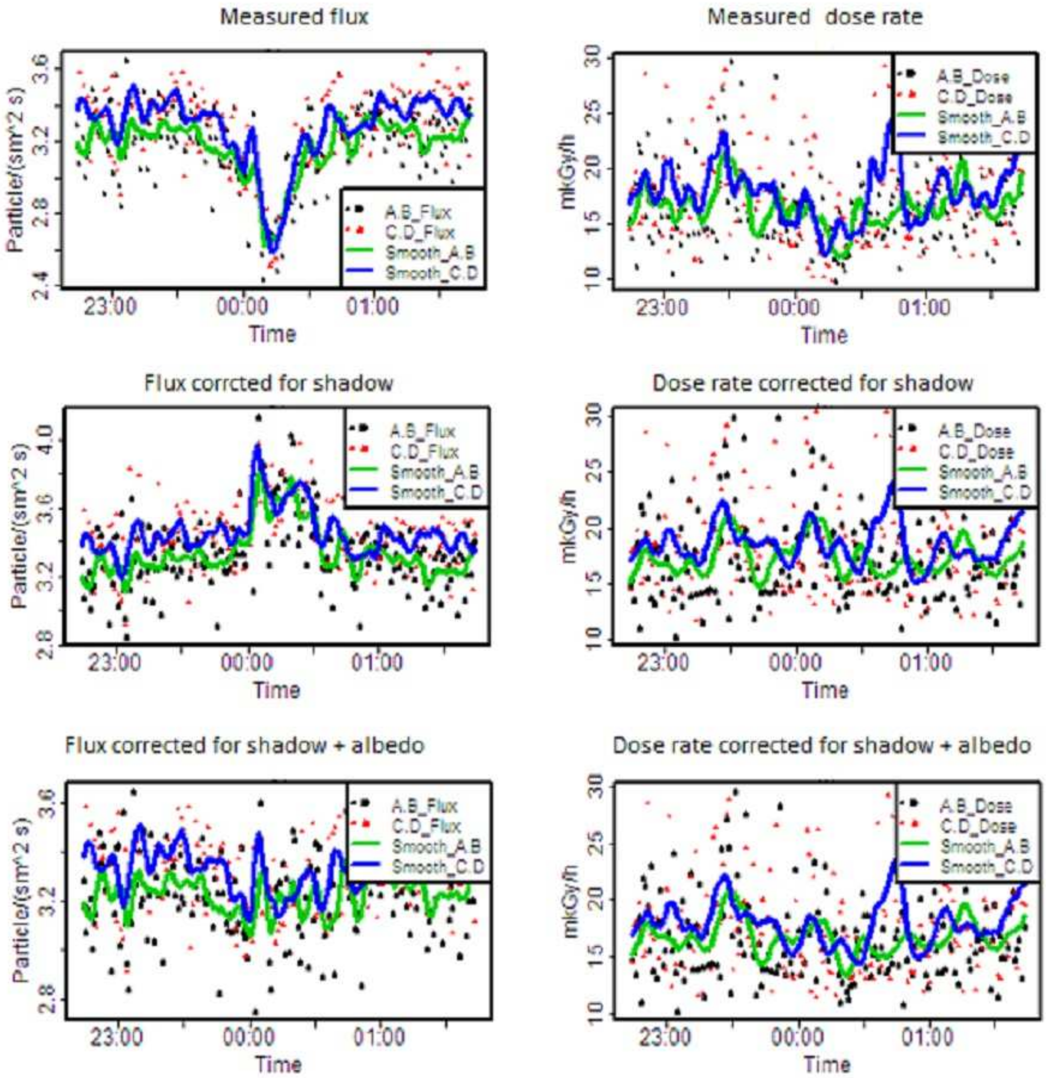

Fig.6.2.1.4. Top: the flux (left) and dose rates (right) measured by Liulin-MO on 25 February 2017 near and at the pericenter of TGO; middle plots: the same values corrected by a simple geometrical correction of FOV shading by Mars; bottom: the same values corrected for the FOV shading and for the albedo particles.

A statistical study gives albedo contribution of 6 – 12 percent. As a zero approximation we assume that in Mars orbit the flux is 0.88 of the flux in deep space and the dose rate is 0.82 from that in deep space. This estimation is based on the analyses of all 38 cases of data available for pericenter crossing during Mars capture orbit phase of TGO.

In Fig. 6.2.1.4. the bottom plot shows the corrected for the FOV shading and for the albedo particles values, i.e. these are the flux and dose rate in free space at about 1.5 AU

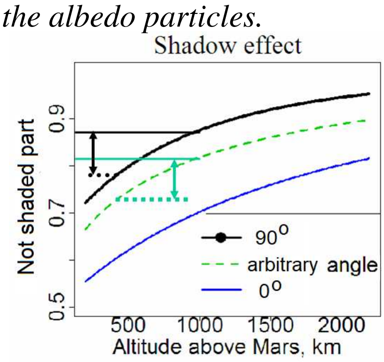

Fig.6.2.1.5. Dependence of the non - shaded part of flux on the altitude above Mars for 3 different orientations of Liulin-MO sensors relative to the nadir and difference in the fraction of unshaded flux for the actual and effective height.

Second approach: modeling and calculation of the albedo flux on circular orbit

An evaluation of Mars albedo contribution to the measured particle flux was performed by mathematical methods, using different approximations and model distribution functions. These modeling estimated the albedo contribution to about 7% to 10%. They clearly demonstrated that to estimate the albedo contribution correctly we need to know:

At 400 km height above Mars:

- The energy distribution of the albedo particles to determine which of them enter behind our shielding.
- The intensity of the albedo relative the interplanetary GCR flux.
- Their angular distribution to calculate what part of the albedo flux hits our sensors.

Two foreign researchers, experts in Mars atmosphere and soil modelling – Dr. Guo and Dr. Da Pieve were contacted and an agreement was received that they will try to model the albedo particles hitting Liulin-MO.

Dr. Guo provided us with detailed modelled spectra of the albedo particles (Semkova et al, 2022). She provided the spectra of particles at 80 km height obtained from the AtRIS model (Guo *et al*, 2019). Spectra are provided for two surface pressure conditions - 82 Pa and 1200 Pa, which refer to two extreme cases of total atmospheric thickness. The solar modulation condition for the input GCR is chosen as 400 MV from the Badhwar O'Neil model which is a proxy of solar minimum. The flux unit is in $cm^{-2}s^{-1}MeV^{-1}ster^{-1}$. In our estimations further we took into account only the contributions from protons and alpha particles as dominating charged particles; from neutrons and gamma rays.

A brief description of the procedure for calculating the fluxes recorded by Liulin-MO detectors

Using the OLTARIS tools (**https://oltaris.larc.nasa.gov/**) the contribution of the albedo particles to Liulin-MO fluxes for different orientations of the satellite and different angular distributions were calculated.

The calculations were carried out on the basis of a detectors shielding model using 64802 rays. For each ray the shielding thickness and the incident flux, accounting for Mars shading were calculated. The flux dependence on the shielding thickness is calculated using the method of linear interpolation from tables.

Calculation of the proton and alpha particles albedo

The albedo table was calculated from the upward proton differential spectrum for atmospheric pressure 1200 Pa.

From the spectrum j in $cm^{-2}s^{-1}MeV^{-1}ster^{-1}$, the integral spectrum in $cm^{-2}s^{-1}ster^{-1}$ was calculated. Then, the tabular values of the proton energy in the integral spectrum were compared with the values of the proton ranges in aluminum. The resulting table was further used for interpolation the dependence of the flux on the shielding thickness. The flux of alpha particles, as well the secondary radiation due to nuclear interactions, were not taken into account at this stage. When calculating the flux incident on the detector from different directions the following cosine angular distribution over the zenith angle λ was considered:

$(n+1)\cdot j(h)\cdot \cos^n(\lambda)$

The (n+1) coefficient used further reflects the case when j(h) is the mean for all upward directions. In case j(h) is the flux directed to zenith the coefficient is 1 and all results for the albedo flux should be divided by (n+1).

The GCR particle flux was calculated using the Badhwar 2020 model for December 1, 2018 (this is the last month for which data is currently available) was used. The calculation was made for a set of aluminum thicknesses from 0 to 400 g.cm^{-2}.

Several calculations of the contributions of GCR and the proton albedo to the flux values that should be recorded by the detectors have been performed. Three variants of the spacecraft orientation and four variants of the angular distribution of albedo particles are considered. Table 6.2.1.1 shows the effect of orientation when the angular distribution of the albedo prortons is $j(h)\cdot\cos(\lambda)$. When calculating the contribution of the albedo protons, in addition to the fluxes in the detectors, the values that would register an isotropic spherical detector of a unit area, placed in the same shielding conditions were calculated. This parameter is denoted as Jisotrop. Flux is in units cm^{-2}s^{-1}.

Table 6.2.1.1. Assessment of the effect of detectors' orientation on the flux recorded by them

Altitude km	Orientation angles, degree		Orientation Description	GCR contribution to the registered flux		Albedo protons contribution to the registered flux		
	θ	φ		BA	DC	J isotrop	J BA	J DC
400	0	0	The axis of the telescope BA is directed to the nadir, and the axis of telescope DC is directed to the horizon	1.619	2.045	0.1486	0.1076	0.0580
400	90	0	The axis of the telescope BA is directed to the horizon, and the axis of the telescope DC is directed to the nadir	2.113	1.637	0.1114	0.0491	0.0779
400	90	90	The axes of both telescopes are directed to horizon	2.088	2.057	0.1335	0.0575	0.0515

It can be seen that the effect of orientation, causing different shading of the GCR flux by Mars, significantly exceeds the effect from the albedo flux, the latter varies from 2.3% to 6.6% of the flux due to GCR themselves.

Table 6.2.1.2 shows the results of examining the effect of the angular distribution of albedo particles on the flux recorded by the detectors for detectors' orientation θ = 0, φ = 0

Table 6.2.1.2. Estimation of the effect of the albedo particles angular distribution on the flux recorded by the detectors

Exponent **n** in distribution $\cos^n\lambda$	GCR contribution to the registered flux		Albedo protons contribution to the registered flux		
	BA	DC	J isotrop	J BA	J DC
0 (isotropic distribution)	1.619	2.045	0.1750	0.1082	0.0801
1	1.619	2.045	0.1486	0.1076	0.0580
2	1.619	2.045	0.1365	0.1076	0.0469
3	1.619	2.045	0.1298	0.1077	0.0402

For BA detectors, whose axis is directed to the nadir, an effect of the exponent **n** on the recorded flux is practically absent. For the second pair of detectors the relative change is much larger but the absolute value of the differences is at the level of 0.01 particles per second, which is not discernible in the experimental data. This allows us to assume that **the form of the angular distribution of albedo protons is not significant.**

A series of calculations was carried out to assess the effect of orientation on the average thickness of the shielding in each direction. Calculations have shown that the albedo contribution to the recorded flux from protons depends more strongly on orientation than on the average shielding thickness. The calculations were carried out for the conditions of pressure 82 Pa (pres82 spectrum) and pressure 1200 Pa (pres1200 spectrum), the exponent in the angular distribution n = 1.

Along with the calculations for protons, the calculations for the alpha particles albedo were carried out using the same procedure. The results are shown in Table 6.2.1.3.

Table 6.2.1.3. Calculation of proton and alpha particles albedo contribution to the registered flux

Spectrum under consideration	S/c orientation angles		Average shielding thickness on the side facing Mars, g/cm^2	Estimated contribution to the registered flux, 1/cm^2/s	
	θ	φ		Detector BA	Detector DC
pres82_Output_proton	90	90	28.907	0.0716	0.0648
	90	180	9.720	0.0867	0.1527
	120	-130	3.171	0.1082	0.1113
pres1200_Output_proton	90	90	28.907	0.0575	0.0514
	90	180	9.720	0.0709	0.1247
	120	-130	3.171	0.0890	0.0915
pres82_Output_alpha	90	90	28.907	0.0031	0.0029
	90	180	9.720	0.0033	0.0059
	120	-130	3.171	0.0039	0.0040
pres1200_Output_alpha	90	90	28.907	0.0030	0.0028

	90	180	9.720	0.0031	0.0056
	120	-130	3.171	0.0037	0.0038

Calculation of the neutron and gamma albedo

The calculation from the upward spectra of neutrons and gamma radiation was carried out using a similar method. The detector sensitivity to neutrons and gamma was taken from the data of physical calibrations and ground tests of Liulin-MO dosimeter. The results from the calculations are shown in Table 6.2.1.4.

Table 6.2.1.4. Calculation for the neutron and gamma albedo contribution to the registered flux

Spectrum under consideration	Flux $1/cm^2/sr/sec$	S/c orientation angles		Average shielding thickness on the side facing Mars g/cm^2	Estimated contribution to the registered flux, $1/cm^2/s$
		θ	φ		
pres82_Output_Spectral_phi_400_Out_neutron	2.02	90	90	28.907	0.170
		90	180	9.720	0.251
		120	-130	3.171	0.284
Pres1200_Output_Spectral_phi_400_Out_neutron	1.30	90	90	28.907	0.109
		90	180	9.720	0.162
		120	-130	3.171	0.183
pres82_Output_Spectral_phi_400_Out_gamma	0.423	90	90	28.907	0.00907
		90	180	9.720	0.0134
		120	-130	3.171	0.0152
Pres1200_Output_Spectral_phi_400_Out_gamma	0.446	90	90	28.907	0.00958
		90	180	9.720	0.0142
		120	-130	3.171	0.0160

Based on the above calculations a decision was taken to use further only measurements performed in nominal orientation of TGO, when Liulin-MO sensors look at 90o to nadir.

The results from the calculations of the albedo **when Liulin-MO sensors look at 90^o to nadir** show that **the contribution of the total albedo (protons+alpha+neutrons+gamma) to the measured total flux from GCR and albedo is respectively 7.9% for detector BA and 7.8% for detector DC for surface pressure conditions 1200 Pa. The corresponding values for surface pressure conditions 82 Pa are 10.8% for detector BA and 10.7% for detector DC. These values are in the range of the estimated albedo contribution to the measured flux from the statistical studies and are used in the S/W developed for extrapolating Liulin-MO fluxes data to deep (free) space** (see below).

The data for the fluxes in free space at 1.5 AU are important for the benchmarking the models of the radiation fields in space.

It is very difficult and time consuming to calculate the contribution of the albedo to the measured dose rate using the albedo spectra. That's why, taking into account the good correlation between the results for calculation the fluxes in free space using the two approaches described above we decided **in the S/W developed for extrapolating Liulin-MO dose rate data to deep space to use the conversion coefficient of 0.82 obtained from the measurements in TGO high elliptic orbit** (see below). This coefficient accounts for both the shading by Mars and the albedo contribution to the measured dose.

Description of the procedure for extrapolating the particle flux and dose rates in free space at 1.5 AU

The procedure for extrapolation the particle flux and dose rates in free space at 1.5 AU includes the following steps:

- In the internal data base of Liulin-MO[*] select the time interval for which data are required.
- In the Liulin-MO database extract the minute calibrated values of the fluxes

FBA=FB0+FBA0+FDB0+FA1+FAB1;

FDC=FD0+FDC0+FDB0+FC1+FCD1;

and dose rates

DBA = DB0+ DBA0+DBD0+DA1+DAB1;

DDC = DD0+ DDC0+ DDB0+DC1+DCD1

using the ***"Flux rate"*** and ***"Dose rate"*** calculating procedures. As a result of selecting the desired values and saving them four files of type .csv containing the minute values of the fluxes and dose rates for the selected time intervals are created.

- In the Liulin-MO database extract the coordinates of the spacecraft calculated by the SPICE software for the same time interval. After selecting and saving the data a file of .csv type is created.
- Use the newly developed S/W (see below) to relate the data for the minute values of the fluxes and dose rates to the orbital parameters and extract only the values when Liulin-MO sensors look at $90^{o}\pm5^{o}$ to nadir. As a result a file containing the data for the measured fluxes and dose rates at $90^{o}\pm5^{o}$ to nadir during the selected period is created.
- Use the newly developed S/W (see below) to calculate from the measured fluxes and dose rates at $90^{o}\pm5^{o}$ to nadir the values meaningful for the free space at 1.5 AU as follow:

A) For atmospheric pressure 1200 Pa:

$Ffree_i =(Fmeas_i -0.079\ Fmeas_i)/(1-Ksh_i)=0.921Fmeas_i/(1-Ksh_i)$. This is the formula for the detector BA.

$Ffree_i =(Fmeas_i -0.078\ Fmeas_i)/1-Ksh)_i=0.922Fmeas_i/(1-Ksh_i)$. This is the formula for the detector DC.

B) For atmospheric pressure 82 Pa:

$Ffree_i =(Fmeas_i -0.108\ Fmeas_i)/(1-Ksh_i)=0.892Fmeas_i/(1-Ksh_i)$. This is the formula for the detector BA.

$Ffree_i =(Fmeas_i -0.107\ Fmeas_i)/(1-Ksh_i)= 0.893Fmeas_i/(1-Ksh_i)$. This is the formula for the detector DC.

---

[*] The internal database of Liulin-MO is developed under Contract No. 4000117692/16/NL/NDe DOSIMETRY: Dosimetry science payloads for ExoMars TGO & surface platform. Unified web-based database with Liulin type instruments' cosmic radiation data and described in the attached Dosimetry_Deliverable_D04.02-Rev1.pdf

In these relations *Fmeas* is the measured flux, *Ffree* is the free-space flux without shading from Mars, *Ksh* is the shading coefficient from Mars, and *i* is the sequence number of the measurement.

C) $Dfree_i = Dmeas_i/0.82$, where *Dfree* is the dose rate in free space and *Dmeas* is the measured dose rate, *i* is the sequence number of the measurement. The coefficient *0.82* is applied to both detectors BA and DC.

Description of the S/W for extrapolating the particle flux and dose rates in free space at 1.5 AU

The S/W ALL3PROGS.FOR developed for extrapolation the particle flux and dose rates in free space at 1.5 AU is based on the above described procedure. It is a FORTRAN program. It calculates the extrapolated values in 3 consecutive phases.

- In the first phase the subroutine *CRT_TAB_M* looks for four (4) files of the type

MinuteDoseRate_DB0+DBA0+DA1+DAB1+BD0……….csv,
MinuteDoseRate__DD0+DDC0+DC1+DCD1+BD0……….csv,
MinuteFLuxRate_FB0+FBA0+FDB0+FA1+FAB1……….csv,
MinuteFLuxRate_ FD0+FDC0+FDB0+FC1+FCD1……….csv

extracted from Liulin-MO database and creates a corresponding ".tab" file.

- In the second phase the subroutine *COMBINE_TAB_ORB_M* mixes data from the '.tab' file created by the previous sub–routine program with coordinate data, contained into 'Spice_xxxx xxxxx_yyyy yyyy.csv' file extracted from Liulin-MO database. It creates file of type YYYY_MM.csv, containing data for the orbital parameters, measured fluxes and dose rates in detectors AB and CD and angles in the range $90^o \pm 5^o$ to nadir in which these values are measured.

- In the third phase the subroutine *CRT_DERIVED_TAB* calculates from a file of type YYYY_MM.csv the values of the fluxes and dose rates in the free space at 1.5 AU and saves them in a file of type YYYY_MM _derived_type.tab.

As an example the file 2021_06_derived_type.tab with the values of the fluxes (calculated for surface pressure conditions 1200 Pa and 82 Pa) and dose rates in the free space at 1.5 AU for June 2021 was submitted as an attachment to TN01.01.

The S/W for evaluation the particle flux and dose rates at free space at 1.5 AU was delivered together with TN01.01.

Analysis

The analysis of the fluxes in the free space obtained for the extreme surface pressure conditions 1200 Pa and 82 Pa shows a difference between the values for the different conditions within ± 4%. The uncertainties of the measured fluxes are ± 5%. The resulting uncertainties of the estimated fluxes in the free space at 1.5 AU are ± 10%.

The uncertainties of the measured dose rates (statistical and systematic) are ± 10% (Semkova *et al*, 2018, 2021). We assume the same differences of the dose rates in the free space obtained for the extreme surface pressure conditions 1200 Pa and 82 as for the fluxes, i.e. uncertainties ± 4%. The resulting uncertainties of the estimated dose rates in the free space at 1.5 AU are ± 15%.

As a further development the details of calculations of GCR, Mars surface and atmosphere albedo contribution and Mars shading effect on the measured fluxes in TGO Mars orbit were described in Semkova et al, 2022.

6.2.2. TN01.02. Review of Liulin-MO results during the first year of the contract

Additional reference documents for TN01.02.

1. *Koleva R., et al,* 2018. **S**olar wind modulation of galactic cosmic rays observed on board of ExoMars TGO, 2018, EPSC Abstracts, Vol. 12, EPSC2018-576
2. *Krastev K et al,* (2021).Temporal analysis of the GCR flux obtained from the Liulin instrument in orbit around Mars, Proceedings of the Thirteenth Workshop "Solar Influences on the Magnetosphere, Ionosphere and Atmosphere" September, 2021, Primorsko, Bulgaria, pp.45-49
3. *Matthiä, D., T. Berger, A. I. Mrigakshi, and G. Reitz* (2013), A ready-to-use galactic cosmic ray model, Advances in Space Research, 51, 329-338, **DOI: 10.1016/j.asr.2012.09.022**
4. *Semkova, J., et al*, (2021b). Radiation environment in the interplanetary space and Mars orbit during the declining phase of 24th and beginning of 25th solar cycles according measurements aboard ExoMars Trace Gas Orbiter, paper presented at the Thirteenth Workshop "Solar Influences on the Magnetosphere, Ionosphere and Atmosphere" September, 2021, Primorsko, Bulgaria, **http://ws-sozopol.stil.bas.bg/**
5. *Semkova, J., et al*, (2021c)Peculiarities of the radiation environment in Mars orbit in the period May 2018 – October 2021 according experimental investigations aboard ExoMars Trace Gas Orbiter, plenary paper presented at SES 2021 conference, Sofia, 20 – 22 October 2021, **http://space.bas.bg/bg/news/files/events/2021_SES_Program.pdf**
6. *Semkova, J. on behalf of FREND team*, (2021d). Observation of solar particle events in July-October 2021 according to radiation measurements on ExoMars TGO, TGO – MEX joint Science Session, Webex Teleconference, 17-18 November 2021
7. *Zeitlin, C., et al, 2*016, Solar modulation of the deep space galactic cosmic ray lineal energy spectrum measured by CRaTER, 2009–2014, Space Weather, 14, 247–258, **doi:10.1002/2015SW001314**
8. *Kozyrev et al.2022:* Observation of solar particle events from MGNS experiment onboard BepiColombo mission, HEND experiment onboard Mars Odyssey mission, and also FREND and Liulin-MO experiments onboard TGO mission during July-October 2021, EGU General Assembly 2022, Vienna, Austria, 23–27 May 2022, EGU22-11521, DOI: **10.5194/egusphere-egu22-11521**
9. *Benghin et al, 2022,* Comparison of the flux and dose rate measured by the Liulin-MO device aboard ExoMars TGO with calculated estimations, Thirteenth Moscow Solar System symposium 13m-S3 October 10-14, 2022. Space Research Institute of Russian Academy of Sciences Moscow, Russia ISBN: 978-5-00015-057-3, **doi: 10.21046/13MS3-2022**
10. *Semkova J. et al*, 2022 a, Observation of solar energetic particle events onboard ExoMars TGO in July 2021-March 2022, Proceedings of the Fourteenth Workshop "Solar Influences on the Magnetosphere, Ionosphere and Atmosphere" June, 2022, ISSN 2367-7570, ,pp. 55-60, **https://spaceclimate.bas.bg/ws-sozopol/pdf/Proceedings2022.pdf**
11. *Semkova, J. et al*,2022b, Radiation environment in Mars orbit in the period May 2018 -January 2022 according measurements aboard ExoMars TGO, 44th COSPAR Scientific Assembly, Held 16-24 July, 2022, Athens, Greece, Abstract F2.3-0014-22, **https://ui.adsabs.harvard.edu/abs/2022cosp...44.2700S/abstract**
12. *Semkova J. et al*, 2022c , Comparison of the flux measured by Liulin-MO dosimeter in ExoMars TGO science orbit with the calculations, LSSR, ISSN 2214-5524, **https://doi.org/10.1016/j.lssr.2022.08.007**
13. *Guo J et al*, 2023, The First Ground Level Enhancement Seen on Three Planetary Surfaces: Earth, Moon, and Mars, Geophysical Research Letters, 2023, *50*, e2023GL103069. **https://doi.org/10.1029/2023GL103069**, Online ISSN:1944-8007

14. *Semkova J. et al*,2023b Observation of the solar energetic particle events in Mars orbit in July 2021- March 2022, Conference of Deep Space Sciences in China, April 24-30, 2023 in Hefei, Anhui, China, **https://planet.ustc.edu.cn/icdss,** **https://planet.ustc.edu.cn/web/viewer.html?file=/attachs/file/20230411/s2.pdf**
15. *Semkova J. et al*, 2023c, Update of the science results from the radiation investigations in Mars orbit aboard ExoMars TGO in 2018-2023, Fifteenth Workshop Solar Influences on the Magnetosphere, Ionosphere and Atmosphere, 5-9 June 2023 in Primorsko, Bulgaria, 2023, Book of Abstracts, **doi: 10.31401/WSoz.2023.abs**, pp.7
16. *Koleva R et al*, Where did the solar energetic protons observed in Mars orbit come from?, Fifteenth Workshop Solar Influences on the Magnetosphere, Ionosphere and Atmosphere, 5-9 June 2023 in Primorsko, Bulgaria, 2023, Book of Abstracts, **doi: 10.31401/WSoz.2023.abs**, pp.4
17. *Liu W. et al*, Modeling the Radiation Environment of Energetic Particles at Mars Orbit and a first validation against TGO Measurements, The Astrophysical Journal, 2023 , **949-** 77, DOI: **10.3847/1538-4357/acce3c**

Liulin-MO data in TGO Mars science orbit and discussion

Particle fluxes and dose rates

The dependence of the particle fluxes and dose rates on the solar cycle development are investigated in (Semkova et al, 2021a-e). In Fig. 6.2.2.1. are plotted the sunspot numbers from 2010 to 2022 and the periods of available Liulin-MO data imposed on it.

The fluxes and dose rates recorded in the perpendicular detectors B(A) and D(C) of Liulin-MO and count rates of Oulu neutron monitor (http://cosmicrays.oulu.fi/) for the period from 1 May 2018 to 10 November 2021 are shown in Fig. 6.2.2.2. The fluxes and dose rates are calculated from hourly measurements of the corresponding energy deposition spectra and include both stopping and penetrating particles in every one of the detectors.

• An increase of the dose rates and fluxes is observed from May 2018 to February 2020 in TGO orbit which corresponds to the increase of GCR intensity during the declining of the solar activity in 24th solar cycle; The averaged dose rate for the period is 14.7/15.3 μGy h^{-1} at two perpendicular directions and the averaged particle flux is 3.09/3.19 cm^{-2} s^{-1} at two perpendicular directions.• **From March to August 2020** the measured radiation values are practically equal, corresponding to the minimum of 24th cycle and transition to 25th cycle. The **highest values of the dose rate (15.5/16.2 μGy h^{-1} at two perpendicular directions) and particle flux (3.24/3.33 cm^{-2} s^{-1} at two perpendicular directions) are registered in this period.**

• Since September 2020 a decrease of the dose rates and fluxes is observed, corresponding to the decrease of GCR intensity during the inclination phase of the 25th cycle. At the moment of writing the final report (June 2023) the dose rates and flux of GCR is about 55% of the values during the minimum of 24th solar cycle (Semkova et al, 2023c).

• A good correlation between Liulin-MO and Oulu neutron monitor measurements in periods of Mars - Earth opposition (2018, 2020) is observed.

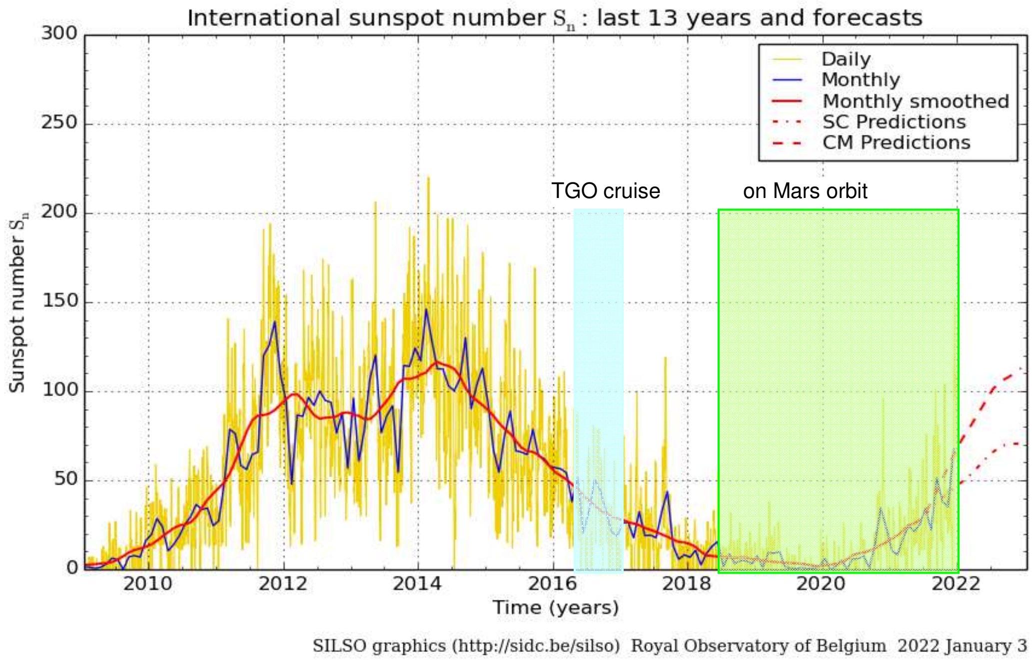

Fig. 6.2.2.1. Solar cycle development and the periods of available Liulin-MO data imposed on it.

• The sharp increases in the fluxes and dose rates in July, September and October 2021 are related to SEP registrations and will be discussed below.

The short-term modulations of GCR fluxes and dose rates have the same characteristics as those registered during TGO cruise. The latter were analysed in details in Koleva et al., 2018,

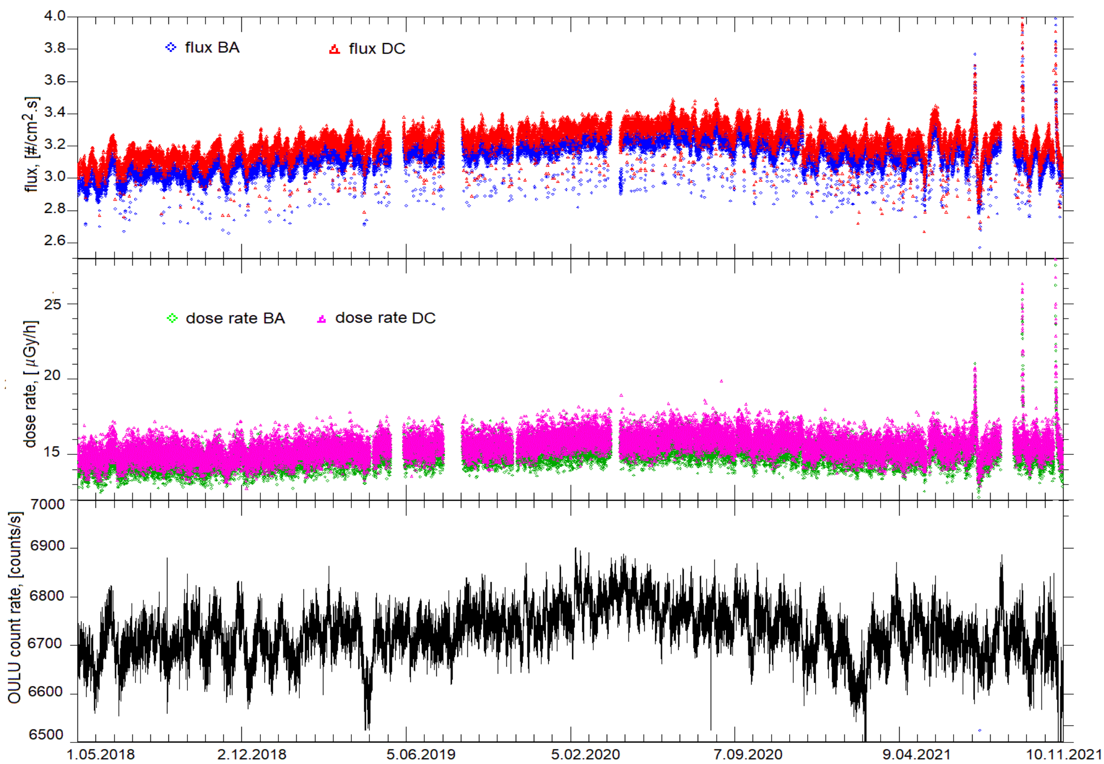

Fig. 6.2.2.2. From top to bottom: Liulin-MO particle flux, Liulin-MO dose rate, Oulu count rate in linear scale from 01.05.2018 to 10.11.2021

where it was shown that they were due to the interaction of GCR with the corotating interaction regions of the solar wind.

In Mars circular orbit the planet shades detectors' field of view (FOV), thus cutting part of GCR flux. The cut part of FOV is an angle dependent on TGO orientation and its altitude. TGO orientation can vary by 180^0 though not often and for short time interval of about 2 hours; TGO altitude varies within 50 km in every orbital pass. Most of the time TGO –Y axis is oriented along nadir and the angle between detector's axis and Mars direction is ~ 90^0. In this 'nominal' orientation the FOV shading for a single detector is about 23% (Krastev et al, 2019). The dominant part of data presented in Fig. 6.2.2.2 relate to this orientation. The narrow sharp drops of the measured flux coincide with the increases of the shading effect up to about 40% when the angle between detector's axis and Mars direction approaches zero. The absorbed dose depends insignificantly on the change of the shading.

Comparison of time profiles of particles measured by Liulin-MO and FREND neutron detectors

In our analysis we added comparison between Liulin-MO and FREND neutron detectors

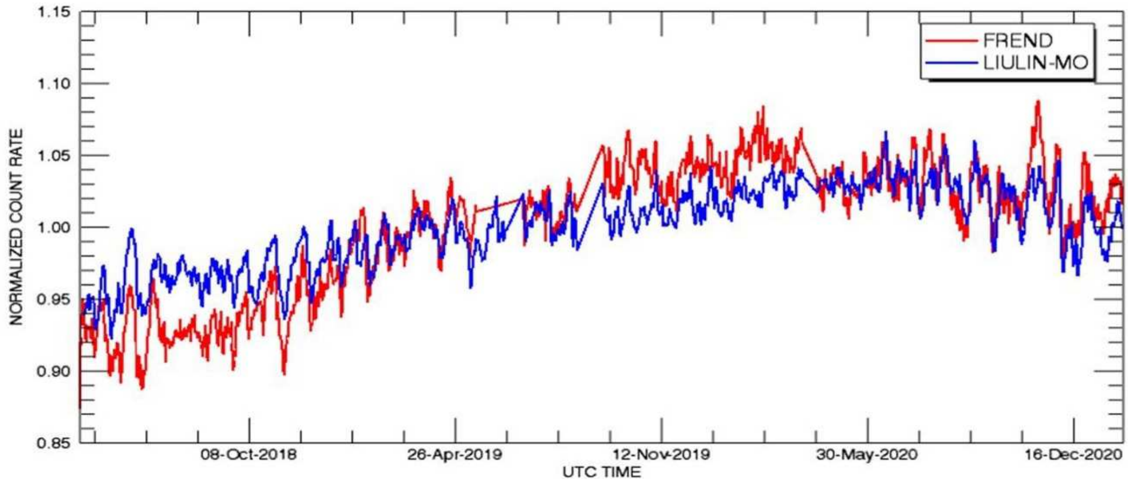

Fig. 6.2.2.3. Time profiles of GCR daily variations measured by Liulin-MO and FREND neutron detectors in May 2018 –February 2021 in Mars orbit

time profiles (Semkova et al, 2021b) taking into account that we have a possibility to compare their observations for the same period of time (May 2018 –March 2021). For simplicity we compared FREND neutron detectors signals measured in soft channels populated with charged particles.

To minimize instrumental effects and different sensitivities of these instruments we normalized all time profiles to their mean values observed between May 2018 and March, 2021 and selected time resolution equal to one Earth day. It allows us to compare relative amplitude of variations observed by different instruments on the long-term base. The results of such a comparison are presented in Fig. 6.2.2.3.

These time profiles demonstrate a good correlation on a local time scale (days) and show similar growth on long term scale (months). The difference in the amplitude of long-term variations (8-11%) might be addressed to how the solar modulation variations are visible for GCR particles with different energies.

Observation of Solar particle events in July-October 2021

In July, September and October 2021 events related to coronal mass ejections (CME) and/or flare are registered (Krastev et al, 2021, Semkova et al, 2021 c-e, 2022).

These are the only SEP events registered in Liulin-MO data till the moment of writing the TN01.02. On 17.07.2021 at 09:06 UTC started an increase in the flux and dose rate. During 20-28.07.2021 a Forbush decrease of GCR is observed (Fig. 6.2.2.4). The analysis of the energy deposition spectra shows that at least 60% of SEP forming the peak in the flux and dose rate are in the energy range 30-40 MeV. The time profile of the July 17 event shows that first Liulin-MO is hit by the accelerated at the front of the CME to high energies SEP, forming the pick in the particle flux. After several days to Mars arrives the dense solar plasma which causes the Forbush decrease of GCR. For the entire event from 16.07.2021 to 28.07.2021 a decrease of the dose rate by 0.5 μGy/h compared to quite conditions before the event is

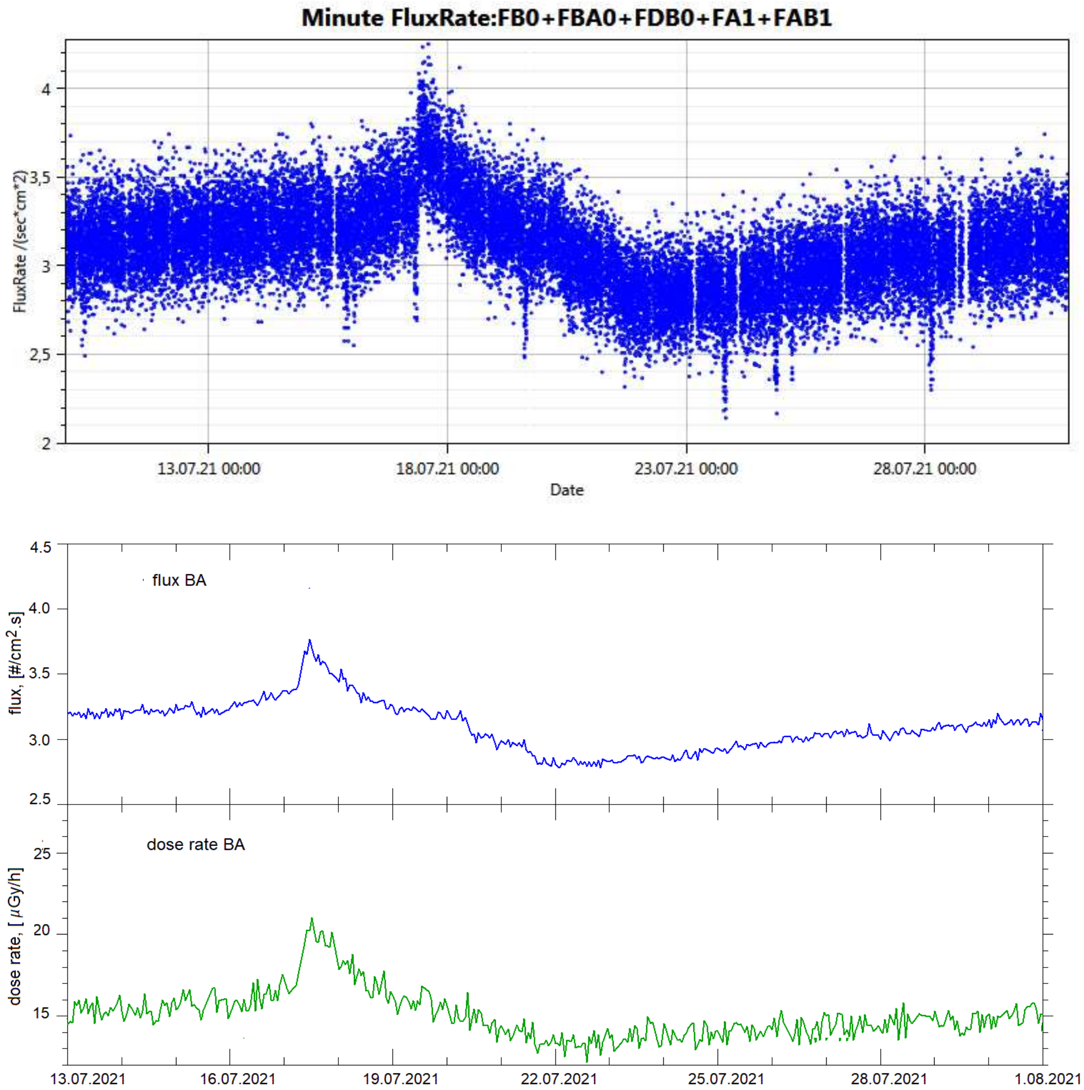

Fig. 6.2.2.4. Time profiles of the minute and hour particle flux and dose rate during the event 17-28.07.2021

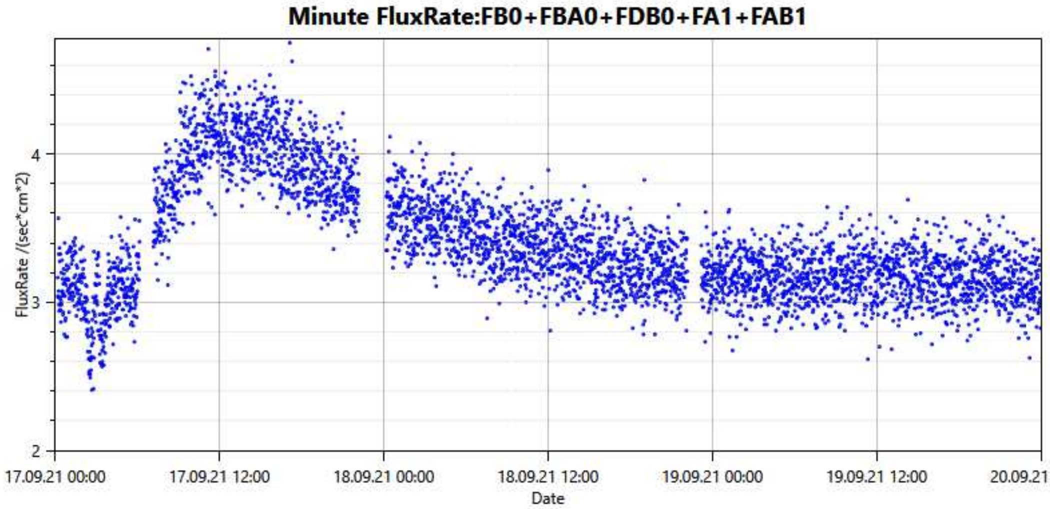

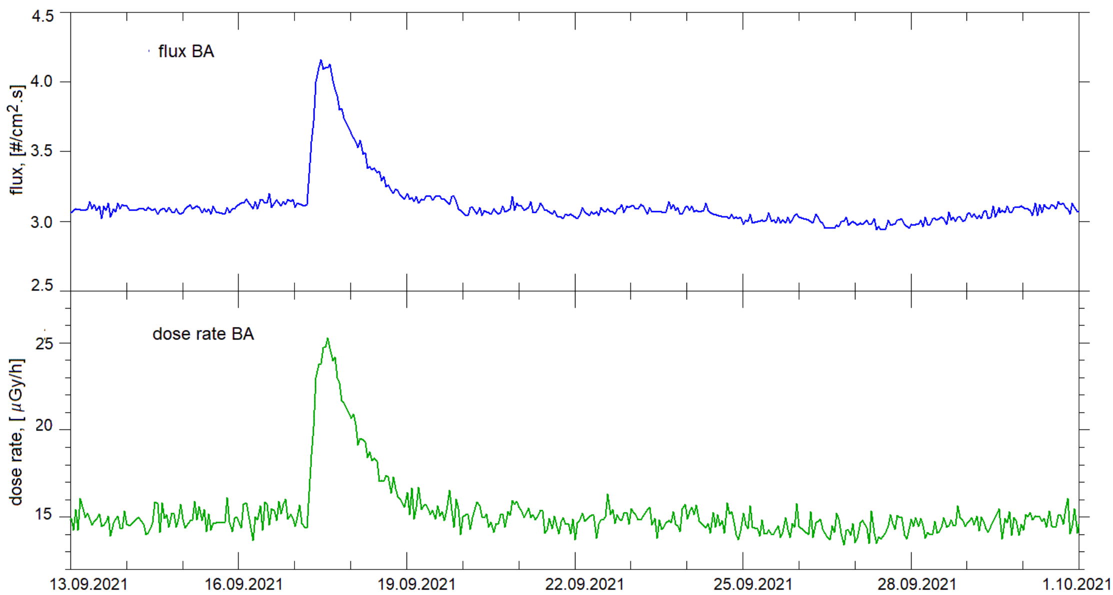

Fig. 6.2.2.5. Time profiles of the minute and hour particle flux and dose rate during the SEP event 17-18.09. 2021

On 17.09.2021 at 07:12 UTC started another increase in the flux and dose rate. The preliminary analysis shows that this event is connected to a solar flare visible from Mars, that cannot be seen by SDO or LASCO instruments in Earth orbit. The time profiles of this event are plotted in Fig. 6.2.2.5. The total dose from SEP received during 17-18.09.2021 event is 156 µGy –less than the half of daily dose from GCR.On 28.10.2021 was registered the most powerful SPE in Liulin-MO data till now. At 16:55 UTC started an increase in the flux and dose rate. The time profiles of this event are plotted in Fig. 6.2.2.6. It is possible on TGO we see the SEP accelerated at the front of the CME, well defined at 14:36 in LASCO/SOHO data (about 2H20min before registration on TGO). The CME plasma dose not reach Mars, no Forbush decrease is observed. The total dose from SEP for 28-31.10.2021 event is about 7 mGy, which is equal to the dose received from GCR for 19 days during quite conditions.

The data for SEP events on TGO in July-October 2021 contribute to the details for the solar activity at a time when Mars is on the opposite side of the Sun from Earth and are quite helpful for understanding the heliospheric space weather condition at this period. The analysis of these events and comparison with the observations of other instruments on different space missions and on Earth has been done. At TGO – MEX joint science session teleconference held 17-18 November 2021 a comparison of Liulin-MO observations of these events with simultaneous observations on MGNS-BepiColombo, HEND-Mars Odysee and FREND neutron detectors-TGO was presented. These observations have been reported at EGU 2022 General Assembly (Kozyrev et al, 2022). A paper on October 2021 SPE event as observed in Mars orbit and surface, on Moon orbit and surface and on Earth has been published by an international team with the inclusion of Liulin-MO data (Guo et al, 2023).

Later more SEP events were registered and in continuation of this work after the completion of the task they were analysed in details (Semkova et al 2022 a,b; 2023, b,c; Dachev et al, 2022; Koleva et al, 2023). The 15-19 February 2022 SEP event is the most powerful in our data. During this event the SEPs dose is equal to the dose for 38 days from

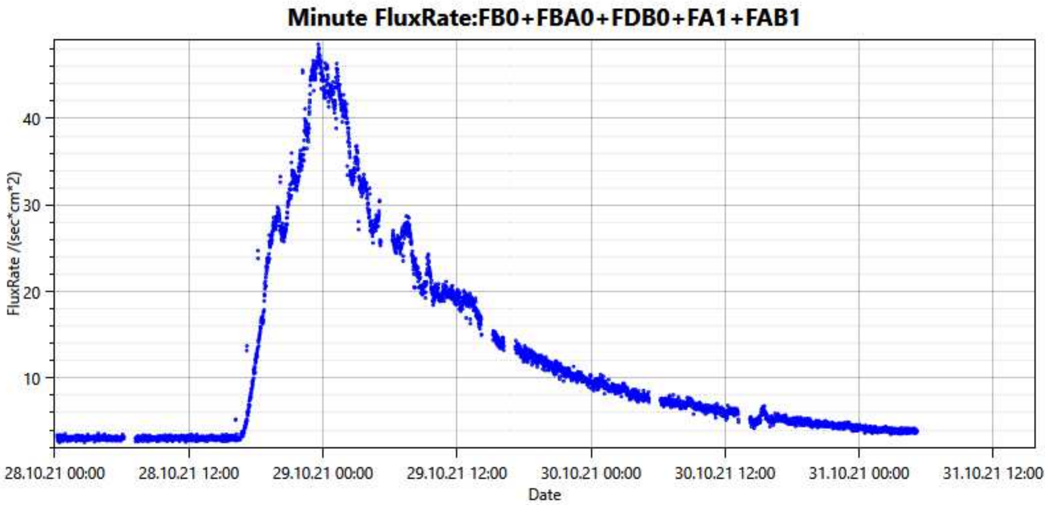

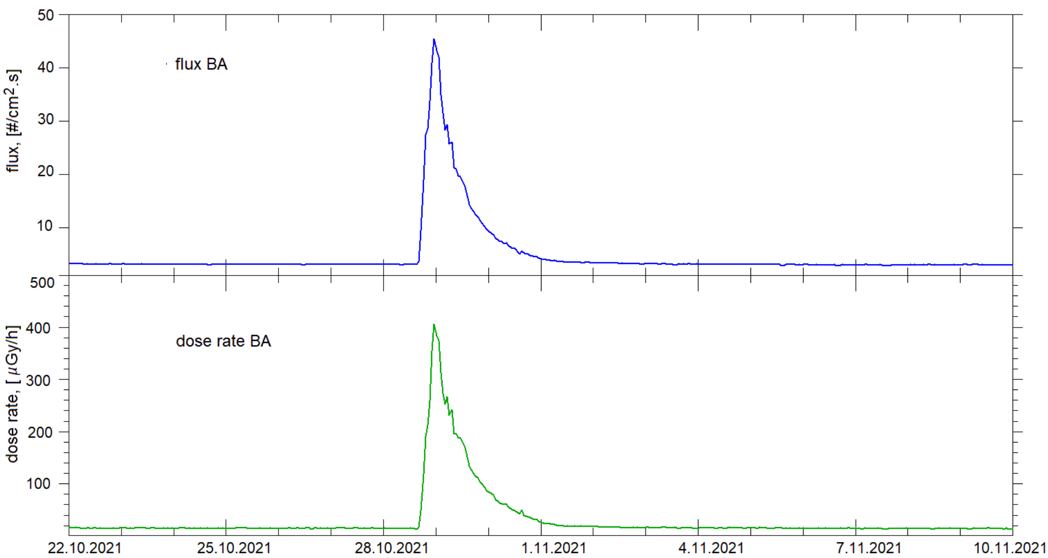

Fig. 6.2.2.6. Time profiles of the minute and hour particle flux and dose rate during the SEP event 28-31.10.2021

GCR in undisturbed conditions, the biologically significant dose equivalent from SEPs is equal to the dose equivalent for 13 days from GCR in undisturbed conditions. The doses from 28-31 October 2021 SEP event are about 2 times less.***Comparison of measured parameters with model results***One of the scientific objectives of Liulin-MO experiment is to provide data for verification and benchmarking of the radiation environment models. Models of GCR describe their spectra and intensity in free space, away from any celestial body.

We have compared with model results Liulin-MO measurements during the transit to Mars and on the high elliptic orbit MCO1 (Semkova et al, 2021 a, c).

Simulations of dose rate were carried out with OLTARIS simulation tool (**https://oltaris.larc.nasa.gov/**). As an input the GCR model of Matthia et al., 2013 was used and distribution of matter along the direction of penetrating radiation. A radiations shield thickness metafile for detector B(A) based on Liulin-MO detectors' shielding model and the example of a 969 rays thickness distribution metafile available on OLTARIS site was created. With these assumptions the parameters which are expected to be measured by detector B(A) were calculated. A comparison between the simulations and measurements of the dose rate and flux during the TGO transit to Mars from May to September 2019 and in high elliptic Mars orbit in November-December 2016 is presented in Fig. 6.2.2.7. At high elliptic Mars orbit since 01 November 2016 only the data from measurements at distances higher than 1500 km from Mars surface, i.e. the measurements in free space were taken into account in this comparison.

The obtained results show that **during the TGO transit to Mars the measured dose rate behind the shielding of the detectors of Liulin-MO is about 25% higher than the simulated values. The measured flux is about 40% higher than the simulated one.** The simulation results are preliminary, the discrepancy needs further clarification of the input settings and probably testing of another GCR models.

To compare Liulin-MO data measured on Mars circular orbit (400 km altitude) with models they should be extrapolated to deep space, i.e. corrected for the presence of Mars - shading of the GCR flux from Mars and the contribution of albedo particles from Mars atmosphere and surface. While the effect from Mars shading is easy to calculate the effect of albedo particles at 400 km height, above the atmosphere, is much more complicated. Recently we have

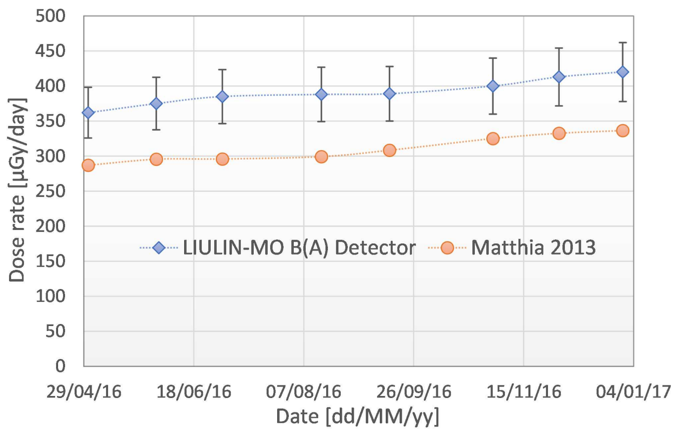

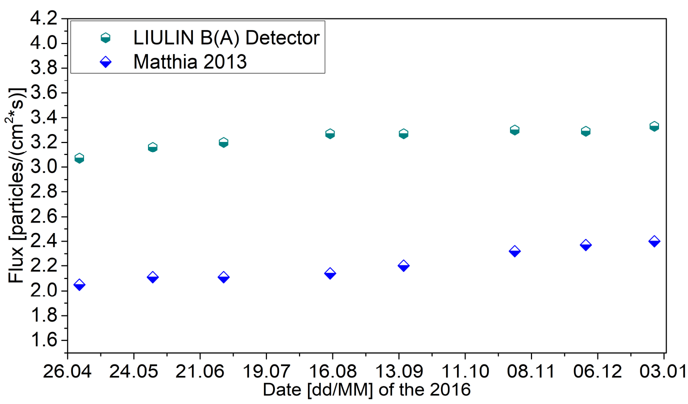

Fig. 6.2.2.7. Comparison between the daily dose rates and flux measured by Liulin-MO detector B(A) and the simulated dose rates and flux

made some additional evaluation of the albedo (see TN01.01), which will be used for extrapolation of the existing Lulin-MO orbital data to deep space and more accurate comparison with GCR models.

As a further development of this research we have compared with model results Liulin-MO measurements in TGO Mars science orbit (Benghin et al, 2022, Semkova et al, 2022c, Liu et al, 2023). The obtained results show that the measured dose rate and flux behind the shielding of the detectors of Liulin-MO are higher than the simulated values. The reasons for that are the secondary particles, anomalous cosmic rays and the gradient of GCR spectrum from 1 AU to 1.5 AU which are not included in the models. Accounting for these differences, the calculated flux and dose rate may increase to match the measurement results. The results can serve for the benchmarking of GCRs models**.**

Worsening of the radiation conditions in interplanetary space

One of the science objectives of Liulin-MO is together with the neutron detectors of FREND to provide data for verification and benchmarking of the radiation environment models and assessment of the radiation risk to the crewmembers of future exploratory flights.

To achieve this objective Liulin-MO data measured on Mars circular orbit (400 km altitude) should be extrapolated to deep space, i.e. corrected for the shading of the detectors and for the presence of Mars (shading of the GCR flux from Mars and the contribution of albedo particles from Mars atmosphere and surface).

To estimate the contribution of the albedo particles is a rather complicated problem as theoretically it can depend except on the incident primary GCR flux also on the season, the relief, on soil composition, atmospheric composition, etc. At a zero approximation we evaluated the albedo contribution to be in the range of 6% to 11% (Semkova et al, 2021 a). This has been confirmed from recent evaluations of the albedo contributions (see TN01.01).

We assume that in Mars orbit the flux is 0.88 of the flux in deep space and the dose rate is 0.82 from that in deep space. The above coefficients account both for the shading from Mars and for albedo contributions. Under this assumption the cosmic ray fluxes and doses measured in Mars orbit are recalculated into values meaningful for the deep interplanetary space at about 1.5 AU.

The results show that the radiation conditions in the interplanetary space worsen in the minimum of the solar activity in 24th solar cycle (Semkova et al, 2021b). With respect to the values measured during TGO transit to Mars in April-September 2016 (Semkova et al, 2018), in August 2020 the particle flux has increased at least by 17.9% (to 3.68 $cm^{-2} \cdot s^{-1}$) and the dose rate – by 21.9% (to 19 $\mu Gy \cdot h^{-1}$).

The dose rate in free space in 24th cycle minimum (at least 19 $\mu Gy \cdot h^{-1}$) is significantly higher the dose rate of 13.25 $\mu Gy \cdot h^{-1}$ measured during the previous 23rd solar minimum in 2009/2010 by CRaTER instrument on LRO (Zeitlin, C., et al., 2016). This demonstrates the peculiarities of the passed 24th solar cycle.

Conclusion

The experimental data and obtained results for the radiation environment conditions in Mars' orbit and in the interplanetary space during the declining and minimum of 24th solar cycle and beginning of 25th cycle may be helpful for benchmarking of the GCR models, understanding the heliospheric space weather condition, assessing the radiation risk for human and robotic missions and for planning the future manned missions to Mars.

6.2.3. TN01.03 Review of the results from the comparison with SREM fluxes on Rosetta mission

Additional reference documents for TN01.03.

1. *Evans, H. D. R., Bühler, P., Hajdas, W., Daly, E. J., Nieminen, P., and Mohammadzadeh, A.* Results from the ESA SREM monitors and comparison with existing radiation belt models, Adv. Space Res., 42, 1527–1537, 2008.
2. *Geiseler et al. 2008.* The radial gradient of galactic cosmic rays: Ulysses KET and ACE CRIS Measurements. International Cosmic Ray Conference 1, 571–574)
3. *Geisler and Heber,* 2016. Spatial gradients of GCR protons in the inner heliosphere derived from Ulysses COSPIN/KET and PAMELA measurements, Astronomy and Astrophysics 589, DOI: 10.1051/0004-6361/201527972.
4. *GOST 25645.204-83.* The method of calculating the shielding of points inside the phantom. Gosstandart, Moscow, 1983
5. *Honig, T., Witasse, O.G., Evans, H., Nieminen, P., Kuulkers, E., Taylor, M.G., Heber, B., Guo, J. and Sánchez-Cano*, B., 2019, September. Multi-point galactic cosmic ray measurements between 1 and 4.5 AU over a full solar cycle. Annales Geophysicae, 37, No. 5, 903-918.
6. *Potgieter, M. S.* 2013. Solar modulation of cosmic rays. Living Reviews in Solar Physics, 10, 3

Review of the results from the comparison with SREM fluxes on Rosetta mission

SREM description

The Standard Radiation Environment Monitor (SREM) is a simple particle detector developed for wide application on ESA satellites. It measures high-energy protons and electrons of the space environment with a 20-degree angular resolution and limited spectral information.

The SREM consists of three detectors (D1, D2, and D3) in two detector head configurations. One system is a single silicon diode detector (D3). The main entrance of the D3 window is covered with 0.7 mm aluminum, which defines the lower energy threshold for electrons to -0.5 MeV and for protons to -10 MeV. The other system uses two silicon diodes (detectors D1/D2) arranged in a telescope configuration. The main entrance of this detector is covered with 2 mm aluminum giving a proton and electron threshold of 20 and 1.5 MeV, respectively. A 1.7-mm-thick aluminum and 0.7 mm thick tantalum layer separate the two diodes of the telescope configuration. The telescope detector allows measurement of the high-energy proton fluxes with enhanced energy resolution. In addition, the shielding between the two diodes in the telescope prevents the passage of electrons. However, protons with energies greater than 43 MeV go through. Thus, using the two diodes in coincidence gives pure proton count rates allowing subtraction of the proton contribution from the electron channels.

Fig. 6.2.3.1. Picture of SREM flight model.

The SREM is mounted in a single box of 20x12n10 cm3 and weighs 2.6 kg, see Fig. 6.2.3.1. The box contains the detector systems with the analog and digital front-end electronics, a power supply, and a TTC-B-01 Telemetry and Telecommand interface protocol. A total of 15 discriminator levels are available to bin the energy of the detected events. Any two of the levels can be used to raise an alarm flag when the count rates exceed a programmable threshold. This alarm signal can then be used to control the operation of the spacecraft and its instruments. The detector electronics is capable of processing a detection rate of 100 kHz with dead-time correction below 20%.

In addition to 15 energy bins, three counters are assigned to detector one to three dead-time correction values, respectively. Table 6.2.3.1 lists all SREM counters. As explained earlier, the D1/D2 configuration measures protons from approximately 20 MeV to infinity. Events detected by this configuration are divided into 10 bins, (including four proton coincidence bins) and 1 heavy ion bin. SREM is incapable of discriminating between various heavy ion particle types and identifies particles as heavy ions, in one bin only, if their deposited energy in D2 is higher than 9 MeV. The D3 sensor is sensitive to electrons with energies from 0.5 MeV, and is also sensitive to protons, requiring that a deconvolution procedure must be applied to obtain particle spectra in mixed environments (Evans et al., 2008).

Table 6.2.3.1

List of the SREM counters and the corresponding energy ranges of protons and electrons detected (Evans et al., 2008).

Bin	Logic	Discriminator level	Proton energy (MeV)			Electron energy (MeV)		
		$\Delta E >$ XX (MeV)	Min (MeV)	Max (MeV)	SCF [#/cm^2]	Min (MeV)	Max (MeV)	SCF (#/cm^2)
TC1	D1	0.085	27	∞	15.8	2.0	∞	118
S12	D1	0.25	26	∞	19.0	2.08	∞	195
S13	D1	0.6	27	∞	16.0	2.23	∞	519
S14	D1	2.0	24	542	38.5	3.2	∞	25403
S15	D1	3.0	23	434	65.6	8.18	∞	5460
TC2	D2	0.085	49	∞	13.1	2.8	∞	191
S25	D2	9.0	48	270	208.8	n/a	n/a	
C1	D1 × D2	0.6, 2.0	43	86	107.22	n/a	n/a	
C2	D1 × D2	0.6, 1.1–2.0	52	278	75.6	n/a	n/a	
C3	D1 × D2	0.6, 0.6–1.1	76	450	35.1	n/a	n/a	
C4	D1 × D2	0.085–0.6, 0.085–0.6	164	∞	10.4	8.10	∞	155
TC3	D3	0.085	12	∞	49.3	0.8	∞	101
S32	D3	0.25	12	∞	49.3	0.75	∞	189
S33	D3	0.75	12	∞	40.2	1.05	∞	1162
S34	D3	2.0	12	∞	63.8	2.08	∞	93077

Data used

In this work we present a review of the results from the comparison of Liulin-MO fluxes on ExoMars TGO mission with SREM count rates on Rosetta mission obtained in the period April - September 2016.

Liulin-MO data

From Liulin-MO measurements we use the data for the minute particle fluxes provided by single detector B(A) (omnidirectional) in the energy deposition range > 0.08 MeV. All events with energy deposition > 190 MeV are registered and are considered as events with 190 MeV energy deposition in the measured fluxes. The geometry factor of a single detector is ~ 12.56 cm^2 sr.

The data from measurements of Liulun-MO fluxes presented below must be understood in the context of the shielding from the free-space radiation environment provided by the mass of materials surrounding the instrument's detectors. A model of Liulin-MO shielding was created on basis of the Russian standard GOST 25645.204-83 (GOST, 1983), using the documentation of the FREND instrument and data for TGO spacecraft obtained from http://spaceflight101.com/exomars/trace-gas-orbiter-instruments and http://sci-lib.com/article1181.html. Using this model the shielding distribution probability density was calculated (Semkova et al., 2018, 2021). It was estimated that there are no significant differences in the shielding caused by the dosimeter itself plus the rest of FREND modules and

TGO materials to any of the four Liulin-MO detectors. Representative for the shielding of Liulin-MO detectors is the central point between the detectors located at equal distances from the detectors. The first momentums of the shielding distribution probability density is about 20 g cm^{-2} (see Fig. 4b in Semkova et al, 2021). The shielding values are assumed to be aluminum-equivalent, the actual shielding consists of several different materials. The energy threshold for the minimum shielding is 1.7 MeV for electrons, 30 MeV for protons and 6.8 GeV for iron ions.

The measurements of Liulin-MO used are conducted during the ExoMars TGO cruise to Mars from about 1.1 AU to about 1.4 AU.

On April 22, 2016 Liulin-MO was turned on. The monitoring was terminated for short periods of the Mid-Cruise Checkout and for the Deep Space Maneuver performed between July 18 – August 11, 2016. Since August 11, 2016 till September 15, 2016 Liulin-MO was turned on periodically. After September 15, 2016 Liulin-MO was turned off during the maneuvers for Mars orbit insertion and EDM release. In April –September 2016 Liulin-MO gathered a good statistic of measurements of galactic cosmic rays (GCR) in free space. No solar energetic particle events were observed during this period.

The data by Liulin-MO used in this work are available at the "Unified web-based database with Liulin-type instruments" (**http://esa-pro.space.bas.bg/LIULIN_MO**) created under ESA Contract under the PECS No. 4000117692/16/NL/NDe.

SREM data

Used are the SREM data from counter TC1 which proton and electron energy ranges, respectively ≥27 MeV and ≥2 MeV (Evans et al, 2008) are closest to the proton ≥30 MeV and electron ≥ 1.7 MeV ranges of Liulin-MO. The discriminator level of 0.085 MeV of TC1 is also close to that of Liulin-MO, which is 0.080 MeV. For the completeness of the comparison with Liulin-MO flux are used also count rates of S32 SREM counter sensitive to low-energy protons, with the sensitivity to electrons, and SREM counter S14 mainly sensitive to protons (Honig et al. 2019).

According to Fig. 4 panel (b) of Honig et al. (2019) in the period April-September 2016 Rosetta spacecraft is flying on the surface of the comet at a distance between 2.8 and 3.7 AU.

The SREM data are downloaded from http://srem.psi.ch/html/rosetta_summaryplots.shtml (plots) and ESA Planetary Space Archive (PSA) at https://archives.esac.esa.int/psa/, https://archives.esac.esa.int/psa/#!Table%20View/SREM=instrument.

The Oulu neutron monitor data are downloaded from http://cosmicrays.oulu.fi.

The sunspot number data are downloaded from https://www.swpc.noaa.gov/products/solar-cycle-progression

Comparison of data obtained by SREM on Rosetta and Liulin-MO on ExoMars TGO

The method used for obtaining the correlation between SREM and Liulin-MO data sets contains the following steps:

1. Comparison of the count rates of SREM counters and Liulin-MO flux with the data for the solar activity for the period April-September 2016, represented by the sunspot numbers and Oulu Neutron monitor (NM) count rates.

2. Comparison of the average monthly values of 3 SREM counters on Rosetta with Liulin-MO flux rate in the same period April – September 2016.

Comparison with summary plots for the SREM on Rosetta count rates from S14 and S32 counters

On the site **http://srem.psi.ch/html/rosetta_summaryplots.shtml** we found 6 graphics for the period April-September 2016. In the LEGEND there we found is the following:

Legend

The Rosetta/SREM summary plots show the time course of the two SREM counters TC3 and S14. Counter TC3 is sensitive to highly energetic protons and electrons and counter S14 is mainly sensitive to protons. The background level is caused by cosmic rays and is normally around 2 c/sec in TC3 and 0.2 c/sec in S14.

In fact, in the summary plots at the above site the time course of S32 and S14 counters are plotted.

Fig. 6.2.3.3. shows the first graphic with a comparison for April 2016. In the figure together the SREM S14 (red markers) and S32 (blue markers) counters and the Liulin-MO flux (black markers) are seen. On the vertical axes the two SREM counters in (counts/sec) and the Liulin-MO flux in (cm^{-2} s^{-1}) are plotted. On the horizontal axes the date from 1st of April to 1st of May 2016 is plotted. It is seen that all three parameters have very similar behaviors with slowly variations around fixed values, which are a result of measurements under quiet solar conditions of the galactic cosmic rays (GCR) radiation source.

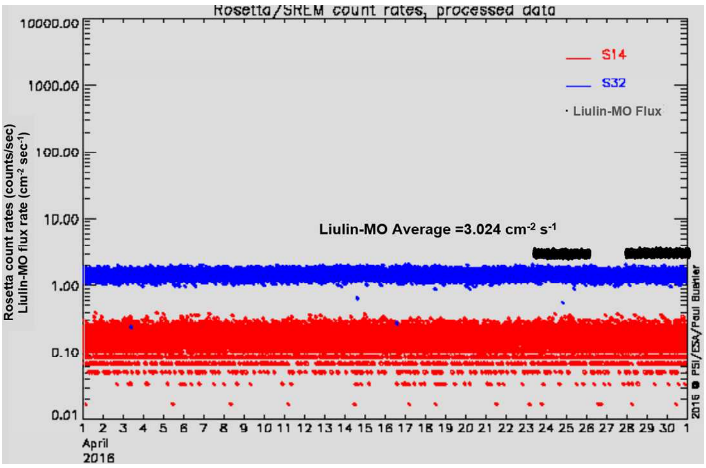

Fig. 6.2.3.3. Comparison of data between SREM and Liulin-MO instruments for April 2016

Figures 6.2.3.4- 6.2.3.8 present the results of SREM-Liulin-MO comparisons for the months May to September 2016.

Figure 6.2.3.9 summarizes all figures 6.2.3.4- 6.2.3.8 for the period 20 April-17 September 2016. The plotted parameters are the same as in figures 6.2.3.3-6.2.3.8. A linear trendline on the Liulin-MO flux data with a formula seen in the right upper corner of Fig. 6.2.3.9 is added. The small positive coefficient of 0.0007 in front of the linear term of the equation confirms the linear anti correlation of the Liulin-MO flux from the monthly smoothed solar sunspot number (**https://www.swpc.noaa.gov/products/solar-cycle-progression**) shown with magenta line and points.

Except the dependence from the sunspot numbers another shorter-term variations are seen in the SREM and Liulin-MO data. To reveal this dependence we prepare Fig. 6.2.3.10.

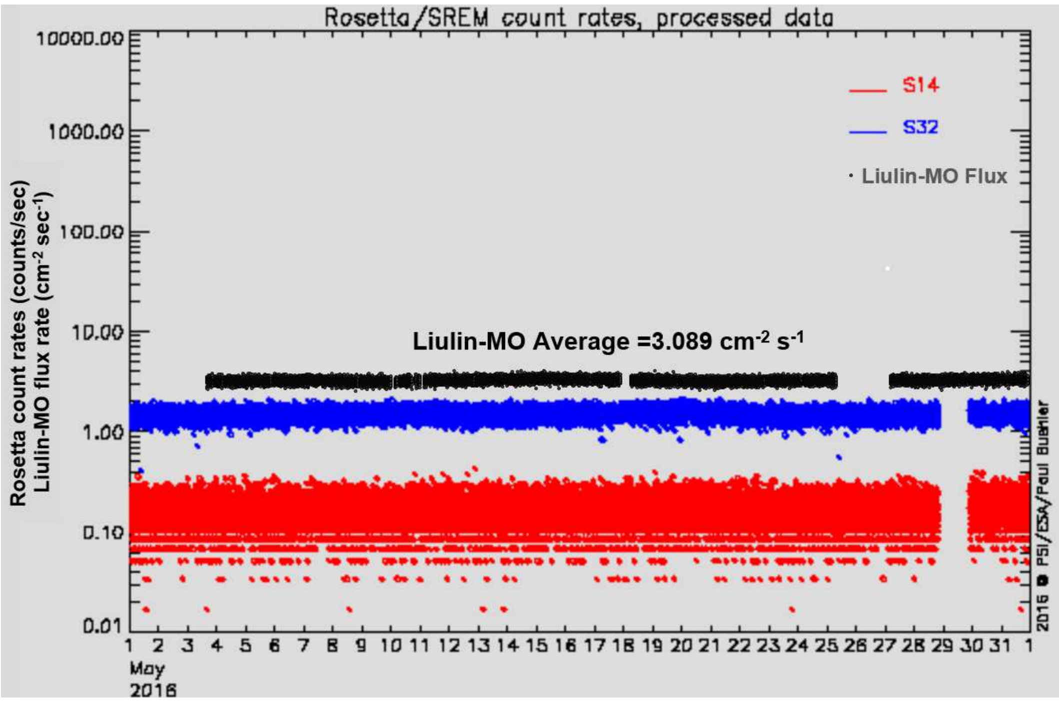

Fig.6.2.3.4. Comparison of data between SREM and Liulin-MO instruments for May 2016.

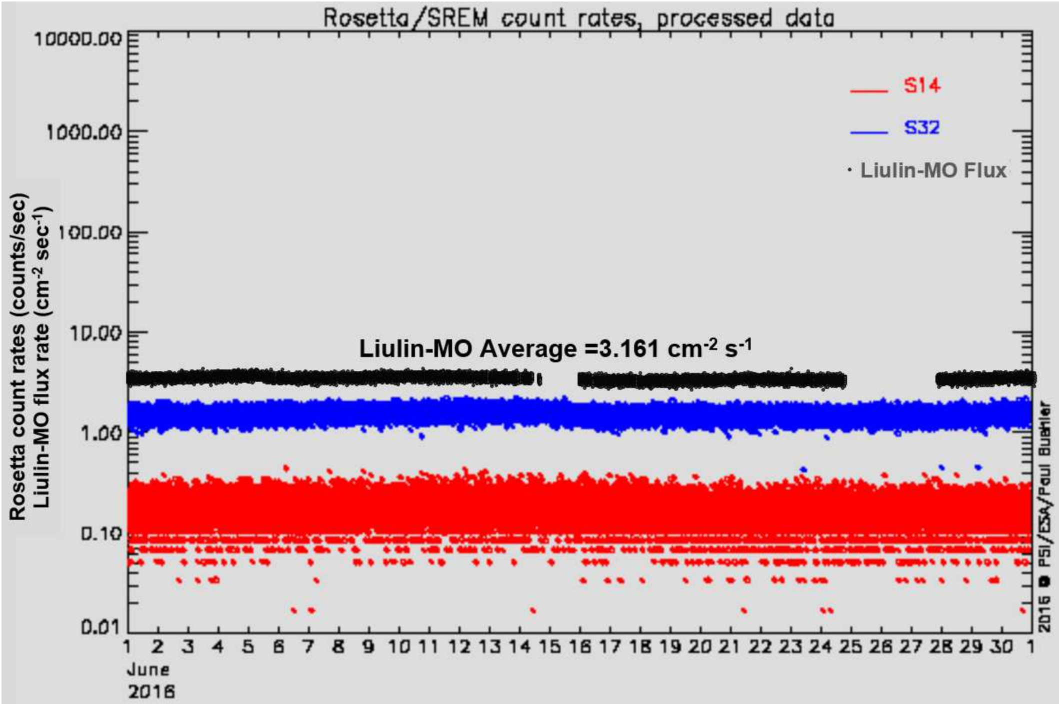

Fig.6.2.3.5. Comparison of data between SREM and Liulin-MO instruments for June2016.

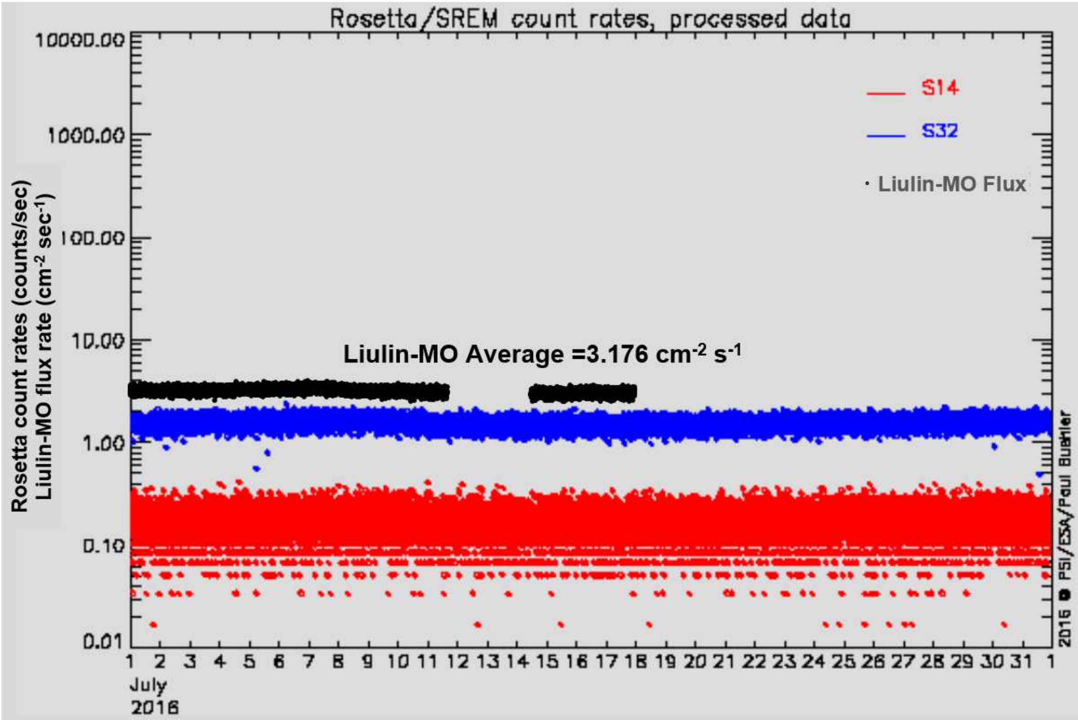

Fig.6.2.3.6. Comparison of data between SREM and Liulin-MO instruments for July2016.

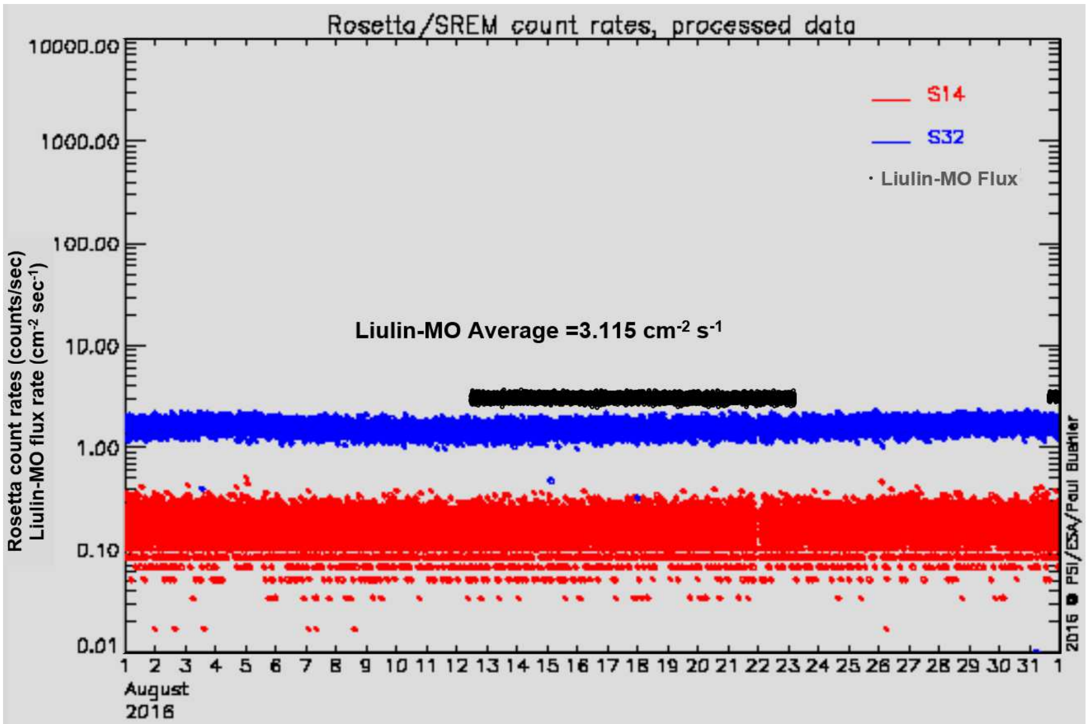

Fig.6.2.3.7. Comparison of data between SREM and Liulin-MO instruments for August 2016.

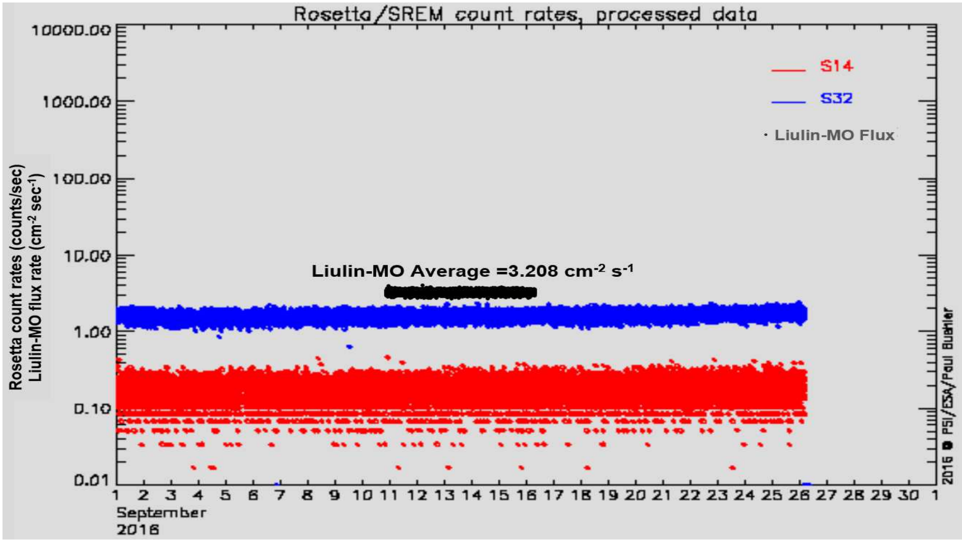

Fig.6.2.3.8. Comparison of data between SREM and Liulin-MO instruments for September 2016.

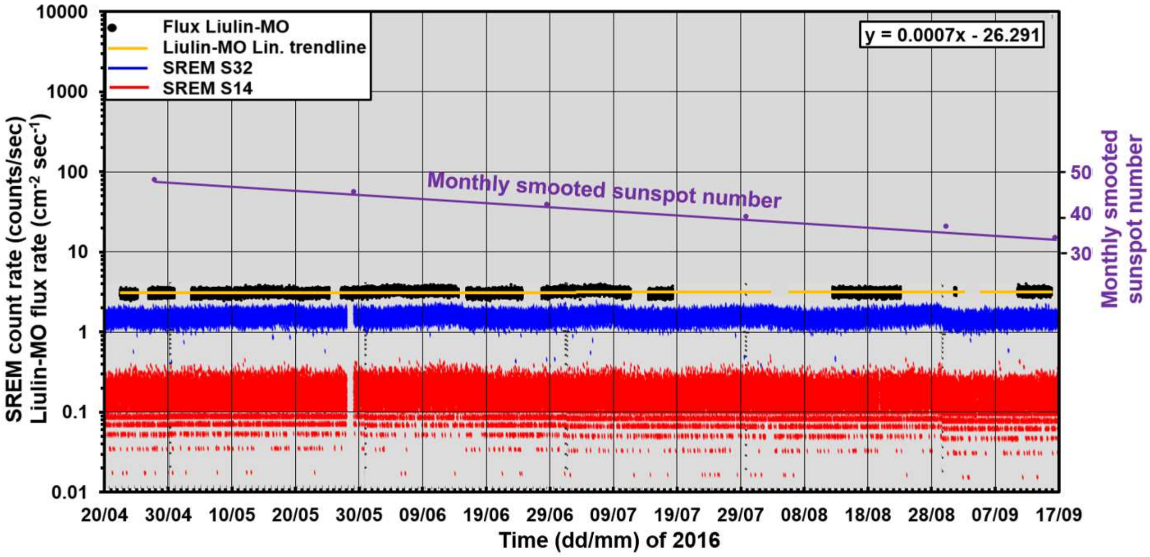

Fig.6.2.3.9. Comparison of data between SREM and Liulin-MO instruments for the period April-September 2016. The instruments data are compared with the graphics of the monthly smoothed sunspot number also.

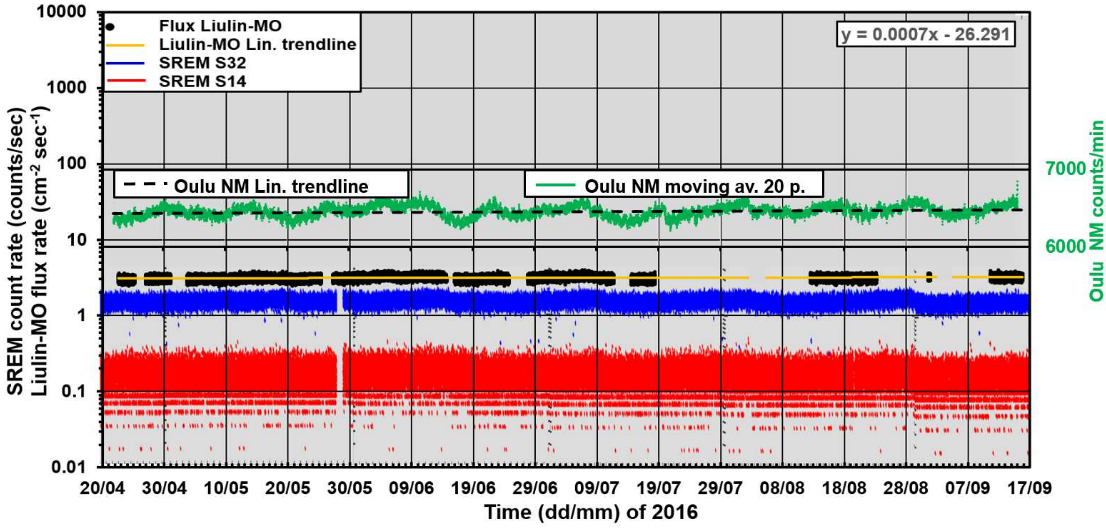

Fig.6.2.3.10. Comparison of data between SREM and Liulin-MO instruments for the period April-September 2016. The instruments data are compared with the graphics (green line) of the Oulu NM count rate.

In Fig.6.2.3.10 except the instruments' data, the variations of the Oulu Neutron monitor counts rate (https://cosmicrays.oulu.fi/) are plotted with green line. The Oulu NM linear trend line with equation y=0.3297x-7474.6 also shows positive raising count rate in accordance with Liulin-MO positive flux rate.

For better understanding of the correlation between the Liulin-MO flux and Oulu NM counts rate we prepare Fig. 6.2.3.11. Two parameters are plotted - Liulin-MO minute flux rate with black points and Oulu NM hourly counts rate. Good correlation between the two parameters is observed.

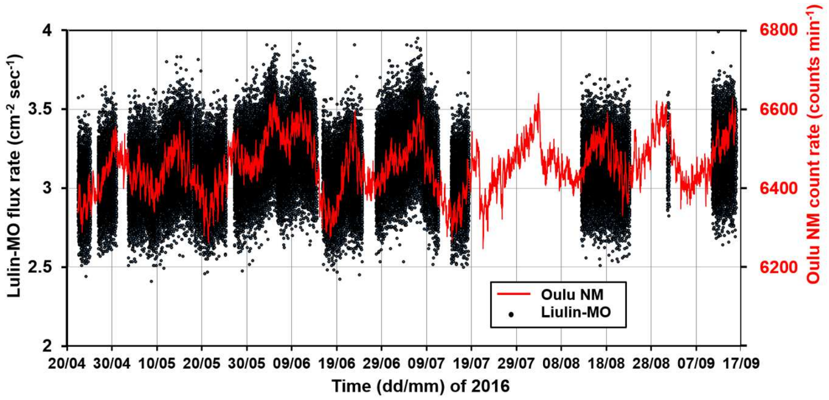

Fig.6.2.3.11. Comparison of data between Liulin-MO flux rate and Oulu NM count rate.

Comparison of numeric values of SREM count rates from TC1, S14 and S32 counters with Liulin-MO flux rate

Fig 6.2.3.12 presents graphics of the numeric data from the following parameters: SREM TC1 couther with 160-s resolution, SREM S12 couther with 160-s resolution, SREM S32 couther with 160-s resolution, Liulin-MO flux with 60-s resolution, Oulu NM counts with 1-hour resolution. Linear trendlines from Liulin-MO flux, SREM TC1 and Oulu NM are also shown.

The analysis of Fig. 6.2.3.12 reveals the following:

1) A long-term enhancement of all parameters is observed. This is in response of the falling trend of the solar activity in 2016 toward the solar cycle 24 minimum in 2019. The SREM parameters rising trends in 2016 were shown by Honig et al. (2019) The Liulin-MO parameters rising trends in 2016 were revealed by Semkova et al. (2018), pls. see Fig 8 therein.

2) The linear rising trends of Liulin-MO flux, SREM TC1 counter and Oulu MN count rate anti correlate with the solar activity because during the periods of low solar activity larger amount of GCR particles penetrate in the Solar system in conditions of a smaller solar wind and embedded magnetic field (Potgieter, 2013).

3) All measured parameters from SREM and Liulin-MO instruments follow relatively well the shorter-term variations of the GCR flux, monitored by Oulu NM.

The comparison of the count rates of SREM counters and Liulin-MO flux with the data for the solar activity for the period April-September 2016, represented by the sunspot numbers and Oulu NM count rates reveals enhancement of both SREM counts and Liulin-MO flux in response of the falling trend of the solar activity in this period and increase of GCR intensity.

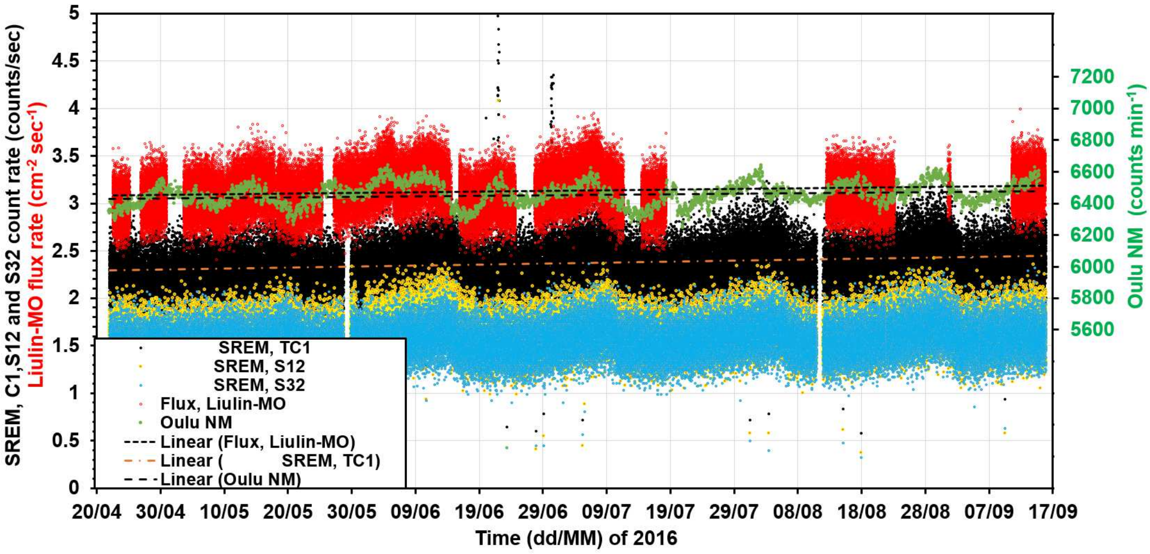

Fig.6.2.3.12. Comparison of numeric data between SREM and Liulin-MO instruments for the period April-September 2016. The instruments data are compared with the graphics (green line) of the Oulu NM counts rate

<u>Comparison of the average monthly values of SREM count rates from TC1, S14 and S32 counters with Liulin-MO flux rate in April – September 2016</u>

We are unable to make a real inter-calibration between the SREM and Liulin-MO data because at the time of the simultaneous measurements of both instruments Rosetta and ExoMars TGO are at very different heliocentric distances. The inter-calibration is not a subject of TN01.03.

A cross-calibration trough other SREM instruments (like in Honig et al, 2019) on other missions, operating at about 1 AU (Proba-1 and INTEGRAL) in April – September 2016 and examination of the radial gradient of cosmic rays may be a subject of a future investigation.

Nevertheless in Table 6.2.3.2 and Fig. 6.2.3.13 are compared the average monthly values of the SREM count rates from TC1, S14 and S32 counters with Liulin-MO flux for the time of simultaneous measurements of both instruments in April – September 2016. In the figure the linear approximations of the dependences between the average values measured by both instruments are also shown.

A good correlation between SREM and Liulin-MO data sets is observed, particularly between Liulin-MO flux and TC1 count rate.

In September 2016 we observe about 6.1 % increase of the Liulin-MO flux in comparison to the flux measured in April 2016. In September 2016 observed is about 6.25 %-7.1 % increase of the TC1, S32, S12 SREM counts in comparison to the counts measured in April 2016. The increase in Liulin-MO flux and SREM count rates is due to the decrease of the solar activity and the radial gradient of GCR. During the analyzed period TGO increased its radial distance from 1.1 to 1.4 AU, Rosseta - from 2.8 to 3.7 AU.

In the obtained results we did no extrapolation about GCR propagation, the radial gradient of CGR is not a resolved problem yet (please note that investigation of the gradient of CGR is not a direct subject of TN01.03).

- In Geiseler et al. 2008, during the 23rd solar cycle the radial gradient of GCR in the inner heliosphere was evaluated to be 4.5±0.6%/AU, assuming it was the same during 1998 - 2004. If this figure is applicable for the 24th solar cycle, then ~ 1.7% of Liulin-MO flux increase and

~ 4.05-4.6% of TC1, S32, S12 SREM counts increase could be due to the increase of the radial distances. This would give ~ 4.4 % increase of Liulin-MO flux and ~ 2.2 - 1.6% increase in TC1 count rate due to decrease of solar activity;

Table 6.2.3.2.

Average monthly values of the SREM count rates from TC1, S14 and S32 counters with Liulin-MO flux rate for April – September 2016.

Date	Liulin-MO	S12	S32	TC1
30/04/2016 00:00:00	3.024	1.543	1.472	2.24
30/05/2016 00:00:00	3.089	1.585	1.501	2.28
30/06/2016 00:00:00	3.177	1.664	1.534	2.48
30/07/2016 00:00:00	3.173	1.635	1.562	2.36
30/08/2016 00:00:00	3.115	1.673	1.591	2.31
15/09/2016 00:00:00	3.209	1.652	1.573	2.38

- In Honig et al, 2019 the radial gradient for the period 21 October 2004 -21 May 2011 is evaluated to be 2.96%±0.12%/AU. In this case ~ 0.95 - 1.2% of Liulin-MO increase and ~2.5 - 2.8% of TC1 increase due to radial gradient. Correspondingly the increase due to decrease of solar activity would give ~ 4.9 - 5.16% for Liulin-MO and ~ 3.45 - 3.75% for TC1.

These results are quite controversial (regarding the relation of the contribution of the solar activity and heliocentric distance to the observed in both data sets increase of GCR count rate in the period April-September 2016). The evaluations demonstrate that the problem of GCR is complicated. According Honig et al, 2019 during the comet phase from early 2014 to September 2016, the radial gradient changed, equivalent to an overall 8% attenuation in the count rate of GCR, which is unexpected and unexplained. Geisler and Heber, 2016 showed that the radial gradient depends on protons energy.

Nevertheless the results from comparison of Liulin-MO on TGO and SREM-Rosetta data sets provide confirmation of the modulation of galactic cosmic rays (at different locations in the inner heliosphere) with respect to solar activity, which was our hypothesis as well as they provide some useful insights into the behaviour of the galactic cosmic ray propagation within the inner heliosphere.

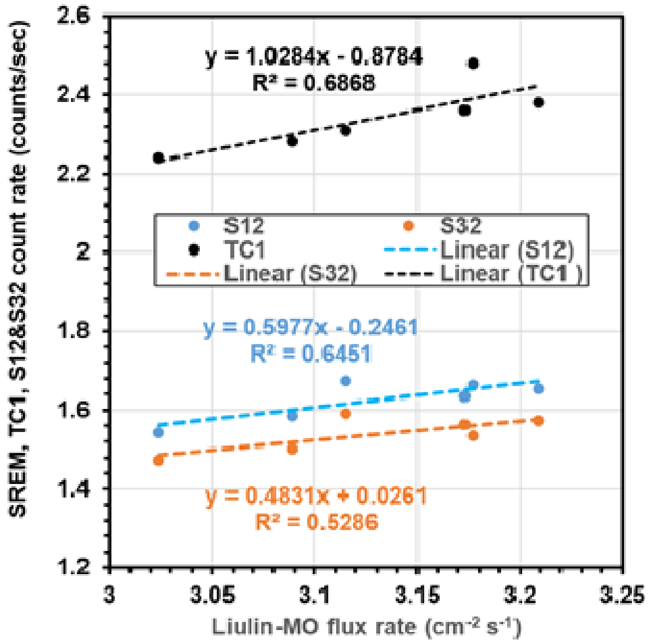

Fig.6.2.3.13. Comparison between the Average monthly values of SREM count rates from TC1, S14 and S32 counters with Liulin-MO flux rate for April – September 2016 and linear fitting of the corresponding dependencies.

Conclusion

Reviewed are the results from the comparison of Liulin-MO fluxes on ExoMars TGO mission with SREM TC1, S32 and S14 count rates on Rosetta mission obtained in the period April - September 2016 at different heliocentric distances in the interplanetary space.

The main results from the comparison show:

1) A long-term enhancement of all parameters is observed. This is in response of the falling trend of the solar activity in 2016 toward the solar cycle 24 minimum in 2019. The SREM parameters rising trends in 2016 were shown by Honig et al (2019). The Liulin-MO parameters rising trends in 2016 were revealed by Semkova et al. (2018).

2) The linear rising trends of Liulin-MO flux, SREM TC1 counter and Oulu MN count rate anti correlate with the solar activity because during the periods of low solar activity larger amount of GCR particles penetrate in the Solar system in conditions of a smaller solar wind and embedded magnetic field (Potgieter, 2013).

3) All measured parameters from SREM and Liulin-MO instruments follow relatively well the shorter-term variations of the GCR flux, monitored by Oulu NM.

4) A good correlation between monthly averaged SREM and Liulin-MO data sets is observed, particularly between Liulin-MO flux and TC1 count rate.

5) A good inter-calibration between the SREM and Liulin-MO data cannot be made because Rosetta and ExoMars TGO were at very different locations at the time of data collection. The inter-calibration is not a subject of TN01.03. Nevertheless the results from comparison of Liulin-MO on TGO and SREM-Rosetta data sets provide confirmation of the modulation of galactic cosmic rays with respect to solar activity, which was our hypothesis as well as they provide some useful insights into the behaviour of the galactic cosmic ray propagation within the inner heliosphere.

6) A cross-calibration of Liulun-MO data on ExoMars TGO and SREM data on Rosetta trough other SREM instruments (like in Honig et al, 2019) on other missions, operating at about 1 AU (Proba-1 and INTEGRAL) in April – September 2016 with subsequent inter-calibration between SREM-Rosetta and Liulin-MO data and examination of the radial gradient of cosmic rays in this period may be a subject of a future joint investigation with the SREM team.

6.2.4. TN01.04. Liulin-MO data products prepared for delivery to ESA PSA: Review of results

Additional reference documents for TN01.04.

1. *Benghin V., et al,* 2019. Comparison of Liulin-MO Dosimeter Radiation Measurements during ExoMars 2016 TGO Mars Circular Orbit with Dose Estimations Based on Galactic Cosmic Ray Models, paper presented at the 11 th workshop "Solar Influences on the Magnetosphere, Ionosphere and Atmosphere", Primorsko, Bulgaria, June 3-7, 2019, Program & Presentations, **http://ws-sozopol.stil.bas.bg/**
2. FREND Experiment Archive Interface Control Document (EAICD), EXM-FR-ICD-IKI-0086, version 2.2 of 28.03.2022

Liulin-MO data and their processing

As Liulin-MO is an ESA experiment we are obliged to provide our data to ESA Planetary Science Archive, developed and maintained by ESAC. Data processing is done in **two independent brunches** - by PSA in cooperation with us and by our team.

The flow of Liulin-MO data processing and the relations with PSA are depicted in Fig. 6.2.4.1.

All data products in PSA should be in PDS (Planetary Data System) compliant format. In the latest PDS 4 version each data file consists of a label file in *xml* format and a file with data themselves. The label file carries information about the data file: its identification in the

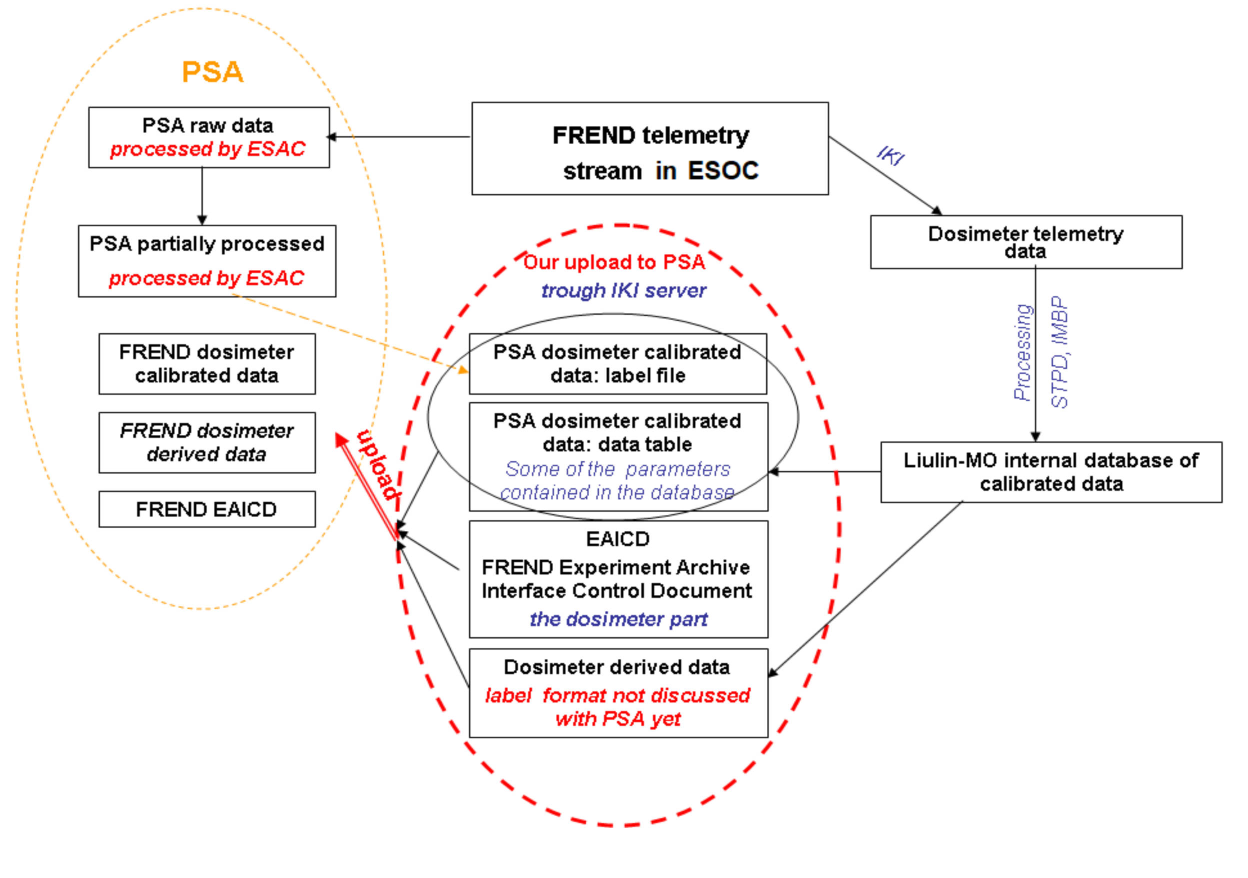

Fig. 6.2.4.1. Flow diagram of Liulin-MO data processing

archive, data content and the related PSA products.

Data processed by ESAC

- **Level 1 data - telemetry**. Liulin-MO is a part of the FREND experiment, so FREND telemetry blocks received in ESOC are retrieved by PSA (in ESAC) and archived. Users and even data providers have no access to these data products.

- Level 2 data - raw data. These are corrected for telemetry errors and split or decomentated into a data set for a given instrument. Data are also tagged with time. The content of the raw data products is suggested, agreed with the experiment team and verified by us.

- **Partially processed data**. These are data in an intermediate stage of calibration. The output electronic signals are converted to physical parameters characteristic for the particular instrument. The content of the partially processed data products is suggested, agreed with the experimenters and verified by us.

Data processed and provided by Liulin-MO team

We use directly the telemetry blocks containing Liulin-MO data, provided by FREND manager and retrieved from IKI server ASAP. Data immediately undergo express analysis for verification and control. Then they are processed to calibrated level and supplied to the internal database[*].

- Level 3 data - calibrated data. In our case these are data about the measured particle flux in units particles/cm^2.s and dose rate in units μGy/h. These data are compiled from the data in the internal database. Files are organized on a monthly base and are of two types - containing data measured with time resolution of one minute –‘minute data' - and data measured with time resolution one hour – ‘hour data’.

- Level 4 - derived data. These will be data measured in Mars science orbit, extrapolated to free space at 1.5 a.u. calculated by the algorithm described in TN 01.01.

EAICD - FREND Experiment Archive Interface Control Document

PSA is not a database but a data storage. The EAICD is aimed to PSA user not from FREND team to get acquainted with the experiment and to be able from the raw data to calculate the calibrated and derived data. It contains description of the instruments, of the experiment itself, description of its data in PSA and algorithms for consecutively processing data: from telemetry to raw, from raw to partially processed, from partially processed to calibrated, from calibrated to derived. The EAICD is common for the neutron and dosimeter parts of the experiment. We provide the necessary parts for the dosimeter. The whole document is compiled and provided to PSA by the FREND manager from IKI.

Current stage of the work on Liulin-MO data processing

Work done prior the start of the contract

Initially (up to 2020) it was agreed that PSA would contain only raw, calibrated and derived Liulin-MO data. Till the end of January 2020 the structure and content of the calibrated

[*] The internal database of Liulin-MO is developed under Contract No. 4000117692/16/NL/NDe DOSIMETRY: Dosimetry science payloads for ExoMars TGO & surface platform. Unified web-based database with Liulin type instruments' cosmic radiation data

label and data files was agreed and approved, 52 files with calibrated data were uploaded to PSA. According PSA rules data should go review. In October and November 2020 two online meetings with the reviewers and all data producers involved was held. From these meetings two major problems arose: 1) One of the reviewers was categorically disagreed with the form of the raw data files and insisted on their re-formatting and re-processing, removing files with wrong data; 2) We as data providers argued that the existing organization of the raw data on a 6-hour base is inappropriate and insisted on providing raw files for a day, as their description is directly connected with the content of the labels for our calibrated files. As a result a new structure of the raw data products was proposed and PSA developers suggested producing Partially Processed Products (PPP).

Work done under the contract

Raw data products

The structure of the raw data files was easily agreed and files with raw data on a daily base at the end of 2020, prior the start of the contract. At that time in PSA there were a lot of raw data products containing wrong data of various types, particularly for intervals when Liulin-MO was not operating. During the contract we provided our PSA collaborators with criteria for wrong and test data and a provisional list of intervals of wrong data. Now these files and intervals are removed from the archive. In March 2022 all Liulin-MO raw products were reprocessed in the new form by the PSA team. Nevertheless these products are not yet released for the public because of internal for the archive rules.

Partially processed data products

We proposed and our PSA collaborators agreed that the PPP products would be of two types: 1) containing data with one hour time resolution; 2) containing data with one minute time resolution. We proposed the names of the variables in the data files. After a one year of continuous mutual discussions and error corrections, in March 2022 the final structure of the PPP was agreed and our PSA collaborators were able to proceed on with their preparation. At present in PSA are ingested partially processed files from 1.07.2022 till now and several exemplary files for the first half of 2022. Data are not publicly released.

Calibrated data products

Our team is on duty to process Liulin-MO data to the level of calibrated and provide them to PSA. As described in the previous section calibrated data are calculated in a timely manner and supplied to the internal database. Problems arose with compiling the label files. In order to preserve traceability in the archive the labels of the calibrated products have to contain a list of the raw and PP products used as an input for calculating the calibrated data. We could not list non-existing files. **Occasionally** in November 2022, after regular checking PSA, we noticed that PP files have appeared starting form June 2022. In December 2022 we stared uploading test files to PSA. At the end of February 2023, after several iterations clearing PDS4 syntax errors, the label files were agreed and we prepared the calibrated products. The PSA team responsible for Liulin-MO data is not yet ready to ingest calibrated data into the archive because of the lack of PPP. We discussed with them the problem and agreed that we upload the calibrated data and they will store them in a test directory till it will be possible to ingest them. So we uploaded all our calibrated data for the period 2016 – 2022 to the corresponding test directory of the IKI server.

Derived data

The program of producing derived data is developed, the algorithm reported in TN 01.01 and the software in SW 01.01. Now we started the procedure of discussion with PSA collaborators and settlement of the label files. In particular the derived data should be assigned a PDS logical identifier.

The Experiment Archive Interface Control Document EAICD

The Liulin-MO updates of the EAICD done under the contract are as follows:

- New table description of the raw data product;

- New table description of the partially processed data products; assigning names to the parameter fields;

- New algorithm for data processing from telemetry to raw level;

- Algorithm for data processing from raw to partially processed level;

- Algorithm for data processing from partially processed to calibrated level;

- Algorithm for data processing from calibrated to derived level.

These updates are included in version 2.2 of the EAICD dated 28.03.2022.

Improving quality of data supplied to PSA

Processing Liulin-MO calibrated data we noticed in the 'minute' data files one serious shortcoming which we will name briefly ‘backward time jumps’. To explain the problem we first will briefly describe how data are organised on board and transmitted to the telemetry.

Liulin-MO data highlights

- Liulin-MO measurement cycle lasts 1 hour
- Liulin-MO data consist of **Measurement Frames** that are generated **every 1 hour**. Within the Measurement Frame parameters measured with time resolution 1 minute represent a ‘minute’ block of a certain length. Such blocks are repeated 60 times, each containing measured parameters for the 60 consecutive minutes of the given hour.
- Each Measurement Frame is transmitted to the telemetry by 20 packets every 3 minute, i.e. each frame is recorded during exactly 1 hour – 60 minutes.
- The Measurement Frame does not contain the time of the measurements. The beginning of the measurement cycle is defined by the time in which the first packet was recorded; let’s denote it by T0. Then the time in which the parameters of each one–minute block are measured is calculated adding to T0 the number of that block in the sequential series of blocks.

Inconsistencies in calibrated ‘minute' data files

In some cases measurements for intervals of several minutes are repeated with different values of the parameters. In the consecutive records this looks like a backward jump in time. For example:

Date	Time	Dose rate
07-Sep-18	17:59:54	13.3529816043377
07-Sep-18	18:00:54	15.123623456955
07-Sep-18	18:01:54	14.1942467653751
07-Sep-18	18:00:37	22.0868338608742
07-Sep-18	18:01:37	13.336671795845
07-Sep-18	18:02:37	18.6449618005753

In all data starting with April 2016 till present we found 25 such cases. We checked the records in the raw data files in PSA and found out that this happens when for unknown reason the time interval within which the Measurement Frames are recorded is less than 60 minutes. – ‘short cycles'. Note that even the time interval is less than 60 minutes, the data contain measurements for 60 minutes. Figure 6.2.4.2 presents in details how backward jumps happen.

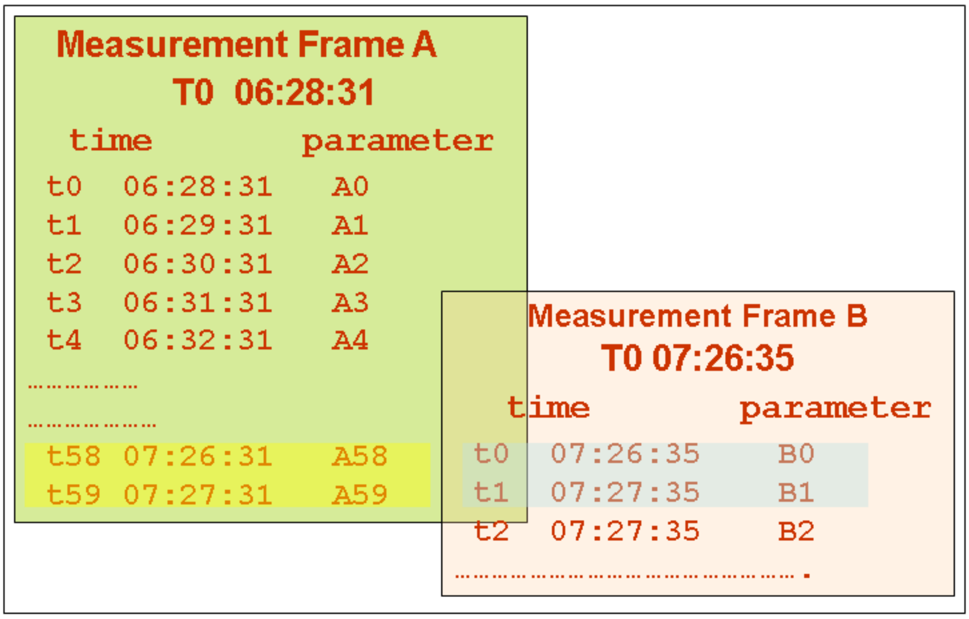

Fig. 6.2.4.2. How backward time jumps are received in the process of deciphering the telemetry records.

In some cases – e.g. records for 19.02.2020, we observe such jumps in our calibrated data, but not in the raw data files in PSA. Such cases can happen when during the communication session with TGO there were some errors in FREND telemetry blocks. We download the telemetry record on the same day of the session. ESOC team checks the validity of the records, corrects the errors if possible and in 2-3- days uploads the corrected blocks, removing the erroneous. In such cases we ask FREND manager to download the telemetry blocks again and process the already correct data.

Algorithm for overcoming the inconsistencies

1. When preparing the calculated 'minutes' files for PSA check the time intervals between the consecutive records of the parameters in the internal database. If a backward time jump is found, write in a specialised file the times of the corresponding records

2. In the corresponding raw data file in PSA check for the presence of ‘short cycles’, which could be the reason for the backward time jump.

3. If a 'short cycle’ is present in the raw data, omit the duplicated time interval from the short cycle data. For example, in the case of 7 September 2018 cited above, omit the records coloured in yellow.

4. If a short cycle is not present in the raw data file, ask FREND manager to reload Liulin-MO telemetry records for the given period. Recalculate the calibrated parameters from the new records.

N.B. The presence of short cycles in the raw data file in PSA will lead to a backward time jump in the partially processed data as well. We initiated an on-line discussion with our colleagues from PSA, pointed out and explained the problem. We informed them how we overcome this inconsistency and provided them a list of the found backward time jumps.

Conclusions

In the course of the contract a lot work on PSA dosimeter data files was done aimed to facilitate the user. Mutual work of Liulin-MO team and PSA collaborators led to a more readable structure of the raw data products, removing raw files with wrong data, appropriate structure of partially processed data products and a lot of improvements in the EAICD.

The new structure helped to prepare an algorithm for overcoming the backward time jumps in calibrated data. The improved calibrated data for the whole period – TGO transit to Mars in2016 and TGO science orbit since May 2018 till now – are uploaded to PSA.

Work with PSA team goes very slowly which puzzles us. PSA decision to use PDS4 for the label files with the constant change of the information model leads to many corrections in the label files, which takes a lot of time. The basic structure of Liulin-MO calibrated files lasted 2 years, from 2018 till the end of 2019. To produce all raw data products in the new structure it took PSA team almost 1.5 years, data are not publicly released yet. Partially processed data are not yet produced and ingested in the archive.

The uploaded calibrated files are parked in the system and we cannot predict when they will be published. The luck of publicity of our data hinders our publication work as journals require visibility of the data used in the science papers. We partially overcome this difficulty due to the Liulin instruments data base, created under the contract Dosimetry with ESA. The data base contains data from 10 missions with Liulin type instruments, including Liulin-MO data. Liulin-MO data are regularly updated in this database and is accessible at http://esa-pro.space.bas.bg/database.

6.3. Activities for WP2

Work Package 2 is aimed at developmental of numerical model of Liulin-MO in order to account for the effects of the surrounding matter on the LET spectra leading to errors in calculating of the quality factor and dose equivalent rates. The work is organized in 3 tasks and is reported in 4 deliverables:

Deliverable number	Deliverable title
TN02.01	Numerical simulations of Liulin-MO; Review of results
TN02.02	Algorithm and S/W for subtracting the secondary effects on LET spectra. Review.
SW02.02	S/W for subtracting the secondary effects on LET spectra
TN02.03	Reprocessed data for the LET spectra, quality factors and dose equivalent rates and

6.3.1. Necessity for numerical simulations

The charged particles registered by Liulin-MO prior hitting the instruments sensors interact with the surrounding materials and undergo changes in energy and eventually produce secondary particles, which in turn could hit the sensors and contaminate the measured LET spectra. The death time of Liulin-MO electronics is 50 ns, so the primary particle and its secondaries are registered as one particle and the energy deposited by them – as one energy pulse. Fig. 6.3.1.1 presents a schematic view of Liulin-MO sensors and their surroundings.

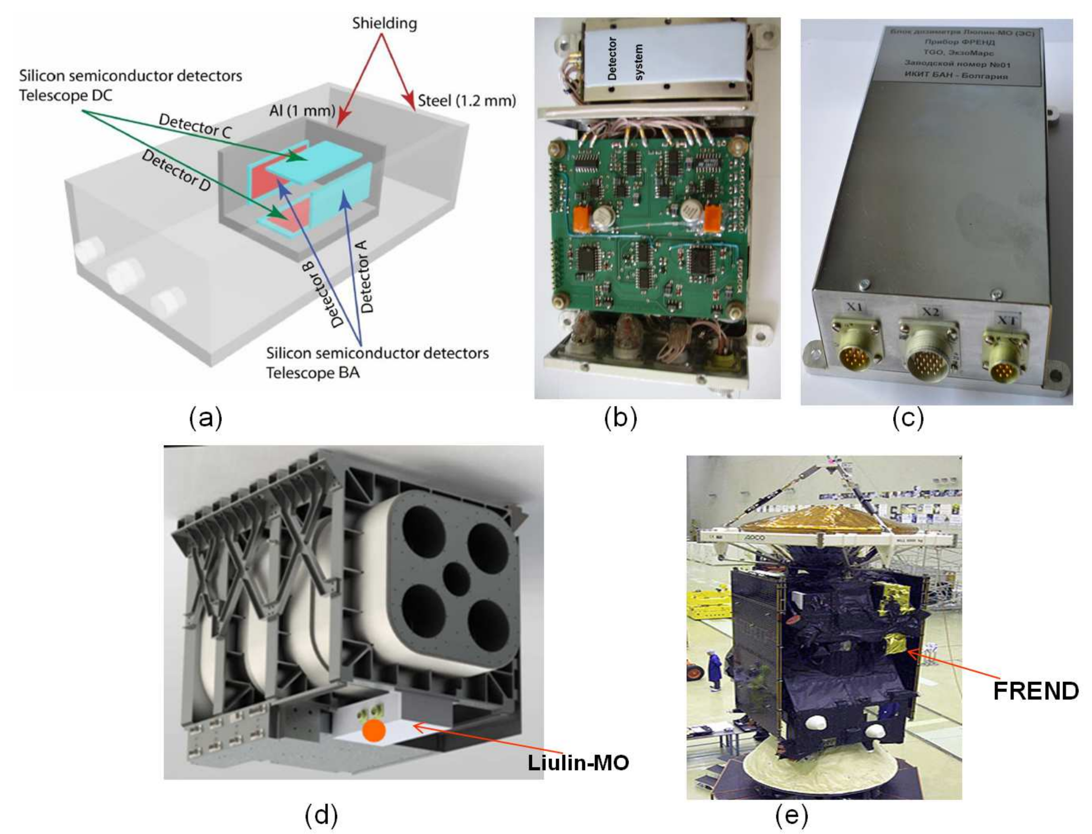

Figure 6.3.1.1 (a) Schematic view of the location of the detectors inside the box of Liulin-MO; (b) the detector system inside the instrument box; (c) Liulin-MO unit; (d) FREND instrument with Liulin-MO on it; (e) TGO ready forlaunch

The earlier investigations (Semkova et al, 2018) show that if we use the coincidence spectra in BA and DC telescopes for evaluating the LET spectra, we obtain too high values for the radiation quality factor *<Q>* (higher than 10), leading to unreliable high dose equivalent estimations.

A tentative simulation of Liulin-MO indicated that a reason for that could be false coincidence signals produced by ions hitting detector A (or C) with secondary electrons (or ions) hitting detectors B (or D) and vise versa.

6.3.2. TN02.01. Numerical simulations of Liulin-MO; Review of results

Additional reference documents for TN02.01.

1. *Agostinelli, S., et al.*, "Geant4 – a simulation toolkit", Nuclear Instruments and Methods in Physics Research Section A: Accelerators, Spectrometers, Detectors and Associated Equipment, Vol. 506, Issue 3, Pages 250-303, 2003.
2. *Benghin V., et al,* 2019. Comparison of Liulin-MO Dosimeter Radiation Measurements during ExoMars 2016 TGO Mars Circular Orbit with Dose Estimations Based on Galactic Cosmic Ray Models, paper presented at the 11 th workshop "Solar Influences on the Magnetosphere, Ionosphere and Atmosphere", Primorsko, Bulgaria, June 3-7, 2019, Program & Presentations, **http://ws-sozopol.stil.bas.bg/**
3. *Krastev, K.**,** Semkova J**,** Koleva R.**,** Benghin V, Drobishev S.* Numerical simulation of LLIULIN-MO dosimeter, Proceedings of the 18th International Scientific Conference "Space, Ecology, Safety, 2022", © Space Research and Technologies Institute Bulgarian Academy of Sciences, p-ISSN 2603 – 3313, e-ISSN 2603 – 3321, pp. 18-22 (*in Bulgarian*)
4. *Pak, S., et al.,* A numerical method to analyze geometric factors of a space particle detector relative to omnidirectional proton and electron fluxes, Journal of the Korean Astronomical Society, August 2018
5. *Slaba, T. C., & Whitman, K.* The Badhwar-O'Neill 2020 GCR model.Space Weather, 18, e2020SW002456. **https://doi.org/10.1029/2020SW002456**
6. *Zhao, X., et al.*, A Geometric Factor Calculation Method Based on the Isotropic Flux Assumption, CP, 37, 126201, 2013.

Description of Liulin-MO numerical model

General remarks about the used software

There are various software packages for numerical simulation of charged particles interaction with matter; many of them are dedicated to particular problems. Geant4 is an open-source toolkit that enables to simulate particle passage through matter. It is written in C++ and offers a wide range of tools for users to employ in their applications (*Agostinelly et al.*) GEANT4 is developed by the large international Geant4 Collaboration and detailed description and several kinds of User Guides can be found at https://geant4.web.cern.ch/.

To produce a numerical model of Liulin-MO and simulate the measurement process the application G4APP was created. It works in GEANT4 environment and includes the necessary modules to resolve our task. In particular it includes the Geant4 Material Database, 87 electromagnetic processes, 129 hadronic and 2 decay processes, 496 particles - mesons, leptons, baryons, nuclei, quarks and diquarks. The necessary geometry is described in a text file. In this work we simulate the functioning of Liulin-MO in free space when only galactic cosmic rays are measured.

To process Liulin-MO data to the state of the art level numerical simulations of the measurements is necessary. The simulations are performed using GEANT 4 software in two steps: i) model only Liulin-MO box masses and materials; ii) upgrading the model with the masses and materials of the FREND neutron spectrometer and the satellite's body surrounding Liulin-MO.

Input

The input data are organized in a macro file.

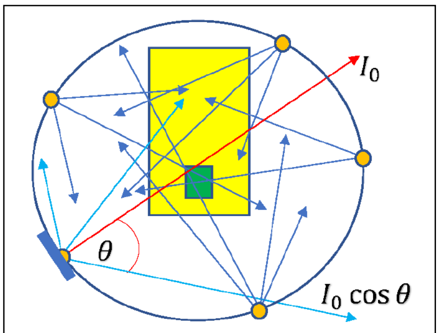

Fig.6.3.2.1. Scheme of the simulation

As a source of charged particles serves the surface of a sphere with an appropriate radius so that the whole instrument and surrounding matter be inside the sphere. The center of the sphere, respectively the center of the coordinate system used, is located at the center of the detector system. Figure 6.3.2.1. shows the used geometry in the case when only Liulin-MO box is modelled, the detector system is drawn in green. The isotropic nature of the galactic cosmic rays is simulated by generation from each point of the sphere a monoenergetic flux with cosine distribution (Zhao, X., et al.).

In the present work we investigate Liulin-MO measurements during TGO transit to Mars in 2016, when only GCR were registered (Semkova et al., 2018). For the input spectral distribution of GCR we use the Badhwar-O'Neill 2020 (BON 2020) model (*Slaba, and Whitman)*. The table distributions of all 28 elements of GCR are obtained from NASA OLTARIS site https://oltaris.larc.nasa.gov/. Their spectra are presented in Fig. 6.3.2.2. Each spectrum is described by 125 energies with the corresponding density.

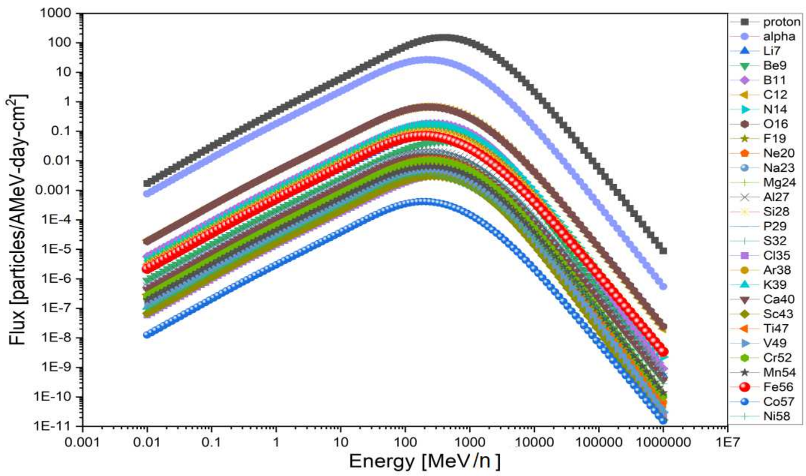

Fig. 6.3.2.2. Energy distribution of GCR in BON 2020 model for year 2016.

Logics of particles registration by the telescopes

The numbers of energy channels and their corresponding energies is done as described in (Semkova *et al,* 2018, 2021):

For each detector low L and high H energy ranges are constructed:

- $E_B(L)$ = 80 keV, $E_B(H)$ = 15 600 keV

- $E_A(L)$ = 15600 keV, $E_A(H)$ = 190 000 keV

- $E_D(L) = 80$ keV, $E_D(H) = 15\ 800$ keV
- $E_C(L) = 15800$ keV, $E_C(H) = 184\ 000$ keV

In order a particle to be taken into account for the energy spectrum of a given detector it should deliver in that detector energy within the limits defined by the corresponding low and high energy ranges.

The telescope registers a particle generated by the program only if the two detectors composing the telescope register it. Let the registered particle has delivered an energy E(L) in the low energy detector of the telescope (B or D) and E(H) is the energy deposited by the high energy detector of the telescope. The following conditions should be fulfilled:

- For telescope BA:

a) $E(H) > 80$ keV&$E(L) > 80$ keV
b) if $E(H) > E_A(L)$&$E(H) \leq E_A(H)$ the particle is registered in the corresponding channel of the telescope defined by detector A
c) if $E(H) \leq E_A(L)$&$E(L) \leq E_B(H)$ the particle is registered in the corresponding channel of the telescope defined by detector B
d) if $E(H) \leq E_A(L)$&$E(L) \geq E_B(H)$ the particle is registered in the 230 channel of detector B
f) if $E(H) > E_A(H)$ the particle is registered in the 255 channel of detector A (the 464 channel of the telescope)

- For telescope DC:

a) $E(H) > 80$ keV&$E(L) > 80$ keV
b) if $E(H) > E_C(L)$&$E(H) \leq E_C(H)$ the particle is registered in the corresponding channel of the telescope defined by detector C
c) if $E(H) \leq E_C(L)$&$E(L) \leq E_D(H)$ the particle is registered in the corresponding channel of the telescope defined by detector D
d) if $E(H) \leq E_C(L)$&$E(L) \geq E_D(H)$ the particle is registered in the 227 channel of detector B
f) if $E(H) > E_C(H)$ the particle is registered in the 255 channel of detector C (the 460 channel of the telescope)

Results of the first stage of simulations – model of Liulin-MO box

The geometry used in this model is shown in Fig. 6.3.2.1. In yellow is drawn the projection of Liulin-MO box and in green – the detector system. The sphere used as a source of charged particle has a radius of 15 cm.

For each of the 28 nuclei of GCR 125 monoenergetic fluxes with isotropic angular distribution is generated randomly on the source sphere. For protons and alpha particles 10^8 are generated; for the rest 26 masses – 10^7. Fig. 6.3.2.2. presents the obtained individual spectra for some masses.

The count rate C is defined as

$$C = \frac{n}{N}\pi R^2 * J$$

where n is the number of registered particles, N – the number of generated particles, R - the radius of the source sphere, J is the flux from the BON 2020 model.

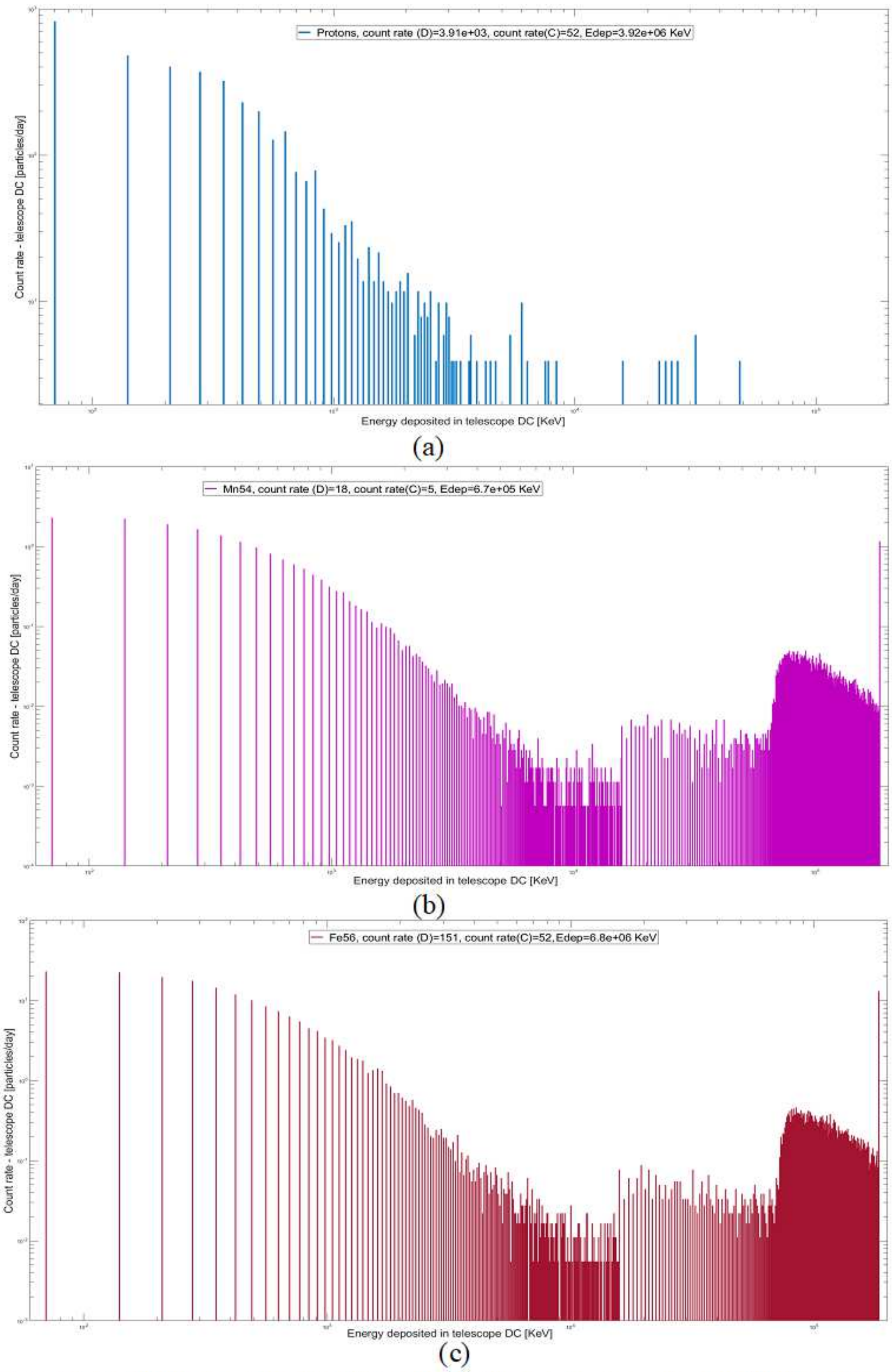

Fig.6.3.2.2.Numerical model of Liulin-MO box: Spectra of some GCR nuclei registered in DC telescope. (a) protons; (b) manganese; (c) iron

The absorbed dose is calculated as

$$D = \frac{\sum_i E_i * n_i}{m}$$

where E_i is the energy deposited in spectral channel i, n_i – the number of particles in that channel and m is the mass of the detectors sensitive volume.

A comparison between the simulated energy deposition spectrum in the telescope and the measured in free space spectra in 2016 during TGO transition to Mars is presented in Figure 6.3.2.3. The numerical simulation allows us to evaluate the contribution to the dose of each GCR component – Fig. 6.2.3.4.

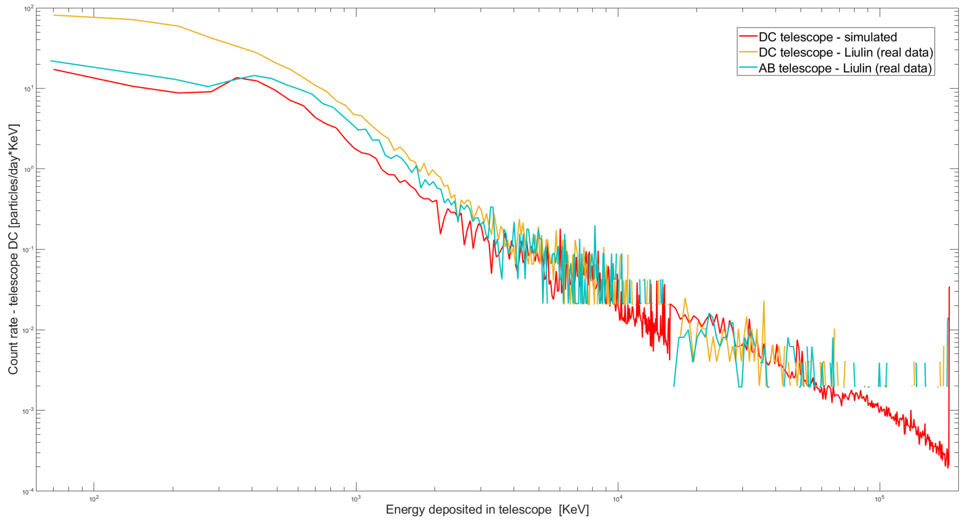

Fig. 6.3.2.3 Comparison between the simulated and measured in 2016 energy deposition spectra

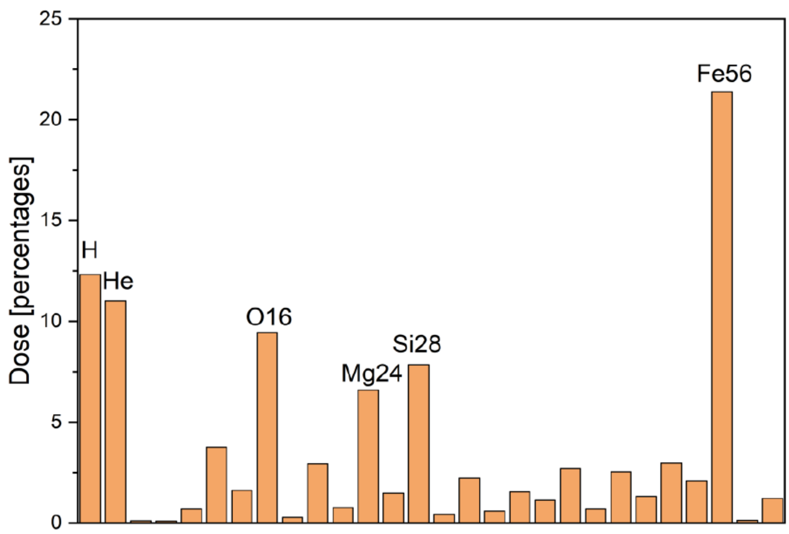

Fig. 6.3.2.4.. Contribution to the dose of the different components of GCR.

Results of the second stage of simulations – model of full geometry

Liulin-MO is surrounded by a lot of different instruments and elements of TGO construction of various materials (pl. see Fig. 6.3.2.1). Restrictions imposed in Bulgaria because the COVID 19 pandemic led to a considerable delay in staring the wok on WP 2 and prevented our access to more powerful computing facilities. All simulations were performed using the computers of the team which proved to be with modest abilities for the purpose of full model of Liulin-MO and the surrounding matter and each run took a considerable time. To overcome this problem we decided to model TGO body (Fig. 6.3.2.1e) by a simple plate with appropriate dimensions. Fig. 6.3.2.5. presents two different views of the used geometry. On the left panel Liulin-MO is drawn in orange, mounted on FREND neutron spectrometer – grey, TGO body is presented as the plate in blue. On the left panel Liulin-MO is drawn in orange, mounted on FREND neutron spectrometer – grey, TGO body is presented as the plate in blue. The right panel shows the dimensions of the model plates. The source sphere has a radius of 150 cm. For protons and alpha particles 10^8 are generated; for the rest 26 masses – 10^7 Fig. 6.3.2.5 demonstrates the energy deposition spectra for manganese and iron, obtained in the full geometry model – in blue, compared with the corresponding spectra in the model of only Liulin-MO box.

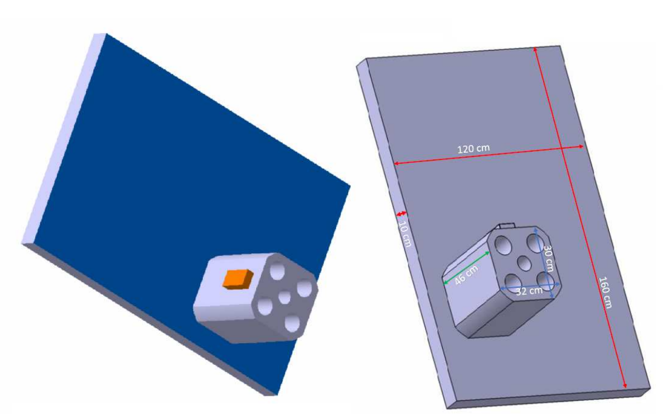

Fig. 6.3.2.5. Two projections of the model geometry, dimensions are shown on the right

Fig. 6.3.2.6. presents the final results from the numerical model – comparison between the simulated and the measured in free space in 2016 spectra by the two telescopes

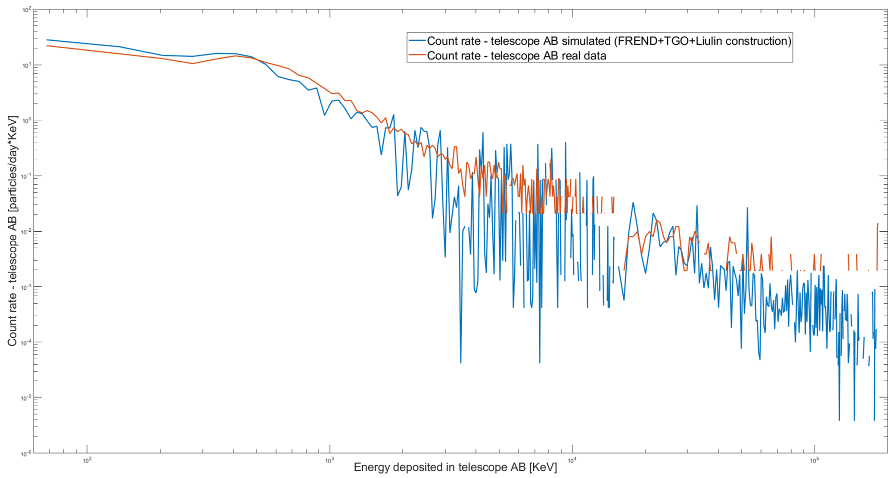

(a)

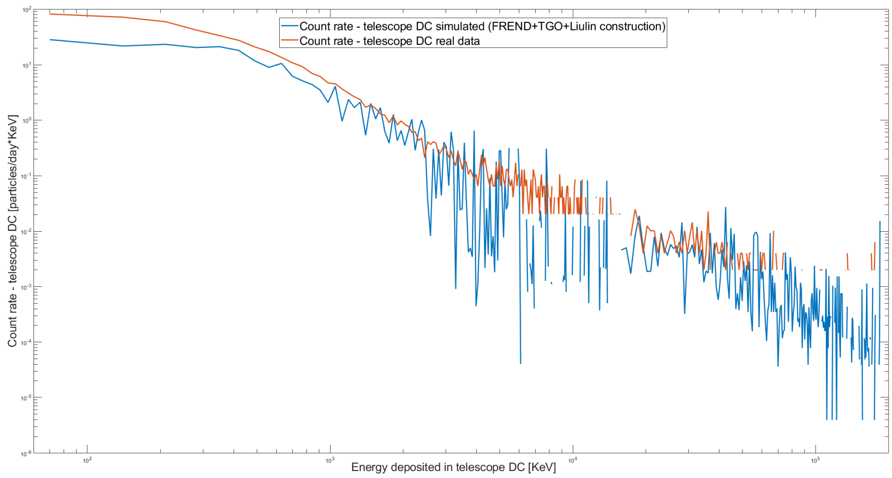

(b)

Fig.6.3.2.6. Comparison between the simulated in the full geometry model energy deposition spectra and the measured ones (a) for telescope BA; (b) for telescope DC.

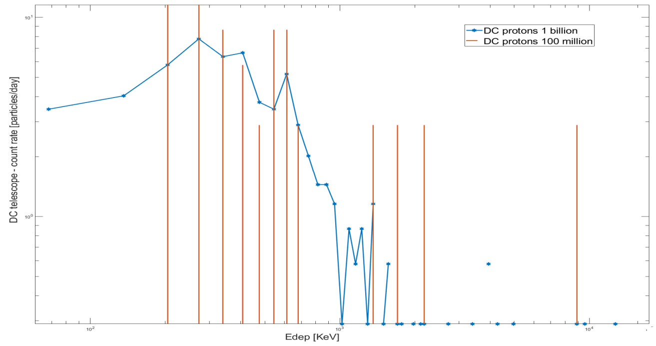

Fig. 6.3.2.7. Effect of the number of generated particles on the simulated spectrum.

The simulated and measured spectra are in quite good correspondence. The considerable scatter in the simulated spectra in the region 200 –1000 keV and around 10000 keV is due to the insufficient statistics. The effect of the number of generated particles is very well demonstrated in Fig. 6.3.2.7, showing the results when 100 millions protons are generated – in red, and those with 1 billions protons – in blue.

Conclusions

A numerical model of Liulin-MO dosimeter mounted on TGO satellite is created. For that purpose a specialized application G4AAP was built, working in GEANT 4 environment. The application allows for simulating the processes of Liulin-MO measurements.

The body of TGO satellite is large in dimensions and with too many constructional details, which provokes a very long time of computations using the computer facilities of the team. To facilitate computations TGO body is modelled as a rectangular plate with dimensions 160x120x10 cm (pl see Fig. 6.3.2.5), which on one hand provide the necessary shielding of 20 gm cm^{-2} to Liulin-MO detectors (Semkova et al, 2021) and on the other hand require a computing volume that is reasonable in time. Input particles are generated from the surface with a 150 cm radius and a center in the center of Liulin-MO detector system. Generated are monoenergetic isotropic fluxes using the energy distribution of 125 energies for each of the 28 nuclei of GCR BON 2020 model. For protons and alpha particles 10^8 are generated; for the rest 26 masses – 10^7.

The behaviour of the simulated spectra of deposited energy very well follows the course of the measured spectra as seen from Fig.6.3.2.6., and provides the possibility to clean the measured LET spectra from false coincidence signals due to secondaries produced in the surrounding matter.

Beyond the end of this contract the model will be developed in two directions:

(i) more detailed descriptions of TGO satellite and instruments' structure (Fig. 6.3.2.8) will be implemented;

(ii) the number of generated particles will be increased. The used number of particles provides sufficient statistics for input particles from the surface of a sphere with 10 cm radius, used in the first stage of simulations. The ensure the same statistics for the second stage where the particles are generated from the surface of a sphere with 150 cm radius the number of input particles should be increased by two orders of magnitude.

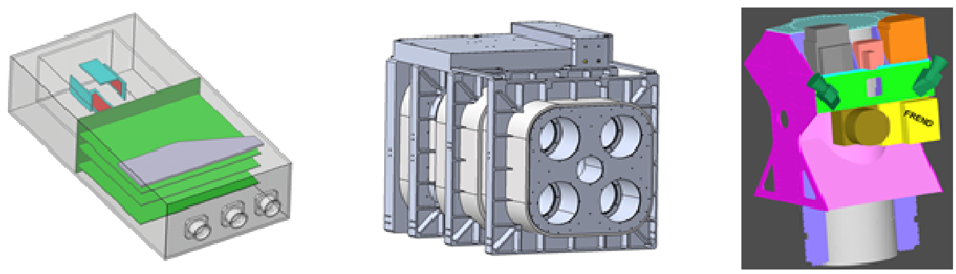

(a) *(b)* *(c)*

Fig. 6.3.2.8. Detailed structural models of: (a) Liulin-MO; (b) FREND neutron spectrometer; (c) TGO satellite body with instruments

6.3.3. TN02.02. Algorithm and S/W for accounting the secondary effects on LET spectra

Description of the method for subtracting the secondary effects on LET spectra

A method was developed for subtracting the secondary effects on LET spectra measured in coincidence mode by Liulin-MO. It includes the following steps:

1. Modeling as described in TN02.01 the energy deposition spectrum in coincidence mode for each of the 28 nuclei of GCR spectrum, using the Badhwar-O'Neill 2020 (BON 2020) GCR model for the period of TGO transit to Mars in April -September 2016 and the full geometry model of the detector's shielding.

2. Subtracting the secondary particle effects on each of the above modeled spectra. The procedure for this is explained by Fig.6.3.3.1a and 6.3.3.1b. (Krastev et al, 2022). Fig. 6.3.3.1a. shows the correspondence between the input iron spectrum (upper plot, obtained using BON 2020 GCR model and NASA OLTARIS, **https://oltaris.larc.nasa.gov/**) and the simulated iron energy deposition spectrum in the telescope DC (bottom plot). In Fig. 6.3.3.1b the part of the input spectrum marked in blue area as cut-off energy are particles with energies that are stopped in the Liulin-MO shielding and do not penetrate to the detectors. The marked in a small black area part of the input spectrum are particles that are stopped in one of the detectors and do not reach the other detector of the telescope. The highest energy part of the input spectrum is projected at the point around the ionization minimum in the energy deposition spectrum (see the bottom plot, where the yellow arrow shows the ionization minimum). We assume that the particles with deposited energies lower than the ionization minimum are secondary particles (SRIM, the Stopping and Range of Ions in Matter, **http://www.srim.org/SRIM/SRIMLEGL.htm**). The area enclosed in green on the bottom plot (called coincidences triggered by electrons) reflects cases where mostly secondary electrons are registered in each of the telescope's two detectors. We subtract the bigger part of these secondary events (mostly electrons but also some ions) from the energy deposition spectrum of the telescope. We use only the part of the telescope's energy deposition spectrum higher than the ionization minimum for construction of the telescope DC energy deposition spectrum with subtracted secondary particles. From this part we also exclude the ions which

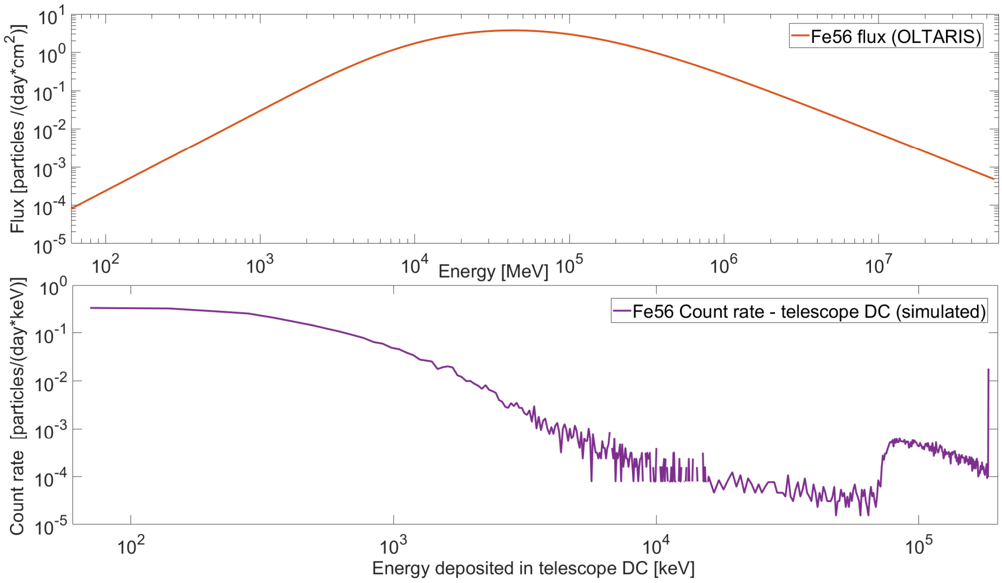

Fig.6.3.3.1a. Input spectrum of iron ions of GCR taken from OLTARIS (upper plot) and output (simulated) energy deposition spectrum in DC telescope (bottom plot)

coincide with electrons. The red arrow marks the maximum of the energy deposition spectrum of iron ions.

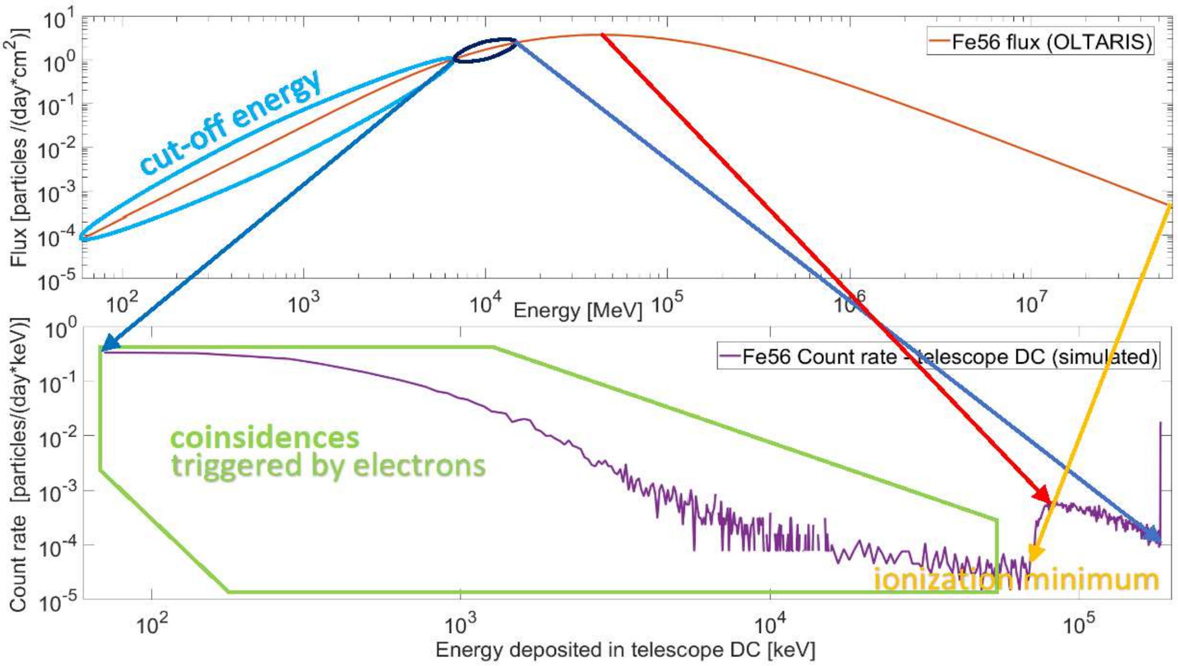

Fig. 6.3.3.1b. The spectra from Fig. 6.3.3.1a with marked areas: the part of the input spectrum marked in blue area as cut-off energy are particles that are stopped in the Liulin-MO shielding and do not penetrate to the detectors. The marked in a small black area part of the input spectrum are particles that are stopped in one of the detectors and do not reach the other detector of the telescope. The area enclosed in green on the bottom plot reflects cases where mainly secondary electrons (but also some secondary ions) are registered in each of the telescope's two detectors. On the bottom plot the yellow arrow shows the ionization minimum in the energy deposition spectrum. The red arrow marks the maximum of the energy deposition spectrum of the iron ions.

The same procedure is applied for obtaining of the telescope BA energy deposition spectrum with subtracted secondary particles.

We divide the elements from hydrogen to nickel into groups, setting a trigger energy threshold (the energy threshold for triggering coincidence signal) for each group that is the same for both telescope detectors. The trigger energy threshold is close to the ionization minimum of elements in the corresponding group.

The energy thresholds are as follow for the different groups of elements:

A) Ni58, Co57, Fe56 – 70 MeV;

B) Mn54, Cr52, V49, Ti47, Sc43 – 50 MeV;

C) Ca40, K39, Ar38 - 35 MeV ;

D) Cl35, S32, P29, Si28 -20 MeV;

E) Al27, Mg24, Na23, Ne20, F19 – 10 MeV;

F) O16, N14, C12, B11 – 3 MeV;

G) Be9, Li7 – 1 MeV;

H) He – 500 KeV.

For protons there is a separate filter in the program that runs under GEANT4. We use energy thresholds for protons equal to 80 keV, equivalent to the lower energy threshold in the telescopes of Liulin-MO.

Trigger energy thresholds can be determined for each element using SRIM. By imposing these restrictions, we thereby clean out secondary particle effects from the telescope's energy deposition spectrum of each element.

Fig. 6.3.3.2 shows the simulated uncleaned and cleaned energy deposition spectrum of iron ions of GCR in the telescope BA.

3. Construct the full energy deposition spectrum in the telescope as a sum of the energy deposition spectra of all 28 masses of GCR with subtracted secondary particles (mainly electrons).

4. Smooth the obtained spectra (cleaned and uncleaned) with the built-in algorithm Moving Averaging of the Origin program.

5. For each spectral channel obtain the relation $K_i = Fsub_i / Fin_i$ where $Fsub_i$ is the number of counts in channel i of the simulated smoothed energy deposition spectrum in the telescope with subtracted secondary effects (as described in point 3), Fin_i is the number of counts in channel i of the simulated smoothed energy deposition spectrum in the telescope without subtracted secondary effects (as described in point 1).

6. For each spectral channel i of the measured by Liulin-MO energy deposition spectrum in the telescope multiply the number of counts in channel i by K_i. In this way we obtain the measured energy deposition spectrum in the corresponding telescope with subtracted secondary particle effects.

7. From the measured energy deposition spectrum obtained in the previous step, the LET spectrum in Si can be obtained using the relation $LET(Si)=(1/\rho)\bullet(dE/dx)$, where dE/dx is the energy lost per unit of path length, ρ is the matter density (2.33 gcm^{-2} for Si). The mean path length in a detector of Liulin-MO telescopes is 327 µm.

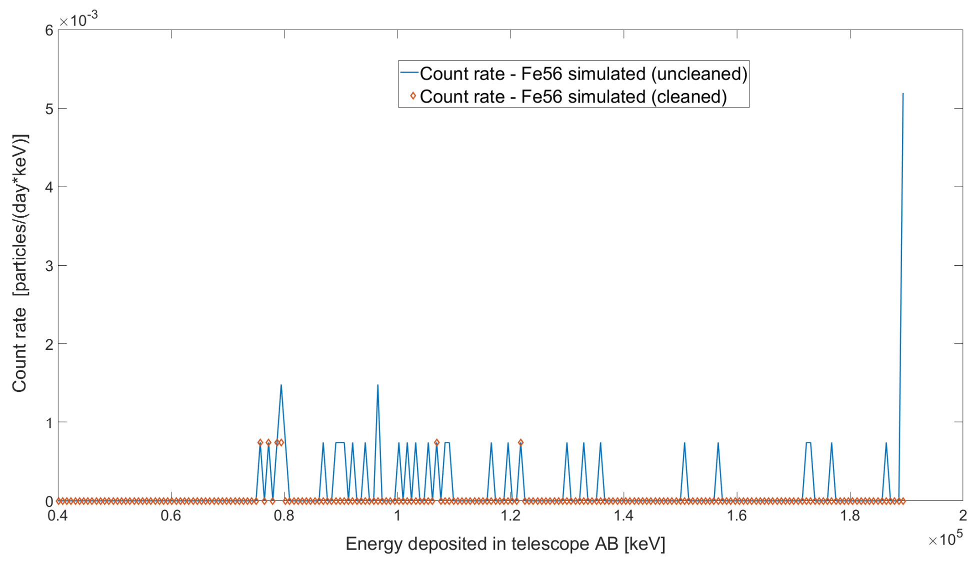

Fig.6.3.3.2. Simulated uncleaned (in blue) and cleaned (in red) energy deposition spectrum of iron ions in BA telescope

<u>Description of the algorithm for subtracting the secondary effects on LET spectra</u>

The algorithm for subtracting the secondary effects on LET spectra includes the following steps:

1. For every spectral channel in the telescopes BA and DC calculate the relation $K_i=Fsub_i/Fin_i$ where $Fsub_i$ is the number of counts in channel i of the smoothed simulated energy deposition spectrum in the corresponding telescope with subtracted secondary effects, Fin_i is the number of counts in channel i of the smoothed simulated energy deposition spectrum in this telescope without subtracted secondary effects.

2. Select the time interval for which data are required in the internal data base of Liulin-MO, developed under Contract No. 4000117692/16/NL/NDe DOSIMETRY: Dosimetry science payloads for ExoMars TGO & surface platform. Unified web-based database with Liulin type instruments' cosmic radiation data and described in Dosimetry_Deliverable_D04.03-Rev1.pdf. The time interval should be in the range 01 May-15 September, corresponding to measurements in the free space during TGO transit to Mars.

3. From Liulin-MO data base extract the measured by Liulin-MO coincidence energy deposition spectra in BA and DC telescopes respectively using the *"SP BA(E) coinc*" and *"SP DC (E) coinc"* procedures of the data base. As a result of selecting the desired values and saving them, two files containing the hourly values of the coincidence energy deposition spectra in the two telescopes for the selected time intervals are created.

4. For every channel i of the measured coincidence energy deposition spectra of every telescope calculate the count rate in *[particles/(day•keV)].*

5. For every spectral channel i of the measured by Liulin-MO coincidence energy deposition spectrum in every telescope multiply the number of counts in channel i by K_i. In this way we obtain the measured energy deposition spectrum in the corresponding telescope with subtracted secondary particle effects.

<u>Description of the S/W for subtracting the secondary effects on LET spectra</u>

The S/W developed for subtracting the secondary effects on LET spectra is based on the above described algorithm. Beside subtracting the secondary effects from the measured LET spectrum, it also calculates the quality factor $<Q>$ from this spectrum.

The program for subtracting the secondary effects on LET spectra and calculating the quality factor works in the environment of the MATLAB package.

The steps involved in these calculations are listed below:

1. Spectra (cleaned and uncleaned) obtained in the GEANT4 simulation for the telescope are smoothed using the Moving Average method.
2. In the MATLAB Workspace, the following variables are created as a column vector:
   a) cs- the cleaned and smoothed spectrum obtained from the simulation
   b) us – the uncleaned and smoothed spectrum obtained from the simulation
   c) rs - the real spectrum measured by the telescope
   d) es - the total energy spectrum of the telescope
   e) ls -the quality factor as a function of L , where L is the unrestricted LET in water ($LET_{Si\rightarrow H_2O} Conversion = 1.3$). **<u>http://icrpaedia.org/Quality_factor</u>**
3. Running a script Q_script.m, described below:

```
for i=1:463;
if us(i)==0
qs(i)=0;
else
qs(i)=cs(i)*rs(i)/us(i);    // reconstruction of the real count rate from the measured count rate and simulated (cleaned and uncleaned)//
end
end
for i=1:463;
ms(i)=es(i)*qs(i)*ls(i); // creates a helper variable//
ns(i)=es(i)*qs(i);       // creates a helper variable//
end
s(1)=ms(1);              // creates a helper variable//
s1(1)=ns(1);             // creates a helper variable//
for i=1:462;
for k=1:i;
s(i+1)=s(i)+ms(i+1);    // creates a helper variable//
s1(i+1)=s1(i)+ns(i+1);  // creates a helper variable//
end
for i=1:463;
Q(i)=s(i)/s1(i);          // calculating the quality factor depending on the number of the first (i) channels we are taking //
end
end
plot(es,Q)              // plots the quality factor graph//
```

4. The steps to run the program are visualized below:
   a) navigate to the folder that contains the attached files Q_factor.mat and Q_script.m (Fig. 6.3.3.3);
   b) in the command window run the command: “load('Q_factor.mat')”. With this command all files in 2 a-e are loaded in the Workspace of MATLAB. (Fig. 6.3.3.4);
   c) in the command window run the command: “run Q_script.m” (Fig. 6.3.3.5).
5. After the execution of the command “run Q_script.m”, in the Workspace of MATLAB, the variable Q is generated (Fig. 6.3.3.6).

The S/W (SW02.02) for subtracting the secondary effects on LET spectra and calculation of $<Q>$ from these spectra is delivered together with TN02.02.

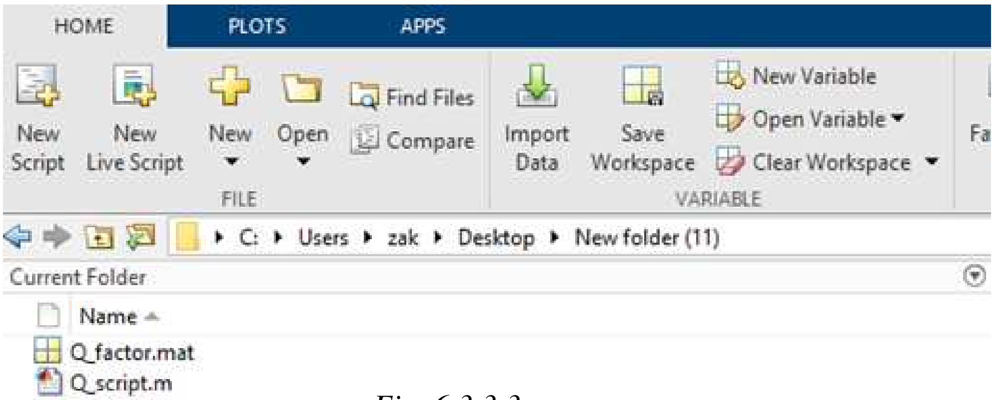

Fig. 6.3.3.3

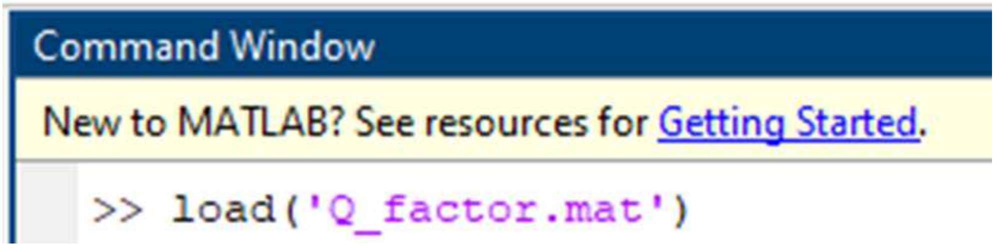

Fig. 6.3.3.4

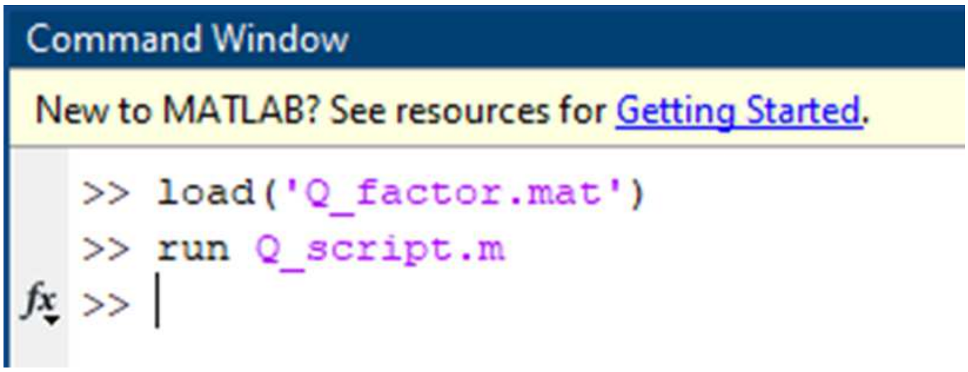

Fig. 6.3.3.5.

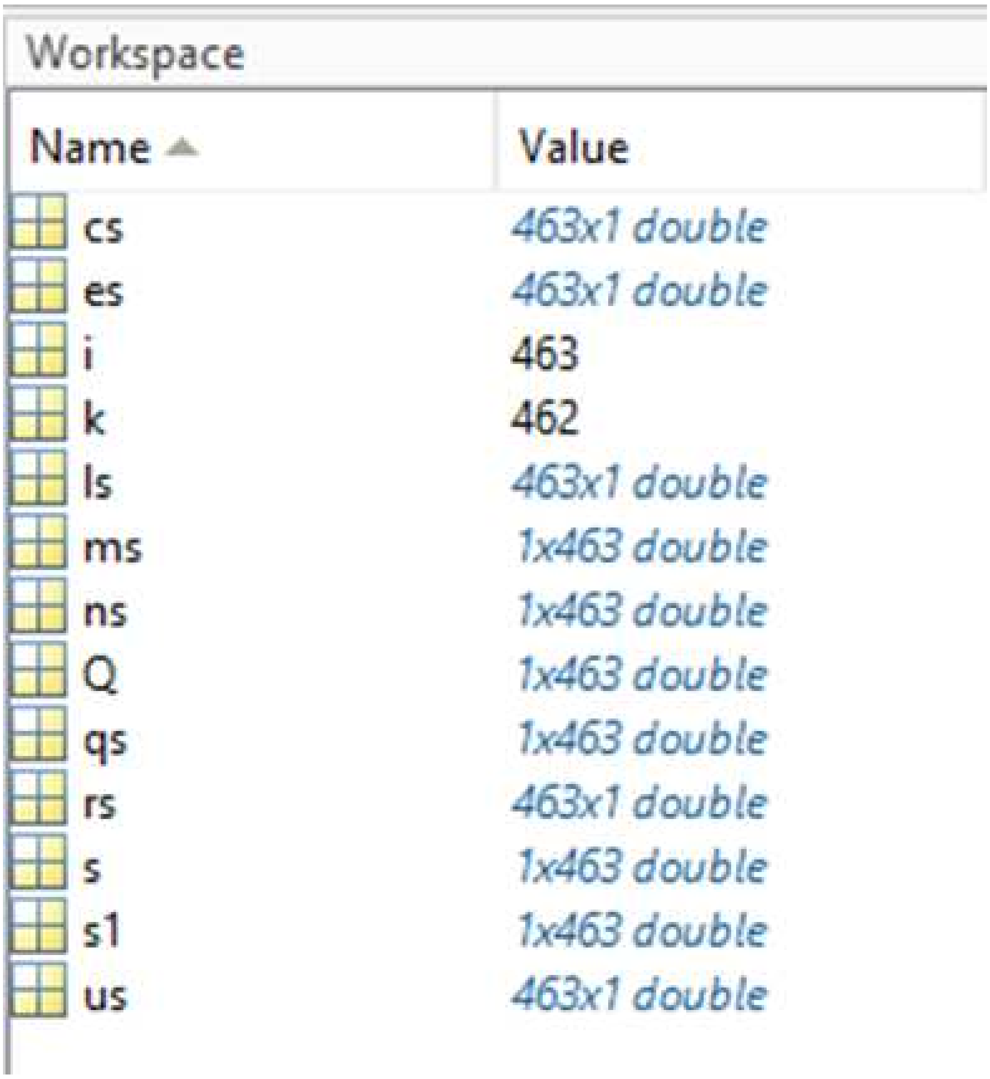

Workspace

Name	Value
cs	463x1 double
es	463x1 double
i	463
k	462
ls	463x1 double
ms	1x463 double
ns	1x463 double
Q	1x463 double
qs	1x463 double
rs	463x1 double
s	1x463 double
s1	1x463 double
us	463x1 double

Fig.6.3.3.6

Conclusion

A method, algorithm and S/W have been developed for subtracting the secondary effects on LET spectra measured by Liulin-MO dosimeter onboard ExoMars TGO during the transit to Mars in May-September 2016. They are based on the developed numerical model of Liulin-MO and the processes in the surrounding materials as describer in TN 02.01.

The S/W also allows calculation of *<Q>* form the measured spectra with subtracted secondary effects.

As an illustration of the developed method, in Fig. *6.3.3.7.* are presented the simulated cleaned and uncleaned from secondary effects energy deposition spectra in the telescope AB for the period May-September 2016. Well seen is the difference between the two spectra, particularly in the low and high energy deposition ranges. The count rate of the cleaned spectrum in the low energy deposition range is higher and in the high energy deposition range it is lower than the count rate of the uncleaned spectrum. This leads to significantly lower *<Q>* calculated from the cleaned spectrum in comparison with *<Q>* calculated from the uncleaned spectrum (see the legend in Fig.6.3.3.7).

The developed SW02.02 and the accompanying files are delivered together with TN02.02.

The developed algorithm and S/W are used for reprocessing the data for the LET spectra, quality factors and dose equivalent rates obtained during the transit to Mars in TN 02.03. There these values are discussed in details.

Future activities beyond this contract include development of an algorithm and S/W for reprocessing the data for the LET spectra, quality factors and dose equivalent rates obtained in Mars orbit for the period since May 2018.

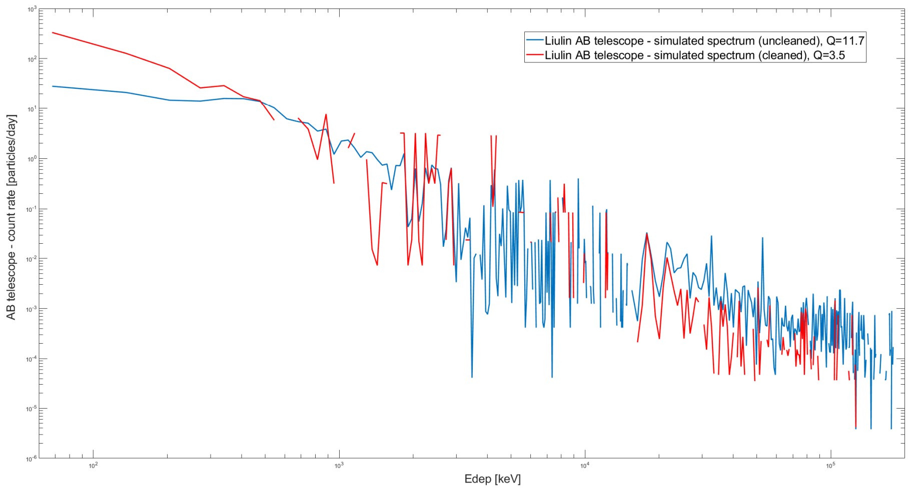

Fig. 6.3.3.7. Simulated cleaned (in red) and uncleaned (in blue) from secondary effects energy deposition spectra in the telescope BA. Data are for the period May-September 2016 during the transit of TGO to Mars.

6.3.4. TN02.03. Reprocessed data for the LET spectra, quality factors and dose equivalent rates and science analysis. Review.

Additional reference documents for TN02.03.

1. *Benton, E., Benton, E., & Frank, A.* (2010). Conversion between different forms of let. Radiation measurements, 45 (8), 957–959. **doi: 10.1016/j.radmeas.2010.05.008**
2. *Berger et al,* The German Aerospace Center M-42 radiation detector—A new development for applications in mixed radiation fields, Rev. Sci. Instrum. **90**, 125115 (2019); **https://doi.org/10.1063/1.5122301**
3. *Doke, T., T. Hayashi, and T.B. Borak*. Comparisons of LET distributions measured in low-earth orbit using tissue-equivalent proportional counters and the position-sensitive silicon-detector telescope (RRMD-III). Radiat. Res., 156 (3), 310–316, 2001, DOI: 10.1667/0033-7587 (2001)
4. *Guo J, Zeitlin C, Wimmer-Schweingruber R. F, Rafkin et a*l. 2015a. Modeling the variations of dose rate measured by RAD during the First MSL Martian Year: 2012–2014. Astrophys J810(1): 24, **https://doi.org/10.1088/0004-637X/810/1/24**
5. *Guo, J., Zeitlin, C., Wimmer-Schweingruber, et al*, "Variations of dose rate observed by MSL/RAD in transit to Mars." Astronomy & Astrophysics 577, A58 (2015b)
6. *ICRP, Report No. 60,* Pergamon Press, Oxford, 1991
7. *Labrenz J., S. Burmeister, T. Berger et al, Matroshk*a DOSTEL measurements onboard the International Space Station (ISS) J SWSC, 5 (A38), 2015, **DOI: 10.(1051)/swsc/2015039**
8. *Schwadron, T. N., A. Baker, B. Blake et al*, 2012. Lunar radiation environment and space weathering from the Cosmic Ray Telescope for the Effects of Radiation (CRaTER), J. Geophys. Res., 117, E00H13, **doi:10.1029/2011JE003978**

Quality factors and dose equivalent rates

The energy deposited is converted to energy lost per unit of path length (*dE/dx)* in silicon. *dE/dx* spectra in silicon can be related to linear energy transfer (LET) spectra in water and the average radiation quality factor $\langle Q \rangle$ can be calculated according to the *Q(LET)* relationship given in ICRP – 60 (ICRP, 1991). The dose equivalent *H* is obtained as $H = D\ (water) \bullet \langle Q \rangle$.

The earlier investigations (Semkova et al, 2018) show that if we use the coincidence spectra in AB and CD telescopes for evaluating the LET spectra, we obtain too high values for the radiation quality factor $\langle Q \rangle$, leading to unreliable dose equivalent estimations. That's why until recently for the calculation of *dE/dx* in silicon the methodology described in Semkova et al, 2018 was applied. We use the full energy deposition spectrum in the single detectors B(A) and D(C) (not only in coincidence mode) and evaluate the LET spectra in the directions BA and DC, assuming a mean path length 600 µm of a particle through the 300 µm thick detector. The value of 600 µm is received from the estimation of the average length of a straight line passing through an infinite flat detector assuming isotropic incidence of particles on the detector. This estimation shows that the average track length is twice the layer thickness. Numerical estimates of the choice of the effective path length 600 µm for several incident LET spectra confirmed the acceptability of this choice (Semkova et al, 2018, 2021, 2023).

To convert the dose rate measured in silicon to dose rate in water and relate $(1/\rho)\bullet(dE/dx)$ in silicon to LET in water we used a factor of 1.3 ± 0.08 (Semkova et al, 2018, 2021, 2023). Here ρ is the matter density. This factor with uncertainties was chosen in Semkova et al, 2018 to allow comparison of LET spectra, $\langle Q \rangle$ and *H* obtained by Liulin – MO and other instruments in the space, providing these values. RAD aboard of NASA Mars Science Laboratory (MSL, Curiosity) uses a factor of 1.38 for these conversions both during the cruise and on Mars surface (Guo et al, 2015 a, b). CRaTER onboard the Lunar Reconnaissance Orbiter uses a conversion factor 1.33 (Schwadron et al, 2012). The silicon-water conversion factor 1.33 is used in Benton et al., 2010. The value of the factor 1.3 ± 0.08 allows a comparison with the commonly used factor of 1.22 - 1.24 for conversion of *(1/ρ)•(dE/dx)* in silicon to LET in water (Doke et al. 2001; Labrenz et al, 2015; Berger et al, 2019). The obtained LET spectrum in water using the conversion factor 1.3 is in the range 0.13 –177 keV/µm. All particles with LET > 177 keV/µm are registered in the last spectral channel and are considered as particles with LET = 177 keV/µm when calculating radiation quality factor <*Q*>, absorbed dose, and dose equivalent.

Review of the reprocessed data for the LET spectra

For the reprocessing of the LET spectra measured in the telescopes BA and DC, the algorithm and S/W developed for subtracting the secondary effects on LET spectra described in TN02.02 are used. As a result we obtain the measured energy deposition spectrum in the telescopes BA and DC with subtracted secondary effects.

From this spectrum the LET spectrum in Si can be obtained using the relation *LET(Si)=(1/ρ)•(dE/dx),* where *dE/dx* is the energy lost per unit of path length, *ρ* is the matter density (2.33 g cm^{-2} for Si). The mean path length in the detector of Liulin-MO telescopes configuration is 327 µm.

The LET spectrum in water is then *LET(Si)=(1/ρ)•(dE/dx) •1.3.*

The calculated in this way range of LET spectrum in water is 0.24-325 keV/µm.

All particles with LET > 325 keV/µm are registered in the last spectral channel and are considered as particles with LET = 325 keV/µm when calculating radiation quality factor <*Q*>, absorbed dose, and dose equivalent.

In Fig. 6.3.4.1a and 6.3.4.1b are plotted the real and reprocessed LET spectra in water measured correspondingly in the telescopes BA and DC during 01 May-15 September 2016 in the interplanetary space. Well seen is the difference between the real and reprocessed LET spectra, particularly in the low and high energy deposition ranges. The count rate of the reprocessed LET spectrum in the low energy deposition range is higher and in the high energy deposition range it is lower than the count rate of the real spectrum.

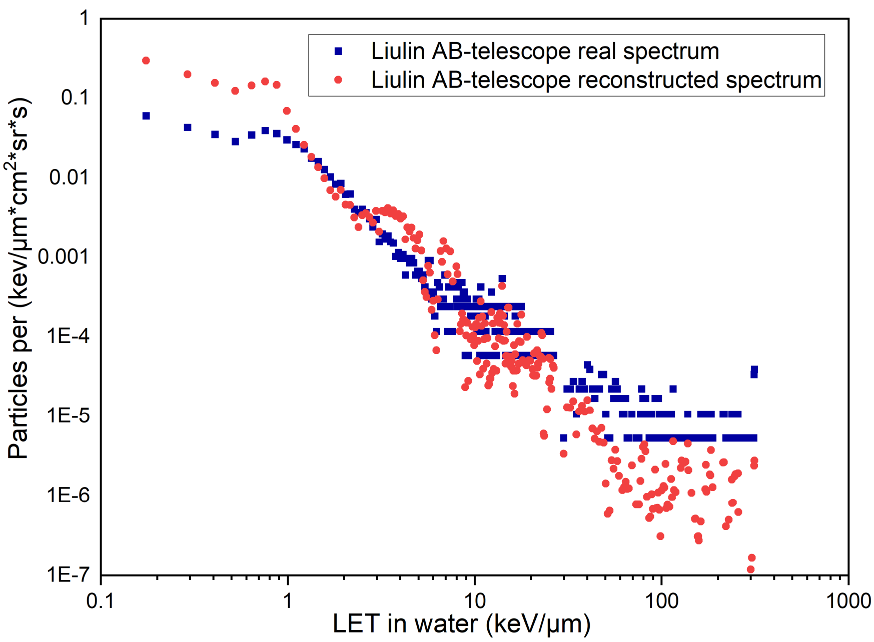

Fig.6.3.4.1a. Real (blue) and reprocessed (red) LET spectra in water measured in the telescope BA during 01 May-15 September 2016 in the interplanetary space.

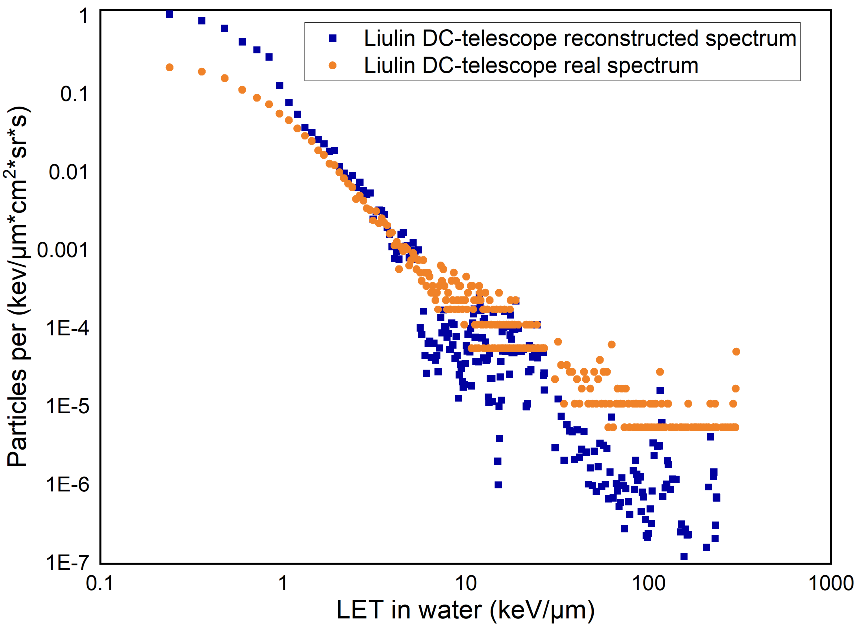

Fig.6.3.4.1b. Real (orange) and reprocessed (blue) LET spectra in water measured in the telescope DC during 01 May-15 September 2016 in the interplanetary space.

Review of the reprocessed data for the quality factor <Q>

The average radiation quality factor *<Q>* is calculated according to the *Q(LET)* relationship given in ICRP – 60 (ICRP, 1991), using the S/W SW02.02 provided with TN02.02.

The average radiation quality factor *<Q>* calculated for the period 01 May-15 September 2016 during the TGO transit to Mars from the reprocessed LET spectra described in the previous section is: *<Q>*=3.9±0.29 for BA telescope and *<Q>*=3.7±0.27 for DC telescope. The uncertainty on *<Q>* is statistical (low count rate at high LET) and systematic (modelling and smoothing of LET spectra, conversion of LET from silicon to water).

Review of the reprocessed data for the dose equivalent

The dose equivalent *H* is obtained as *H = D (water)•<Q>*, where *D* is the absorbed dose rate.

To convert the dose rate *D* measured in silicon to dose rate in water we use a factor of 1.3±0.08 (Semkova et al, 2018, 2021, 2023).

The average dose rate in Si for the period 01 May-15 September 2016 in detectors B(A) is 15.5 ± 0.15 µGy h^{-1}, in detectors D(C) it is 16.2 ± 0.16 µGy h^{-1} (Semkova et al, 2018).

Then the average dose equivalent rate for the same period is 78.6±15.7 µSv h^{-1} in detectors B(A) and 77.9 ± 15.6 µSv h^{-1} in detectors D(C). The uncertainty on *H* is statistical (low count rate at high LET) and systematic (modelling and smoothing of LET spectra, conversion of LET and absorbed dose from silicon to water).

Science analysis of the obtained results from reprocessing the data

The results from the reprocessing the data for LET, <*Q*> and *H* show that during the TGO transit to Mars in May-September 2016: <*Q*>=3.9±0.29 for AB telescope and <*Q*>=3.7±0.27 for CD telescope; *H* = 1.89±0.29 mSv day^{-1} in detectors B(A) and 1.79±0.28 mSv day^{-1} in detectors D(C). These are the data for GCRs. No solar energetic particle events were registered during this period.

It was found that using the full energy deposition spectrum in the single detectors B(A) and D(C), and evaluation the LET spectra in the directions B-A and D-C, assuming a mean path length 600 μm of a particle trough the 300 μm thick detector the mean <*Q*> for 01 May to 15 September 2016 in B-A direction is 4.08±0.3 and in D-C direction it is 4.02±0.3 (Semkova et al, 2018). The uncertainty on <*Q*> is statistical (low count rate at high LET) and systematic (calibration, conversion from silicon to water). In the same work is shown that for the same period in B-A direction the dose equivalent rate is 1.97 ± 0.3 mSv day^{-1}, in D-C direction the dose equivalent rate is 2.04 ± 0.3 mSv day^{-1}. The data was taken during the declining of the solar activity during the 24th solar cycle.

The above results show that a good agreement between the <*Q*> and *H* values obtained using 2 different methods of the calculations of LET (from the full energy deposition spectrum in the single detectors and that from the energy deposition spectrum in the telescopes of Liulin-MO) is observed. The agreement is within the uncertainty of <*Q*> and *H* the values obtained by the two methods of calculation of LET.

The RAD instrument aboard of NASA MSL during its cruise to Mars estimated <*Q*> = 3.82±0.28 and the dose equivalent rate 1.75 ± 0.30 mSv day^{-1} from GCRs in the interplanetary space close to the weak solar maximum in 2012 year (Guo et al. 2015 b).

A very good agreement (within the uncertainty of both instruments) between the calculations of <*Q*> and dose equivalent rates by Liulin-MO and RAD is observed having in mind the different solar cycle conditions and probably the different shielding of both instruments.

All above mentioned results prove the reliability of the simulations of Liulin-MO instrument and processes in it and the reliability of the newly developed method of calculating the LET.

The results for the dose equivalent obtained using the newly developed method and S/W confirm the previous obtained conclusion (Semkova et al, 2018) that during the cruise to Mars and back (6 months in each direction), taken during the declining of solar activity, the crewmembers of future manned flights to Mars will accumulate at least 60% of the total dose limit for the astronaut's career in case their shielding conditions are close to the mean shielding of Liulin-MO detectors – about 20 g cm^{-2}. This is a very important result, regarding the radiation risk and safety for future manned missions to Mars.

7. Conclusion and Recommendations

All technical objectives and tasks of the contract are completed successfully. The main science and technical results are:

- Investigation of the radiation conditions in Mars orbit and in the interplanetary space based on Liulin-MO data were conducted. The dependence of the particle fluxes and dose rates on the solar cycle development are investigated. Shown is that from March to August 2020 the measured radiation values are maximal, corresponding to the minimum of 24th cycle and transition to 25th cycle. The highest values of the dose rate (15.5/16.2 μGy h^{-1} at two perpendicular directions) and particle flux (3.24/3.33 cm^{-2} s^{-1} at two perpendicular directions) are registered in this period. Since September 2020 a decrease of the dose rates and fluxes is observed, corresponding to the decrease of GCR intensity during the inclination phase of the 25th cycle. At the moment of writing the final report (June 2023) the dose rates and flux of GCR are about 55% of the values during the minimum of 24th solar cycle. Analysed are the radiation characteristics of the solar energetic particle (SEP) events, registered since July 2021 in Mars orbit. The 15-19 February 2022 SEP event is the most powerful in our data. During this event the SEPs dose is equal to the dose for 38 days from GCR in undisturbed conditions, the biologically significant dose equivalent from SEPs is equal to the dose equivalent for 13 days from GCR in undisturbed conditions. The doses from 28-31 October 2021 SEP event are about 2 times less. Compared are measurements of GCR time profiles and SEP events by different radiation detectors, including Liulin-MO, located on different satellites in the space and a good agreement is observed. The time profiles of GCR measured by Liulin-MO and FREND neutron detectors on TGO from May 2018 to February 2021 demonstrate a good correlation on a local time scale (days) and show similar growth on long term scale (months). The difference in the amplitude of long-term variations (8-11%) might be addressed to how the solar modulation variations are visible for GCR particles with different energies. During the 28-31 October 2021 SEP the doses measured on Mars orbit, Mars surface, Earth orbit, Moon orbit and Moon surface increased in comparison to undisturbed conditions. On Mars orbit and Earth's high latitude polar orbit the SEP doses are very close (9186 μGy and 10174 μGy), the highest dose is measured in Moon orbit (31191 μGy) due to the lack of magnetosphere and atmosphere, the lowest doses are measured on Mars surface (288 μGy) due to the shielding of SEP by Mars body and atmosphere)
- The values for the radiation doses and particle fluxes necessary for the actualisation of the existing models of cosmic ray fluxes and the evaluation of the radiation hazard to the space vehicles and the crew of future interplanetary missions were obtained. We have compared with model results Liulin-MO measurements during the transit to Mars, on the high elliptic orbit and in Mars science orbit. The obtained results show that in all cases the measured dose rate and flux behind the shielding of the detectors of Liulin-MO are higher than the simulated values. The reasons for that are the secondary particles in the surrounding materials of the detectors, anomalous cosmic rays and the gradient of GCR spectrum from 1 AU to 1.5 AU which are not included in the models. Accounting for these differences, the calculated flux and dose rate may increase to match the measurement results. The results can serve for the benchmarking of GCRs models.
- A method and a S/W for extrapolating Liulin-MO data in Mars orbit to values in deep space at 1.5 a.u. were developed. The method and the S/W account for the GCR and albedo

radiation from Mars surface and atmosphere contribution as well as for the shading effect of Mars on the measured fluxes and dose rates in Mars orbit. The recalculated values represent the derived Liulin-MO data.

- Liulin-MO particle flux and dose rates data from TGO science phase were processed to calibrated and derived levels and in formats agreed with PSA developers as described in FREND Experiment Archiving Interface Control Document (EAICD, EXM-FR-ICD-IKI-0086). The obtained accuracy is within: ± 10% for the calibrated dose rates; ± 5% for the calibrated particle flux; ± 15% for the derived dose rate; ± 10% for the derived particle flux. Mutual work of Liulin-MO team and PSA collaborators led to a more readable structure of the raw data products, removing raw files with wrong data, appropriate structure of partially processed data products and a lot of improvements in the EAICD. Currently all calibrated data for the period 2016 - 2022 are provided in May 2023 to PSA in ESAC, stored and approved. Meanwhile the calibrated data from Liulin-MO measurements are available at http://esa-pro.space.bas.bg/LIULIN_MO_MARS_2 - a database of 10 Liulin type space experiments including Liulin-MO, which was created under the previous contract 4000117692/16/NL/NDe with ESA. Currently all Liulin-MO calibrated data together with the orbital parameters obtained from April 2016 to December 2022 are free accessible.
- A comparison of the measured by Liulin-MO fluxes to SREM flux data on Rosetta mission and their dependence on the solar activity were performed. Reviewed are the results from the comparison of Liulin-MO fluxes on ExoMars TGO mission with SREM TC1, S32 and S14 count rates obtained in the period April - September 2016 at different heliocentric distances in the interplanetary space. A long-term enhancement of all parameters is observed (from April to September 2016 the increase of Liulin-MO flux is 6.1% and increase of the TC1, S32, S12 SREM counts is 6.25 %-7.1 %. A long-term enhancement of all parameters is observed. This is in response of the falling trend of the solar activity in 2016 toward the solar cycle 24 minimum. All measured parameters from SREM and Liulin-MO instruments follow relatively well the shorter-term variations of the GCR flux, monitored by Oulu Neutron Monitor on Earth.
- A numerical model of Liulin-MO was created to investigate and account for the effect of the materials surrounding the instrument on the measured LET spectra. For that purpose a specialized application G4AAP was built, working in GEANT4 environment. The application allows for simulating the processes of Liulin-MO measurements. The results show that the behaviour of the simulated spectra of deposited energy very well follows the course of the measured spectra and provides the possibility to clean the measured LET spectra from false coincidence signals due to secondaries produced in the surrounding matter.
- A method, algorithm and S/W have been developed for subtracting the secondary effects on LET spectra measured by Liulin-MO dosimeter onboard ExoMars TGO during the transit to Mars in May-September 2016. They are based on the developed numerical model of Liulin-MO and the processes in the surrounding materials. The S/W also allows calculation of $\langle Q \rangle$ from the measured spectra with subtracted secondary effects.
- The data for the LET spectra, radiation quality factor $\langle Q \rangle$ and dose equivalent rates from the beginning of Liulin –MO operations were reprocessed and analysed by the above method and S/W. The results from the reprocessing the data show that during the TGO transit to Mars in May-September 2016: $\langle Q \rangle$=3.9±0.29 for BA telescope and

$\langle Q \rangle$=3.7±0.27 for DC telescope; H = 1.89±0.29 mSv day^{-1} in detectors B(A) and 1.79±0.28 mSv day^{-1} in detectors D(C). These are the data for GCRs. The above results are in good agreement with previous estimations of the corresponding values, based on measurements in single detectors of Liulin-MO and with the values of $\langle Q \rangle$ and dose equivalent rates obtained by RAD instrument aboard of NASA MSL during its cruise to Mars. The differences are within the uncertainties of the corresponding parameters (less than 8 %). All above mentioned results prove the reliability of the simulations of Liulin-MO instrument and processes in it and the reliability of the newly developed method of calculating the LET. The results for the dose equivalent obtained using the newly developed method and S/W confirm the previous obtained conclusion (Semkova et al, 2018) that during the cruise to Mars and back (6 months in each direction), taken during the declining of solar activity, the crewmembers of future manned flights to Mars will accumulate at least 60% of the total dose limit for the astronaut's career in case their shielding conditions are close to the mean shielding of Liulin-MO detectors – about 20 g cm^{-2}. This is a very important result, regarding the radiation risk and safety for future manned missions to Mars.

- The scope and schedule of the activity were reviewed and the status of Liulin-MO data and science results have been reported in regular participation in SWT&SOWG ExoMars 2016 meetings (totally 7 meetings during the contract).
- Totally 9 publications in science journals and 14 conference presentations relevant to the objectives of the contract were published.

Recommendations for future activities beyond of this contract

- The ExoMars TGO mission has been extended by ESA to 2025. We recommend and intent to continue the investigation of the radiation conditions in Mars orbit and in the interplanetary space based on existing and upcoming Liulin-MO data, comparison with other radiation measurements in the heliosphere, benchmarking of the cosmic ray models and estimation the radiation risks for future manned and robotic missions to Mars.
- A cross-calibration of Liulun-MO data on ExoMars TGO and SREM data on Rosetta trough other SREM instruments (like in Honig et al, 2019) on other missions, operating at about 1 AU (Proba-1 and INTEGRAL) in April – September 2016 with subsequent inter-calibration between SREM-Rosetta and Liulin-MO data and examination of the radial gradient of cosmic rays in this period may be a subject of a future joint investigation with the SREM team.
- Further development of the numerical model of Liulin-MO in two directions:

(i) more detailed descriptions of TGO satellite and instruments' structure (Fig. 6.3.2.8) will be implemented;

(ii) the number of generated particles will be increased. The used number of particles provides sufficient statistics for input particles from the surface of a sphere with 10 cm radius, used in the first stage of simulations. The ensure the same statistics for the second stage where the particles are generated from the surface of a sphere with 150 cm radius the number of input particles should be increased by two orders of magnitude.

- Development of an algorithm and S/W for reprocessing the data for the LET spectra, quality factors and dose equivalent rates obtained in TGO Mars orbit.

- Reprocessing the data for the LET spectra, quality factors and dose equivalent rates obtained in Mars orbit for the period since May 2018 by above mentioned S/W and comparison with the existing results.
- Continue to provide the new calibrated and derived Liulin-MO data to ESA PSA and maintain and upload the new Liulin-MO data to the Liulin instruments data base http://esa-pro.space.bas.bg/LIULIN_MO_MARS_2**,** created under the previous contract 4000117692/16/NL/NDe with ESA.

General recommendation regarding project management: Maintaining a risk register and close communications with ESA for resolving any problems, issues and risk areas.

8. Acknowledgments

TGORad team is grateful to Michele Iapaolo, Hugh Evans and Jennifer Ngo-Anh for their help, useful recommendations and excellent communications during the contract.

9. List of publications of the team

Published papers

1. Jordanka Semkova, Rositza Koleva, Victor Benghin, Tsvetan Dachev, Yuri Matviichuk, Borislav Tomov, Krasimir Krastev, Stephan Maltchev, Plamen Dimitrov, Nikolay Bankov, Igor Mitrofanov, Alexey Malakhov, Dmitry Golovin, Maxim Mokrousov, Anton Sanin, Maxim Litvak, Alexander Kozyrev, Sergey Nikiforov, Denis Lisov, Artem Anikin, Vyacheslav Shurshakov, Sergey Drobyshev, Results from radiation environment measurements aboard ExoMars Trace Gas Orbiter in Mars science orbit in May 2018–December 2019, Icarus, Volume 361, 2021, 114264,ISSN 0019-1035, **https://doi.org/10.1016/j.icarus.2020.114264**;

2. Jordanka Semkova, Victor Benghin, Jingnan Guo, Jian Zhang, Fabiana Da Pieve, Krasimir Krastev, Yuri Matviichuk, Borislav Tomov, Vyacheslav Shurshakov, Sergey Drobyshev, Igor Mitrofanov, Dmitry Golovin, Maxim Litvak, Comparison of the flux measured by Liulin-MO dosimeter in ExoMars TGO science orbit with the calculations, Life Sciences in Space Research, 2022,ISSN 2214-5524, **https://doi.org/10.1016/j.lssr.2022.08.007**

3. Jordanka Semkova, Rositza Koleva, Victor Benghin, Krasimir Krastev , Krasimir Krastev, Yuri Matviichuk, Borislav Tomov, Stephan Maltchev, Tsvetan Dachev, Nikolay Bankov, Igor Mitrofanov, Alexey Malakhov, Dmitry Golovin, Maxim Litvak, Anton Sanin, Alexander Kozyrev, Maxim Mokrousov, Sergey Nikiforov, Denis Lisov, Artem Anikin, Vyacheslav Shurshakov, Sergey Drobyshev, Nat Gopalswamy, Observation of the radiation environment and solar energetic particle events in Mars orbit in May 2018- June 2022, Life Sciences in Space Research, Available online 31 March 2023, **https://doi.org/10.1016/j.lssr.2023.03.006**
4. Jingnan Guo , Xiaolei Li , Jian Zhang , Mikhail I. Dobynde , Yuming Wang, Zigong Xu , Thomas Berger , Jordanka Semkova , Robert F. Wimmer-Schweingruber , Donald M. Hassler , Cary Zeitlin , Bent Ehresmann , Daniel Matthiä, Bin Zhuang, The First Ground Level Enhancement Seen on Three Planetary Surfaces: Earth, Moon, and Mars, Geophysical Research Letters, 2023, *50*, e2023GL103069. **https://doi.org/10.1029/2023GL103069**, Online ISSN:1944-8007
5. Weihao Liu, Jingnan Guo, Jian Zhang, Jordanka Semkova, Modeling the Radiation Environment of Energetic Particles at Mars Orbit and a first validation against TGO Measurements, The Astrophysical Journal, 2023 , **949-** 77, **DOI:10.3847/1538-4357/acce3c**

6. Krastev K., Semkova J., Koleva R., Benghin V., Drobyshev S. Temporal Analysis of the GCR Flux Obtained from the Liulin-MO Instrument in Orbit around Mars, Proceedings of the Thirteenth Workshop “Solar Influences on the Magnetosphere, Ionosphere and Atmosphere” September, 2021, ISSN 2367-7570, pp. 45-49

7. Dachev T.P., Tomov B.T., Matviichuk Y.N., Dimitrov P.G., Mitev M.G., Semkova J.V. Koleva R.T., Jordanova M.M., Bankov N.G., Krastev K., Malchev S., Mitrofanov I., Litvak M., Kozyrev A, Golovin D., Benghin V.V., Shurshakov, V.A. Overview of the space radiation extreme events observed with Liulin type instruments. Proceedings of the Fourteenth Workshop “Solar Influences on the Magnetosphere, Ionosphere and Atmosphere” June, 2022, ISSN 2367-7570, pp.49-54, **https://spaceclimate.bas.bg/ws-sozopol/pdf/Proceedings2022.pdf**

8. Semkova, J., Koleva, R., Benghin, V., Krastev, K., Matviichuk, Yu., Tomov, B., Bankov, N., Dachev, T., Maltchev, S, Mitrofanov, I., Malakhov, A., Kozyrev, A., Golovin, D., Mokrousov, M., Sanin, A., Litvak M., Nikiforov, S., Liso,v D., Anikin, A., Shurshakov, V., Drobyshev, S., Observation of solar energetic particle events onboard ExoMars TGO in July 2021-March 2022, Proceedings of the Fourteenth Workshop "Solar Influences on the Magnetosphere, Ionosphere and Atmosphere" June, 2022, ISSN 2367-7570, June, 2022, ISSN 2367-7570,pp. 55-60, **https://spaceclimate.bas.bg/ws-sozopol/pdf/Proceedings2022.pdf**
9. Krastev, K., Semkova, J., Koleva, R., Benghin, V., Drobyshev, S., Numerical simulation of Liulin-MO instrument, Proceedings of the Eighteenth International Scientific Conference „Space, Ecology, Safety" SES 2022, 2022, p-ISSN 2603 – 3313, e-ISSN 2603 – 3321, pp. 18-22 (*in Bulgarian*)

Presentations

1. Jordanka Semkova1 and the FREND Liulin-MO team, Radiation environment in the interplanetary space and Mars orbit during the declining phase of 24th solar cycle and transition to 25th cycle according measurements aboard ExoMars TGO, EGU General Assembly 2021, EGU21-2925, **https://doi.org/10.5194/egusphere-egu21-2925**
2. Jordanka Semkova and FREND Liulin-MO team, GCR radiation quantities in the interplanetary space and Mars orbit during the declining phase of 24th solar cycle and transition to 25th cycle according measurements aboard ExoMars TGO, Космическо време в период на вековo понижаване на слънчевата активност, работна среща, 01-05 Юни .2021, Приморско, България, **https://spaceclimate.bas.bg/SW/assets/pdf/Semkova.pdf; https://spaceclimate.bas.bg/SW/prim.php**
3. Krastev K, Semkova J. et al , Thirteenth Workshop "Solar Influences on the Magnetosphere, Ionosphere and Atmosphere" September, 2021, **https://spaceclimate.bas.bg/ws-sozopol/** (see Krastev K, Semkova J., Koleva R., Benghin V., Drobyshev S. Temporal Analysis of the GCR Flux Obtained from the Liulin-MO Instrument in Orbit around Mars, Proceedings of the Thirteenth Workshop "Solar Influences on the Magnetosphere, Ionosphere and Atmosphere" September, 2021, ISSN 2367-7570, pp. 45-49 , DOI: 10.31401/WS.2021.proc)
4. Semkova J., Koleva R., Benghin V., Krastev K., Dachev T., Mitrofanov I., Malakhov A., Golovin D., Litvak M. on behalf of FREND Liulin MO team, Radiation environment in the interplanetary space and Mars orbit during the declining phase of 24th and beginning of 25th solar cycles according measurements aboard ExoMars TGO, Thirteenth Workshop "Solar Influences on the Magnetosphere, Ionosphere and Atmosphere" September, 2021, **https://www.spaceclimate.bas.bg/ws-sozopol/pdf/Friday/Semkova.pdf**.
5. Semkova J., Koleva R., Matviichuk Y., Tomov B., Dachev T., et al., Peculiarities of the radiation environment in Mars orbit in the period May 2018-October 2021 according experimental investigations aboard ExoMars Trace Gas Orbiter, presentation at Seventeenth International Scientific Conference „Space, Ecology, Safety" SES 2021, Sofia, 20 – 22 October 2021

6. Kozyrev, A., Litvak, M., Malakhov, A., Mitrofanov, I., Semkova, J., Koleva, R., Benghin, V., Krastev, K., Matviichuk, Y., Tomov, B., Maltchev, S., Bankov, N., Shurshakov, V., and Drobyshev, S.: Observation of solar particle events from MGNS experiment onboard BepiColombo mission, HEND experiment onboard Mars Odyssey mission, and also FREND and Liulin-MO experiments onboard TGO mission during July-October 2021, EGU General Assembly 2022, Vienna, Austria, 23–27 May 2022, EGU22-11521, 2022, DOI: 10.5194/egusphere-egu22-11521

7. Semkova, Jordanka et al, Radiation environment in Mars orbit in the period May 2018 - January 2022 according measurements aboard ExoMars TGO, 44th COSPAR Scientific Assembly, Held 16-24 July, 2022, Athens, Greece, Abstract F2.3-0014-22, https://ui.adsabs.harvard.edu/abs/2022cosp...44.2700S/abstract

8. Jordanka Semkova, Rositza Koleva, Victor Benghin, Krasimir Krastev, Yuri Matviichuk, Borislav Tomov , Nikolay Bankov, Tsvetan Dachev, Stephan Maltchev' Igor Mitrofanov, Alexey Malakhov, Alexander Kozyrev, Dmitry Golovin, Maxim Mokrousov, Anton Sanin, Maxim Litvak, Sergey Nikiforov, Denis Lisov, Artem Anikin, Vyacheslav Shurshakov, Sergey Drobyshev, Observation of solar energetic particle events onboard ExoMars TGO in July 2021-March 2022, 14th Workshop “Solar Influences on the Magnetosphere, Ionosphere and Atmosphere”, Primorsko, Bulgaria, June 2022, https://spaceclimate.bas.bg/ws-sozopol/pdf/14th/Wednesday/Semkova-Primorsko2022.pdf

9. Jordanka SEMKOVA et al, Radiation environment in ExoMars TGO Mars orbit during solar energetic particle events in July 2021–March 2022, Thirteenth Moscow Solar System symposium 13m-S3 October 10-14, 2022. Space Research Institute of Russian Academy of Sciences Moscow, Russia ISBN: 978-5-00015-057-3, DOI: 10.21046/13MS3-2022

10. Victor Benghin et al, Comparison of the flux and dose rate measured by the Liulin-MO deice aboard ExoMars TGO with calculated estimations, Thirteenth Moscow Solar System symposium 13m-S3 October 10-14, 2022. Space Research Institute of Russian Academy of Sciences Moscow, Russia ISBN: 978-5-00015-057-3, DOI: 10.21046/13MS3-2022

11. Jordanka Semkova, Rositza Koleva, Victor Benghin, Krasimir Krastev, Yuri Matviichuk, Borislav Tomov, Stephan Maltchev, Tsvetan Dachev, Nikolay Bankov, Igor Mitrofanov, Alexey Malakhov, Dmitry Golovin, Maxim Litvak, Anton Sanin, Alexander Kozyrev, Maxim Mokrousov, Sergey Nikiforov, Denis Lisov, Artem Anikin, Vyacheslav Shurshakov, Sergey Drobyshev, Nat Gopalswamy, Observation of the solar energetic particle events in Mars orbit in July 2021- March 2022, Conference of Deep Space Sciences in China during April 24-30, 2023 in Hefei, Anhui, China, https://planet.ustc.edu.cn/icdss, https://planet.ustc.edu.cn/web/viewer.html?file=/attachs/file/20230411/s2.pdf

12. Jordanka Semkova, Rositza Koleva, Victor Benghin, Krasimir Krastev, Yuri Matviichuk, Borislav Tomov, Stephan Maltchev, Tsvetan Dachev, Nikolay Bankov, Igor Mitrofanov, Alexey Malakhov, Dmitry Golovin, Maxim Litvak, Anton Sanin, Alexander Kozyrev, Maxim Mokrousov, Sergey Nikiforov, Denis Lisov, Artem

Anikin, Vyacheslav Shurshakov, Sergey Drobyshev, Nat Gopalswamy, Jingnan Guo, Jian Zhang, Weihao Liu, Update of the science results from the radiation investigations in Mars orbit aboard ExoMars TGO in 2018-2023, Fifteenth Workshop Solar Influences on the Magnetosphere, Ionosphere and Atmosphere, 5-9 June 2023 in Primorsko, Bulgaria, 2023, Book of Abstracts, **DOI: 10.31401/WSoz.2023.abs**, pp.7

13. Koleva R., Semkova J., Benghin V., Krastev K., Matviichuk Y., Tomov B., Bankov N., Maltchev S., Dachev T., Drobyshev S., Gopalswamy N., Mitrofanov I., Malakhov A., Golovin D., Litvak M. Where did the solar energetic protons observed in Mars orbit come from?, Fifteenth Workshop Solar Influences on the Magnetosphere, Ionosphere and Atmosphere, 5-9 June 2023 in Primorsko, Bulgaria, 2023, Book of Abstracts, **DOI: 10.31401/WSoz.2023.abs**, pp.4
14. Krastev Kr., Semkova J., Koleva R., Benghin V., Drobijshev, S., Numerical simulation of the LIULIN-MO device, Fifteenth Workshop Solar Influences on the Magnetosphere, Ionosphere and Atmosphere, 5-9 June 2023 in Primorsko, Bulgaria, 2023, Book of Abstracts, **DOI: 10.31401/WSoz.2023.abs**, pp. 23